Acoustic Trapping of Extracellular Vesicles

Broman, Axel

2024

Acoustic Trapping of Extracellular Vesicles

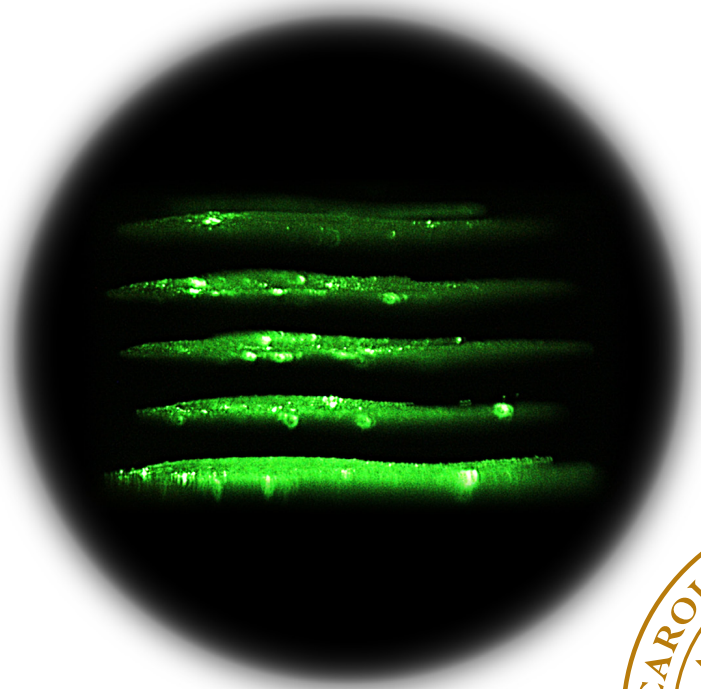

Axel Broman

Department of Biomedical Engineering
Faculty of Engineering
Lund University

Acoustic Trapping of Extracellular Vesicles

Axel Broman

LUND
UNIVERSITY

DOCTORAL DISSERTATION

Doctoral dissertation for the degree of Doctor of Philosophy (PhD) at the Faculty of Engineering at Lund University to be publicly defended on 29th of November at 09:00 in Belfragesalen, Biomedical Center, Sölvegatan 19, Lund, Sweden

Faculty opponent
Prof. David Juncker
McGill University, Canada

Organization: LUND UNIVERSITY, Department of Biomedical Engineering

Document name: Doctoral dissertation **Date of issue** 2024-10-30

Author: Axel Broman **Sponsoring organization:**

Title: Acoustic Trapping of Extracellular Vesicles

Abstract: Extracellular vesicles (EVs) are membrane enclosed biological nanoparticles released by cells. In the past two decades, EVs have gained a lot of attention due to their role in numerous biological processes. However, their small nature complicates isolating them from biological fluids with cumbersome techniques, such as ultracentrifugation. Acoustic trapping is a technique that uses ultrasonic standing waves to isolate particles from their surrounding fluid. In this way, acoustic trapping can be used to isolate EVs. This thesis describes the development of a new acoustic trapping platform, the Multinode Acoustic Trap (MAT). MAT is designed to have higher throughput and capacity than previously reported acoustic trapping platforms. The faster processing by MAT facilitates the study of EVs, and MAT-isolated EVs and their function was further explored in this thesis, mainly through mass spectrometry based proteomics. In **Paper I**, it was shown that MAT was capable of operating at 30 times higher throughput and displayed 40 times higher seed particle capacity than previous systems. We demonstrate that the platform can isolate extracellular vesicles from urine samples and generates sufficient amount of material for RNA and mass spectrometry analysis. In **Paper II**, MAT was used to isolate platelet derived EVs (PEVs) from plasma samples to investigate differences between pathogen-activated platelets and endogenous activation. Complement proteins and IgG3 were found to be enriched in pathogen-activated PEVs. We demonstrate that the MAT produces functionally intact EVs, and that PEVs have immunomodulatory effects. We also show that bacterial M1 protein from *Streptococcus pyogenes* binds to PEVs and can be transported with them, a previously unknown mechanism that could contribute to systemic responses during diseases such as sepsis. In **Paper III**, MAT was used to isolate EVs from small volumes of septic mouse plasma. We demonstrate that EVs during sepsis exhibit changes in their proteomes, with an emphasis on leukocyte migration. We show that the MAT gives fast and easy access to the EV proteome and provides information that cannot be obtained from plasma alone. The small volumes required also means that MAT is suitable for handling biobanked samples and can therefore be used to provide additional information from already collected samples. Finally, **Paper IV** explores the feasibility of combining acoustic trapping with immunoaffinity-based separation, in order to access different subpopulations of EVs. CD9-positive EVs were separated from other EVs by means of functionalized silica beads. Compared to just incubating the beads in plasma, utilizing an acoustic trap gave access to two populations of EVs rather than just the CD9-positive ones. Processing with the acoustic trap was also faster, and the enriched proteins derived from seed particle-bound EVs were more related to CD9, indicating an enrichment of EVs defined by the chosen antibody. As a whole, this thesis broadens the applicability of acoustic trapping as a tool for isolating EVs, and demonstrates the usefulness of the technique through the subsequent analysis of the isolated EVs to reveal new aspects of their biological function.

Key words: Acoustic Trapping, Extracellular Vesicles, Proteomics, Mass spectrometry, Sepsis, Microfluidics, Acoustofluidics

Classification system and/or index terms (if any) Supplementary bibliographical information

Language English **Number of pages**: 73

ISSN and key title: **ISBN (print):** 978-91-8104-272-6
ISBN (electronic): 978-8104-273-3

Recipient's notes **Price** **Security classification**

Signature  Date 2024-10-30

Acoustic Trapping of Extracellular Vesicles

Axel Broman

LUND
UNIVERSITY

Cover photo by Axel Broman. Microparticle clusters levitated in an acoustic field. Green fluorescent nanoparticles are enriched in the microparticle clusters.

Faculty of Engineering

Department of Biomedical Engineering

ISBN (print) 978-91-8104-272-6

ISBN (electronic) 978-91-8104-273-3

ISRN: LUTEDX/TEEM-1139-SE

Report No. 2/24

Printed in Sweden by Tryckeriet in E-Huset, Lund University

Lund 2024

To my dear parents

Table of Contents

Abstract

Extracellular vesicles (EVs) are membrane enclosed biological nanoparticles released by cells. In the past two decades, EVs have gained a lot of attention due to their role in numerous biological processes. However, their small nature complicates isolating them from biological fluids with cumbersome techniques, such as ultracentrifugation. Acoustic trapping is a technique that uses ultrasonic standing waves to isolate particles from their surrounding fluid. In this way, acoustic trapping can be used to isolate EVs. This thesis describes the development of a new acoustic trapping platform, the Multinode Acoustic Trap (MAT). MAT is designed to have higher throughput and capacity than previously reported acoustic trapping platforms. The faster processing by MAT facilitates the study of EVs, and MAT-isolated EVs and their function was further explored in this thesis, mainly through mass spectrometry based proteomics. In **Paper I**, it was shown that MAT was capable of operating at 30 times higher throughput and displayed 40 times higher seed particle capacity than previous systems. We demonstrate that the platform can isolate extracellular vesicles from urine samples and generates sufficient amount of material for RNA and mass spectrometry analysis. In **Paper II**, MAT was used to isolate platelet derived EVs (PEVs) from plasma samples to investigate differences between pathogen-activated platelets and endogenous activation. Complement proteins and IgG3 were found to be enriched in pathogen-activated PEVs. We demonstrate that the MAT produces functionally intact EVs, and that PEVs have immunomodulatory effects. We also show that bacterial M1 protein from *Streptococcus pyogenes* binds to PEVs and can be transported with them, a previously unknown mechanism that could contribute to systemic responses during diseases such as sepsis. In **Paper III**, MAT was used to isolate EVs from small volumes of septic mouse plasma. We demonstrate that EVs during sepsis exhibit changes in their proteomes, with an emphasis on leukocyte migration. We show that the MAT gives fast and easy access to the EV proteome and provides information that cannot be obtained from plasma alone. The small volumes required also means that MAT is suitable for handling biobanked samples and can therefore be used to provide additional information from already collected samples. Finally, **Paper IV** explores the feasibility of combining acoustic trapping with immunoaffinity-based separation, in order to access different subpopulations of EVs. CD9-positive EVs were separated from other EVs by means of functionalized silica beads. Compared to just incubating the beads in plasma, utilizing an acoustic trap gave access to two

populations of EVs rather than just the CD9-positive ones. Processing with the acoustic trap was also faster, and the enriched proteins derived from seed particle-bound EVs were more related to CD9, indicating an enrichment of EVs defined by the chosen antibody. As a whole, this thesis broadens the applicability of acoustic trapping as a tool for isolating EVs, and demonstrates the usefulness of the technique through the subsequent analysis of the isolated EVs to reveal new aspects of their biological function.

Populärvetenskaplig sammanfattning

Alla våra celler skickar ut små membranbundna partiklar som kallas för extracellulära vesiklar. Under de senaste 20 åren har man upptäckt att de spelar viktiga roller i biologiska funktioner. Bland annat hjälper de celler att kommunicera med varandra, kan transportera och leverera biologiska ämnen, och är en viktig del av immunsystemet. Eftersom det har visat sig att de är involverade i många funktioner, har forskning på extracellulära vesiklar ökat kraftigt de senaste åren, men det är fortfarande mycket som man inte vet.

Extracellulära vesiklar är mycket små, vilket gör det svårt att isolera och studera dem. De flesta är under 100 nanometer i storlek, vilket är ungefär 500 gånger mindre än bredden på ett hårstrå. Det tar därför lång tid att isolera och rena dessa partiklar med hjälp av konventionella metoder som centrifugering, vilket försvårar forskningen. Det behövs därför andra metoder för att underlätta forskning på extracellulära vesiklar.

I denna avhandling används en akustisk fälla för att isolera och rena upp vesiklar. Den akustiska fällan använder sig av ultraljud i små flödeskanaler för att manipulera partiklar i vätskan. Genom att matcha ljudvågens frekvens till kanalens resonansfrekvens, kan en stående våg bildas i kanalen. Partiklar i den stående vågen kommer då att röra sig mot specifika punkter där trycket är som lägst. Om även ljudfältet är utformat så att det är starkast i en viss punkt, kan partiklar hållas fast i den punkten, och en akustisk fälla formas. Genom att låta ett biologiskt prov passera genom fällan, kommer partiklarna i provet fastna i fällan och koncentreras, medan vätskan passerar förbi. På så sätt används den akustiska fällan för att rena upp vesiklar från kroppvätskor som blodplasma och urin.

I detta arbete beskrivs utvecklingen av en ny typ av akustisk fälla. Den nya fällan har kraftigt ökad flödeshastighet och kapacitet jämfört med föregående system, vilket används för att enkelt rena upp vesiklar ur större volymer. Vesiklarna studeras sedan främst genom masspektrometri för att analysera vad för typ av proteiner de innehåller och således vilka funktioner de fyller. Bland annat undersöks vesiklarnas roll under infektion. Detta görs genom att titta på vesiklar från blodplättar som stimuleras med ett bakteriellt protein och vesiklar från möss med bakteriell sepsis. Det visades att bakteriella proteiner kan binda till och transporteras med vesiklarna.

Vidare visades att vesiklarna spelade en roll i att attrahera immunceller under infektion.

Slutligen utforskades också möjligheten att kombinera den akustiska fällan med antikroppsinfångning, vilket skulle göra det möjligt att rena upp vesiklar som har proteiner som matchar antikroppen som valts. Detta skulle underlätta forskning på specifika typer av vesiklar, eller vesiklar som kommer från en viss typ av cell, vilket vidare skulle bredda användningsområdet för tekniken. Förhoppningsvis kan en ökad förståelse av vesiklarnas roll i olika sjukdomstillstånd på sikt leda till bättre behandlingar för patienter.

Publications

I. **Axel Broman**, Andreas Lenshof, Mikael Evander, Lotta Happonen, Anson Ku, Johan Malmström and Thomas Laurell. "Multinodal acoustic trapping enables high capacity and high throughput enrichment of extracellular vesicles and microparticles in miRNA and MS proteomics studies." *Analytical Chemistry,* **2021** 93 (8), 3929-3937. DOI: 10.1021/acs.analchem.0c04772

II. Frida Palm*, **Axel Broman***, Genevieve Marcoux, John W. Semple, Thomas Laurell, Johan Malmström and Oonagh Shannon. "Phenotypic characterization of acoustically enriched extracellular vesicles from pathogen activated platelets." *Journal of Innate Immunity*, **2023** 15 (1) 599-613. DOI: 10.1159/000531266

III. **Axel Broman,** Yashuan Chao, Oonagh Shannon, Thomas Laurell and Johan Malmström. "Proteomic profiling of acoustically isolated extracellular vesicles from blood plasma during murine bacterial sepsis." *Submitted manuscript.*

IV. **Axel Broman***, Megan Havers*, Roman Sattarov and Thomas Laurell. Immunoaffinity coupled acoustic trapping: towards extracellular vesicle subpopulation. *Manuscript.*

* *Shared first authorship*

Publications not included in this thesis

V. Megan Havers, **Axel Broman**, Andreas Lenshof, Thomas Laurell. Advancements and obstacles in microfluidics-based isolation of extracellular vesicles. *Analytical and Bioanalytical Chemistry*, **2022** 415 1265–1285. DOI: 10.1007/s00216-022-04362-3

Author's contribution to publications

I. Major part of design and fabrication of the acoustic trapping device, major part of planning, experimental work, data analysis and writing.

II. Large part of planning, experimental work, data analysis and writing.

III. Major part of planning, large part of experimental work, major part of data analysis and writing.

IV. Large part of planning and experimental work, major part of data analysis, large part of writing.

Abbreviations

AT	Acoustic Trapping
CSF	Cerebrospinal Fluid
CD9	Cluster of Differentiation 9
DDA	Data Dependent Acquisition
DIA	Data Independent Acquisition
DIC	Disseminated Intravascular Coagulation
E. coli	Escherichia coli
EV	Extracellular Vesicle
FDR	False Discovery Rate
LC	Liquid Chromatography
MAT	Multinode Acoustic Trap
MS	Mass spectrometry
MVB	Multivesicular Body
NTA	Nanoparticle Tracking Analysis
PEV	Platelet-derived Extracellular Vesicle
PBS	Phosphate Buffered Saline
Re	Reynold's Number
RP-LC	Reverse Phase Liquid Chromatography
SEC	Size Exclusion Chromatography
SOFA	Sequential Organ Failure Assessment
S. pyogenes	Streptococcus pyogenes
SWATH-MS	Sequential Window Acquisition of All Theoretical Mass Spectra
UC	Ultracentrifugation

Introduction

Cells release biological nanoparticles called extracellular vesicles (EVs) into their surroundings. Interest in EVs has grown rapidly in the last 20 years as they have been shown to play an integral role in many biological processes. To study EVs and understand their function, they must first be effectively isolated from their surrounding environment. However, because of their small size, isolating EVs with traditional centrifugation approaches is challenging, which limits their study. Thus, there is an unmet need for faster and more efficient techniques for isolating EVs to facilitate further research.

This thesis explores the use of acoustic trapping, a technique that utilizes ultrasonic waves in microchannels, as a tool for isolating extracellular vesicles EVs. The first aim was to design and develop a new acoustic trapping platform with higher throughput and capacity than previous systems, to make sample processing and EV isolation faster. The second aim was to utilize the acoustic trap in order to study the function and protein content of EVs using mass spectrometry-based proteomics, with a focus on infectious diseases and sepsis. This gives access to a sub proteome based on proteins found in EVs and therefore provides additional information in biomolecular signalling.

This thesis is divided into chapters aimed at explaining key concepts related to the work presented in **Paper I-IV**. It begins with an introduction to extracellular vesicles (EVs), their biological roles and traditional isolation methods. Next, microfluidic concepts are introduced followed by the use of ultrasound in microchannels, referred to as acoustofluidics. The concept of acoustic trapping is then explained, along with a detailed description of the acoustic trapping platform developed in this thesis. The mass spectrometry-based proteomics used to analyze EVs in this thesis is then described. Finally, sepsis and the role of EVs in this complex condition are discussed.

1. Extracellular Vesicles

Extracellular vesicles (EVs) are membrane enclosed particles released by cells into their surroundings. EVs were for a long time considered to be a way for cells to dispose of unwanted components[1] and were consequently understudied. However, EVs have gained a lot of attention in the last two decades and research into EVs and their function has grown exponentially[2]. We now know that most cells release EVs and they have been found in virtually all biofluids, including blood, urine, cerebrospinal fluid (CSF), breast milk, seminal fluid and amniotic fluid[1].

EVs are traditionally categorized into three main groups: exosomes (30-100nm), ectosomes or microvesicles (100-1000 nm), and apoptotic bodies (50-5000 nm), depending on their mechanism of origin[3]. Exosomes are formed in a multivesicular body (MVB) in the cell and released to the surrounding by fusion of the MVB with the plasma membrane. Microvesicles are formed through direct budding of the plasma membrane. Apoptotic bodies are formed as a result of membrane budding during programmed cell death[4]. However, since EVs are most often studied in cell culture media or biofluids, where their origin is not directly observed, it can be hard to classify EVs in this way. Without specific markers of subcellular origin, a more useful categorization is based on the properties of EVs, referring to size range, surface markers or cell type and conditions from which the EV originated[5].

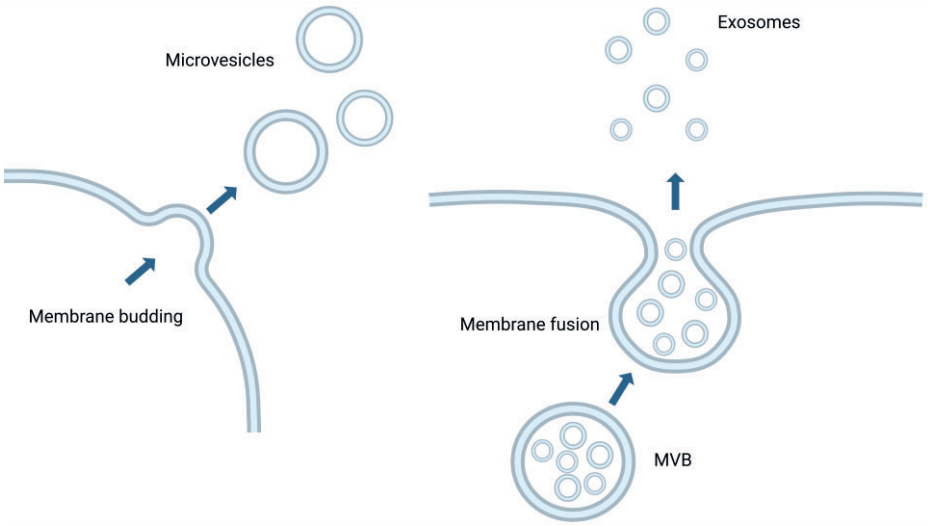

Figure 1: *Formation of extracellular vesicles. Microvesicles are formed through budding of the cell membrane. Exosomes are released through the fusion of a multivesicular body (MVB) with the cell membrane. Figure created with Biorender.*

Since EVs are generated from cells, their contents can reflect cellular processes and the state of the parent cell. This enables a type of liquid biopsy, where information about specific cells and tissue can be gained by analyzing their EVs from biofluids such as blood, urine and CSF[6–8]. EVs have been shown to contain various bioactive molecules, such as proteins, lipids, microRNA (miRNA) and non-coding RNA, cytokines and membrane proteins[5,9–12]. They can act as messengers, shuttling around their cargo and delivering to specific cell types and tissues. Because of this, the biological functions of EVs are broad and complex and have been shown to include cell-cell communication, immune regulation, inflammation, coagulation, homeostasis, response to infection and tumour growth and spread[9]. Additionally, EVs could be used for therapeutic purposes by loading them with specific cargo[11,13], and there have been trials to explore their use in vaccination[14,15]. Given the wealth of biological functions that EVs influence, it is necessary to understand EVs to understand the biology of an organism as a whole.

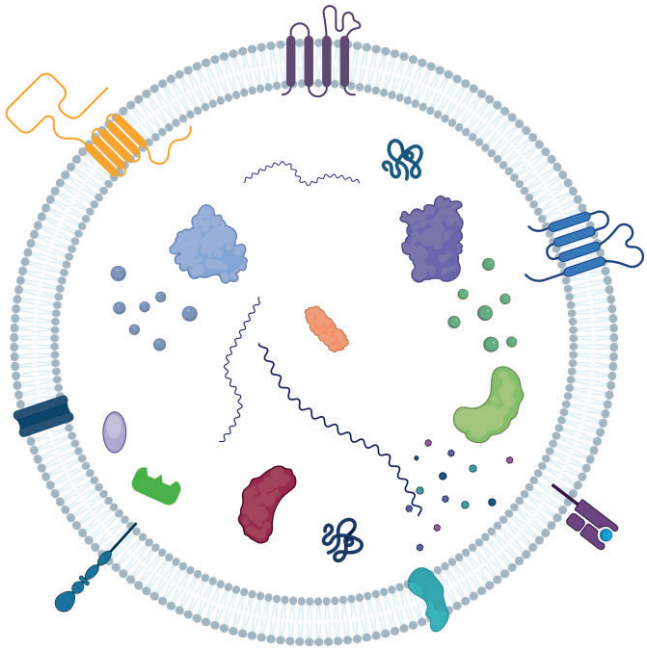

Figure 2: *Schematic cross section of an extracellular vesicle. The vesicle is composed of a lipid bilayer and contains a wide range of membrane proteins and bioactive molecules. Figure created with Biorender.*

In order to study EVs, it is often necessary to isolate them from their supernatant. However, this is often easier said than done. EVs are very small, which makes them hard to separate by a traditional centrifugation approach. In addition, EVs often have to be extracted from a complex biological matrix, further complicating isolation. It is therefore necessary to have good isolation techniques to facilitate the study of EVs. The next section outlines the most common traditional isolation techniques.

1.1 Traditional Isolation Techniques

Ultracentrifugation (UC) has been the most widely used method for isolating EVs. This is because UC is a relatively simple and flexible technique, and most laboratories have access to an ultracentrifuge. Like traditional centrifugation, particles are separated based on their density and hydrodynamic size. However, due to the small size of EVs (~100 nm), very high g-forces (100 000 – 120 000 x *g*) are required for a long period of time, typically around one hour, for small EVs to sediment. This procedure needs to be repeated each time the sedimented EVs are

washed, a procedure necessary to remove background supernatant. This ultimately leads to many hours-long and laborious isolation protocols. One advantage of UC is that successive centrifugation steps can be used to isolate subpopulations of EVs[16], increasing flexibility in EV isolation. However, the high forces involved may induce EV coalescence, which can lead to erroneous conclusions about size and biochemical properties of a population[17]. Additionally, protein aggregates, such as Tamm-Horsfall protein in urine[12,18], can be co-isolated and contaminate the final sample.

Precipitation can be used to quickly separate EVs from the supernatant and dramatically lower the needed centrifugation force and time. In precipitation, additives, often polymers, are added to the biofluid to reduce the solubility of EVs[4]. This causes the EVs to form aggregates, which are then much easier to separate using centrifugation. There are commercial precipitation kits available for purchase, however these tend to require incubation times of several hours. The main advantage is then that it is less labour intensive than UC, and the sample is not subject to extreme forces[16]. However, the addition of additives may reduce the purity of the collected EV fraction. Additionally, comparative studies have found that performance varies across isolation kits and biofluids[19,20]. The International Society for Extracellular Vesicles cautioned against their use in their latest position statement[5].

Size-exclusion chromatography (SEC) is a method that has gained popularity in the last decade[21]. In SEC, a chromatographic column is used to separate EVs based on physical and biochemical properties. A column is packed with porous beads and sample is passed through the column. Small particles, such as free protein, can migrate into the pores in the column, while larger particles such as EVs cannot. The retention time in the column is therefore dependent on particle size, with larger particles eluting before smaller ones. By selecting columns with certain pore sizes, it is possible to separate EVs around a certain size. There are commercially available columns that are aimed towards isolating EVs of different sizes. EV isolation on a SEC column can be done in as little as 15 minutes, with intermediate specificity and recovery[5]. This is significantly faster than UC, however the columns are typically single or 5-times use. Additionally, the sample volume must match the column, and there is a need to know which size of EVs one is aiming for, risking skewed results. There is also a risk of EVs clogging SEC columns, especially ones aimed at isolating smaller EVs[16].

2. Microfluidics

In our everyday world, inertial forces dominate over viscous forces. When we scale down a fluidic system, the behaviour of fluids changes from what we are used to. The surface area to volume ratio increases, which means that surface dependent effects become more influential. Likewise, effects that depend on the bulk become less influential. Most notably, flow goes from turbulent to laminar, moving in parallel layers that do not mix with each other, save for diffusion. Flow resistance in microfluidic channels is typically so high compared to the momentum of the fluid that it stops moving almost immediately when a force is no longer applied. To put it simply, fluids start behaving more like honey and less like water.

There are several benefits of scaling down fluidic systems. Volumes are greatly reduced, requiring less reagents and generating less waste. Reaction times are faster as the distance a reagent needs to diffuse is reduced. The flow is laminar, making flow predictable with computational models and allows for better control of sample, analytes and reagents. For example, this enables the generation of stable concentration gradients in microfluidic cell culture systems[22] and predicted flow behaviour for varying flow rates in acoustofluidic systems[23]. Additionally, the smaller sizes are better suited for probing samples at cellular and subcellular size scales. Because of these various benefits, many different microfluidics-based techniques have been developed for isolating EVs and are outlined briefly at the end of this chapter.

2.1 Flow at the Microscale

2.1.1 Laminar Flow

Whether or not flow in a particular channel will be turbulent or laminar can be estimated with the Reynolds number (Re)[24,25]. Reynolds number is a dimensionless quantity and is calculated by comparing the inertial and viscous forces:

$$Re = \frac{\rho v d}{\eta}$$

Where ρ is the density, v is the velocity, d is the characteristic dimension of the fluidic channel and η is the viscosity. If the Reynolds number is low, the viscous forces dominate the inertial forces and flow will tend to be laminar. Typically, flow goes from turbulent to laminar when Re is less than 2000[26]. The acoustic trapping platform used in **Paper I, II** and **III** has an Re of 1.9 during standard operation, which falls clearly within the laminar regime.

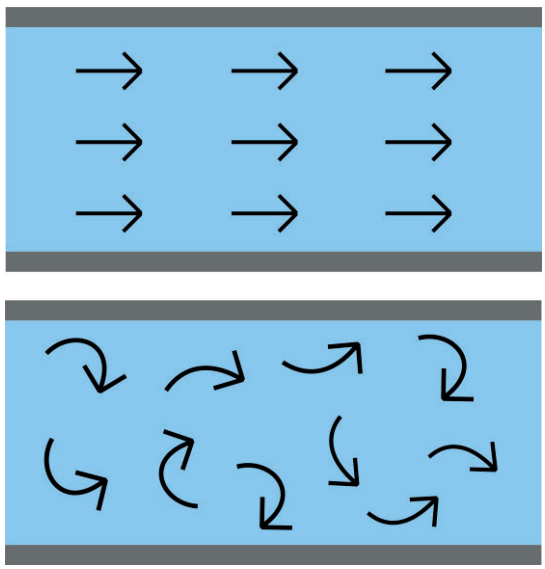

Figure 3: *Schematic illustration of laminar and turbulent flow lines in a fluidic channel.*

2.1.2 Parabolic Flow Profile

When an incompressible, viscous and uniform fluid, often referred to as a "Newtonian fluid", flows with laminar flow through a channel, the flow velocity profile will be parabolic. This is because there will be a no-slip boundary condition at the channel wall that arises from viscous interactions between the wall and the fluid[27]. The flow velocity will be highest in the center of the channel and decrease to zero at the channel wall, resulting in parabolic flow profile, also known as Poiseuille flow[28]. This also means that particles that are suspended in a fluid will move at different velocities and therefore have different retention times according to their proximity to the walls.

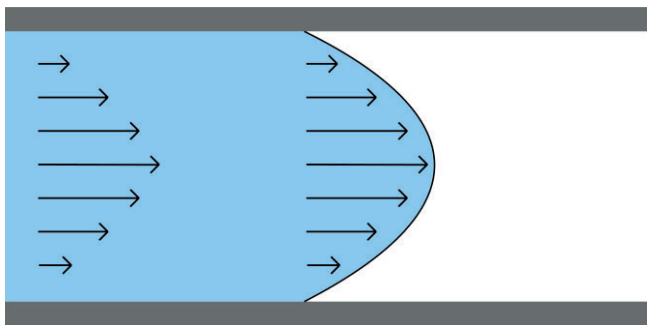

Figure 4: *Parabolic flow profile inside a microfluidic channel. Flow velocity is greatest in the center of the channel and slowest near the walls due to viscous interaction between the fluid and channel walls.*

2.1.3 Fluidic Drag

When a fluid moves relative to a particle, the particle will experience a drag force in the direction of fluid movement. When flow is laminar the drag force F_d can be calculated using Stokes law[25]

$$F_d = 6\pi\eta r v$$

Where η is the viscosity of the fluid, r is the radius of the particle and v is the velocity of the fluid. The drag force on a particle scales with the radius of the particle, but many other external forces, such as magnetic, electric and acoustic radiation forces scale with the volume of the particle. This means that smaller particles are harder to actively manipulate and instead tend to move along with the fluid flow. For many microfluidic isolation techniques, this puts a size limit to how small particles it is possible to manipulate.

2.2 Microfluidic Isolation Techniques

Because of the benefits of scaling down fluidic systems outlined earlier in this chapter, numerous microfluidics-based techniques have been developed for isolating EVs. These include mechanical filtering[29–31], functionalized surfaces[32–34], hydrodynamic focusing[35,36], deterministic lateral displacement (DLD)[37,38], viscoelastic separation[39,40], magnetophoresis[41–44], dielectrophoresis[45,46] and acoustophoresis[18,47–49]. These microfluidic devices have by nature low volumetric throughput. In the above mentioned techniques, the throughput is typically a few microliters per minute, excluding any potential time for incubation or labelling. The low throughput is not inherently a problem, if the sample volume requirements are small. It does, however, slow down processing time and put an upper limit on feasible sample volume, which can be problematic when there are problems getting sufficient material for downstream analyses.

For a detailed overview of these techniques, the reader is referred to the review article by Havers et al.[50] (**Paper V**). A table summarizing the performance, adapted from Havers et al., is provided in Table 1. The acoustic trapping platform developed in **Paper I** operates at several hundred microliters per minute, which is matched only by certain mechanical filtering devices. However, the mechanical filtering device reaching the highest volumetric throughput does not have a mechanism for

eluting EVs, instead cells are grown on top to study EV uptake[51], which makes it unsuitable for other downstream analyses. The field of acoustofluidics and acoustic trapping is explained further in the following chapter.

Table 1: Summary of EV isolation techniques. Reprinted and adapted from[50].

Technique	Separation property	Throughput (µL/min)	Recovery	Purity	Sample type
Ultracentrifugation	Size, density	-	Med	Low	
Precipitation	Size, surface markers	-	High	Low	Plasma, serum, urine
SEC	Size	-	Med	Med	
Mechanical filtering	Size	25 - 1000	Low-High	Med-High	Plasma, urine, cell culture medium
Functionalised surfaces	Surface marker	0.05 - 14	Med	High	Cell culture medium, urine, serum, plasma
Hydrodynamic focusing	Size	4.5 - 23	Med	Med	Plasma, cell culture medium
DLD	Size	< 15	Med	Low	Purified urine exosomes, serum, urine
Viscoelastic separation	Size	3	Med	Low	Purified cell culture media EVs
Acoustophoresis	Size, density, compressibility	0.1 - 500	Low-High	Med	Whole blood, plasma, urine, cell culture medium
Magnetophoresis	Surface marker	0.8 - 3	Med-High	High	Whole blood, plasma, cell culture medium, urine
Dielectrophoresis	Size, charge	3	Med-High	Med	Purified EVs

3. Acoustofluidics

In 1866, August Kundt gave the first report of using acoustic standing waves as a means of manipulating particles[52]. He noted that dust in a tube collected at certain locations in the tube when sound was applied, and by changing the frequency of the sound, it was possible to move the particles to specific locations in the tube. Likewise, it is possible to use acoustic standing waves in microfluidic channels to manipulate particles, a practice referred to as acoustofluidics. Interest in acoustofluidics has grown thanks to its promising potential in lab-on-a-chip devices and biomedical research. A series of 23 papers outlining the field, theories and experiments was published by the Royal Society of Chemistry, and the series was later compiled and summarized as a book in 2015[53]. This chapter aims to explain acoustofluidic concepts and relate them to acoustic trapping.

3.1 Standing Waves

Sound waves are mechanical waves that propagate through a medium. When a sound wave coincides with another wave, the two waves will be superimposed. If the waves have the same frequency and amplitude, a standing wave will form. One way to generate two matching sound waves is to include a reflecting layer in an acoustic device. When a sound wave meets with a medium of different acoustic contrast, part of the wave will be reflected, and part of the wave will be transmitted. The ratio between the reflected wave and the incident wave depends on the difference in acoustic impedance between the media, and is given by

$$\frac{p_r}{p_i} = \frac{z_2 - z_1}{z_2 + z_1}$$

$$z = \rho c$$

Where p_r and p_i are the pressure amplitudes of the reflected and incident waves respectively, z_1 and z_2 are the acoustic impedances of the two different media, ρ is the density and c is the speed of sound in the medium. If there is a large difference in acoustic impedance, most of the acoustic wave will be reflected. Gases, such as air, typically have much lower acoustic impedance than solids, and so very little of the acoustic energy is lost to the surrounding air. This is utilized by including a layer of air underneath the ultrasonic transducer when designing acoustic trapping devices and is discussed further in the next chapter.

A standing wave is not moving in any direction, rather points along the standing wave will experience a constant fluctuation in the pressure field. The areas in the standing wave with the highest pressure amplitude are referred to as the pressure antinodes, and the areas with lowest pressure amplitude are referred to as the pressure nodes.

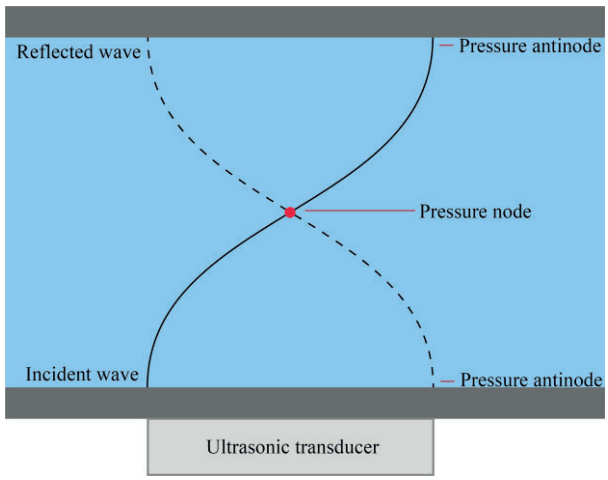

Figure 5: *A standing wave is formed inside a channel when the reflected wave interferes with the incident wave, generating pressure nodes and antinodes.*

3.2 Primary Acoustic Radiation Force

Particles suspended in an acoustic field will experience acoustic radiation forces as a result of sound scattering off the particle. The first analysis of particles in acoustic fields was done by King in 1934[54]. Later, Yosioka and Kawasima expanded the

work to include compressible particles[55]. Their work was summarized and generalized by Gor'kov, describing an acoustic potential based on the monopole and dipole scattering coefficients[56]. The primary radiation force of a plane standing wave on a particle much smaller than the wavelength is the result of a gradient in the acoustic potential U_{rad}, and is given by[57]

$$F_{rad} = -\nabla U_{rad}$$
$$U_{rad} = \frac{4\pi}{3}a^3\left[f_1\frac{1}{2}\kappa_0 p_{in}^2 - f_2\frac{3}{4}\rho_0 v_{in}^2\right]$$
$$f_1(\tilde{\kappa}) = 1 - \tilde{\kappa} \quad \text{and} \quad \tilde{\kappa} = \frac{\kappa_p}{\kappa_0}$$
$$f_2(\tilde{\rho}) = \frac{2(\tilde{\rho}-1)}{2\rho+1} \text{ and } \quad \tilde{\rho} = \frac{\rho_p}{\rho_0}$$

Where a is the radius of the particle, $f_1$is the monopole scattering coefficient, f_2 is the dipole scattering coefficient, κ_0 and κ_p are the compressibilities of the medium and particle, respectively, p_{in} and v_{in} are the pressure and velocity field time averages, and ρ_0 and ρ_p are the densities of the medium and particle respectively.

The direction of the radiation force will be dependent on the particle's density and compressibility in relation to the surrounding medium. We can introduce the acoustic contrast factor Φ to predict whether a given particle will migrate to the pressure node or the antinode. For a 1D planar wave, the acoustic contrast factor can be expressed as[57]

$$\Phi(\tilde{\kappa}, \tilde{\rho}) = \frac{1}{3}\left[\frac{5\tilde{\rho} - 2}{2\tilde{\rho} + 1} - \tilde{\kappa}\right]$$

If the acoustic contrast has a positive value, the particle will migrate to the pressure node, and if it is negative, the particle will migrate to the antinode. Cells, EVs, polystyrene and silica particles typically have positive acoustic contrast in aqueous solutions, and so move towards the pressure node. Lipid particles typically have negative acoustic contrast and move towards the pressure antinode.

If the sound field is localized, which is common practice for acoustic trapping devices, the particles will also experience a lateral radiation force as part of the primary radiation force. This arises from the fact that the sound field has the highest

energy density above the transducer, and the energy density diminishes rapidly outside the transducer region[58]. The radiation force in the lateral direction is responsible for retaining particles against a flow, thus enabling particles to be held in place over the transducer. In an acoustic trap, particles with positive acoustic contrast will migrate to and be held in the pressure node of the standing wave. In the pressure node (z = 0), there is no pressure variation and so the monopole scattering coefficient will not contribute to the radiation force, and the retention force F_r on a particle in the direction x of fluid flow, can be expressed as[59]

$$F_r = -\frac{4\pi}{3}a^3\left[f_2\frac{3p_0^2}{4\omega^2\rho_0}\mathrm{k_x}\mathrm{k_z^2}\cos(\mathrm{k}_x x)\sin(\mathrm{k}_x x)\right]$$

Where ω is the angular frequency and k is the wavenumber. In the pressure node, only the dipole scattering coefficient will contribute to the retention force. Therefore, the particle density in relation to the surrounding medium will determine if a particle can be retained or not. By tuning the density of the medium, it is possible to achieve selective trapping of particles[59]. Since the dipole scattering coefficient is dependent on the density ratio between the particle and the medium, dense particles, such as silica, will experience a much higher retention force than less dense particles, such as polystyrene, and can therefore tolerate much higher drag forces before being carried away with the flow[60].

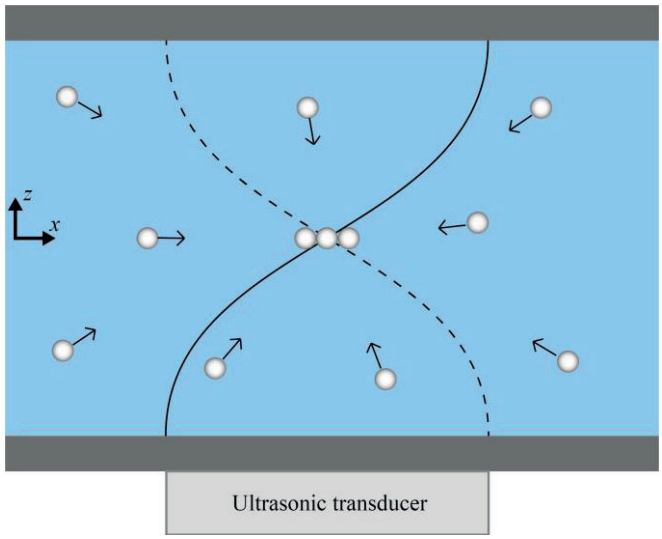

Figure 6: *Primary radiation force on particles in an acoustic standing wave. Particles with positive acoustic contrast experience force both vertically towards the pressure node and horizontally towards where the acoustic field is strongest.*

3.3 Secondary Acoustic Radiation Force

Particles in suspension in an acoustic field will not only experience a primary radiation force, but also a secondary radiation force that arises from sound scattering between particles in suspension. These interparticle forces are sometimes referred to as Bjerknes forces, after his pioneering work studying the force between a pair of bubbles[61]. The interparticle forces were further studied by Crum[62], Weiser et al.[63] and Groschl[64]. More recently, Silva et al. presented a solution to the secondary radiation force[65]. The interparticle force between two spheres will depend on their monopole and dipole scattering coefficients, their sizes, and the angle between the particles in relation to the incoming acoustic wave. However, by only considering particles very close to the pressure node, and angle of $\pi/2$, which is likely for particles held in an acoustic trap, the interparticle force, F_{IP}, can be simplified to[66]

$$F_{IP} = -\frac{6\pi a_s^3 a_p^3 E_{ac} f_{s2} f_{p2}}{d^4}$$

Where a_s and a_p are the radii of the source and probe particle respectively, E_{ac} is the acoustic energy density, f_{s2} and f_{p2} are the dipole scattering coefficients for the source and probe particle respectively, and d is the interparticle distance. What this expression tells us is that the interparticle force is highly dependent on the distance between particles, and so is only significant when particles are very close together.

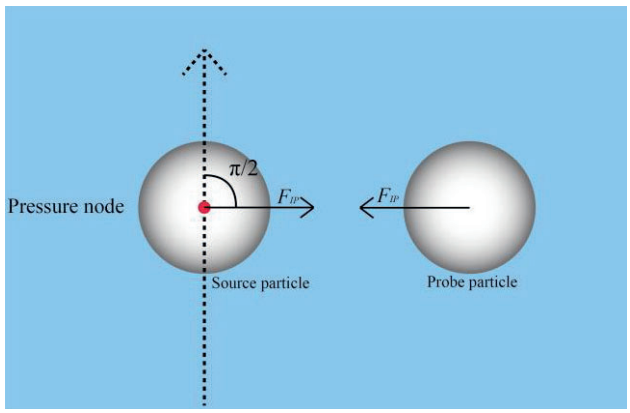

Figure 7: *Interparticle radiation forces on two particles perpendicular to the direction of sound propagation, in the pressure node of an acoustic standing wave.*

3.4 Acoustic Streaming

The acoustic field will not only create forces on the particles in suspension, but also the media itself. These forces result in streaming rolls across different length scales in the fluidic channel. Classically, three different streaming rolls have been described: Schlichting, Rayleigh and Eckart streaming. Schlichting streaming is submicron flows within the viscous boundary layer[67], and arises from dissipation of energy in the viscous boundary layer as flow velocity goes to zero at the no-slip boundary. Rayleigh streaming is wavelength scale rolls[68], and is driven by Schlichting streaming. Eckart streaming is container scale rolls[69] and arises from dissipation of acoustic energy in the bulk of the medium, inducing a fluid jet from the transducer region[70].

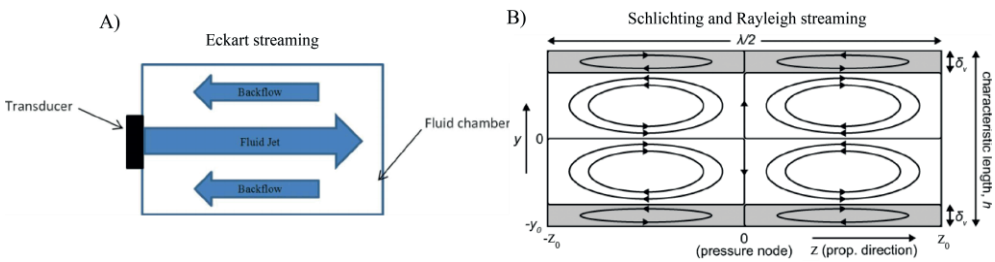

Figure 8: *Representation of streaming in acoustofluidic systems. A) Eckart streaming arising from a fluid jet created by the dissipation of acoustic energy in the medium. B) Schlichting streaming (grey region) in a viscous boundary layer of thickness δ_v and Rayleigh streaming (white region) outside the viscous boundary layer. Adapted from [70] with permission from the Royal Society of Chemistry.*

In addition to the acoustically driven streaming, thermal streaming also occurs when heat dissipates from the ultrasonic transducer into the fluidic channel. Streaming arising from a temperature gradient in the channel has been shown to have a large impact on streaming velocity[71]. Thermal effects have also been shown to influence streaming patterns qualitatively and drive a transition from boundary driven to bulk driven streaming[72]. In the case of a conventional acoustic trap with a single pressure node, the temperature gradient from the transducer results in four streaming rolls horizontally over the transducer[73], Figure 9. Particles that are below a critical size will follow the streaming fluid motion and not focus to the pressure node, which is discussed further in the next chapter.

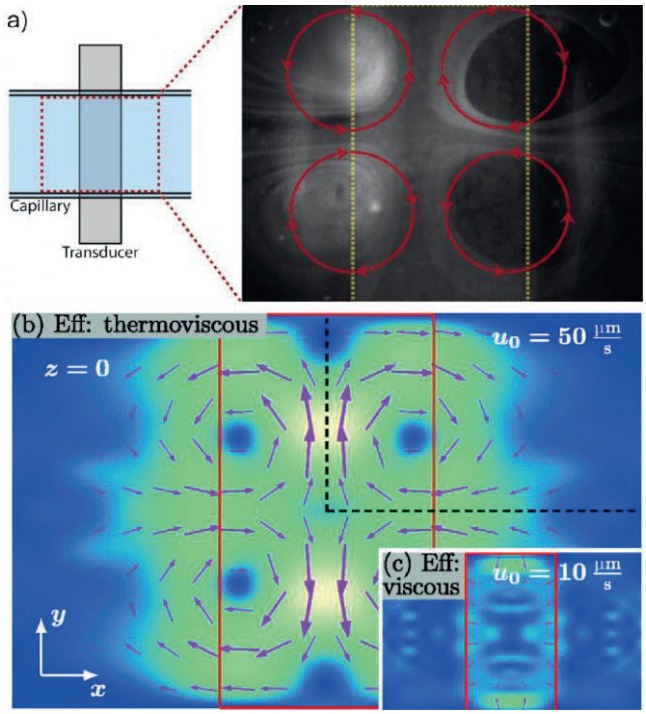

Figure 9: *Thermoviscous streaming over an ultrasonic transducer in an acoustic trapping capillary. A) Acoustic streaming pattern in an acoustic trap, visualized with 490 nm particles. Four streaming rolls are present over the transducer area (outlined in yellow). Figure adapted from [74] with permission from the Royal Society of Chemistry. B) Modelled streaming velocities in the plane of the pressure node when considering both thermal and viscous effects. C) Streaming velocities in the plane of the pressure node considering only viscous effects. The simulated velocity is much lower when disregarding thermal effects. Adapted with permission from [73]. Copyright 2021, Acoustical Society of America.*

3.5 Acoustic Trapping

In acoustic trapping, a localized standing ultrasonic wave is generated inside a fluidic channel. Particles that are denser and less compressible than the surrounding fluid in the vicinity of the trap will migrate to the pressure node where they can be retained against flow. In this way, particles and cells can be enriched in the acoustic field[75]. Since the particles are held in place, it is possible to perform washing and cell staining by switching the buffer that flows past the trapped cluster[76–78]. Acoustic trapping has been shown to be gentle to cells, and it is even possible to culture cells while they are suspended in the trap[78].

There is however a limit to how small particles it is possible to capture in an acoustic trap. This is because the radiation force on a particle scales with the volume of the particle, whereas the fluidic drag force scales with the radius of the particle. As particle size decreases, the radiation force decreases faster than the drag force and at a certain size, particles will be carried along the streaming vortices and not collect into a particle cluster in the pressure node. The cut-off size for streaming dominated motion varies between systems but typically occurs around 2 μm for water-based systems and frequencies in the low MHz range[79]. However, by pre-loading the trap with larger particles, referred to as seed particles, it is possible to circumvent the size limit, which was first demonstrated by Hammarström et al.[74]. Since then, seed-particle enabled acoustic trapping has been used to capture sub-micron particles such as bacteria and extracellular vesicles from plasma, urine, cell culture medium and CSF [18,47,74,80–83]. It has also been integrated with downstream analyses such as RNA analysis and mass spectrometry based proteomics, demonstrating the usefulness of acoustic trapping in biological studies[48,49,81,82,84,85]. It is currently not fully understood to which extent the nanoparticle trapping observed in a seed particle cluster is due to interparticle forces or hydrodynamic effects around the seed particles, but most likely, both effects play a role.

Acoustic trapping has many benefits as an EV isolation tool, such as gentle forces, few manual steps, and ability to handle small sample volumes, which is important as it enables the use of bio banked samples and does not consume large amounts of precious sample. However, acoustic trapping is a non-specific technique, isolating EVs from the entire population in the sample, which can limit its use in studies on specific EVs. **Paper IV** combines acoustic trapping with immunoaffinity based isolation, by using functionalized beads as seed particles, to allow for isolation of subpopulations of EVs. Additionally, the throughput and capacity of acoustic traps

can be limiting when it is needed to process larger, more dilute samples, such as urine. This may lead to multiple trapping runs being pooled to achieve sufficient signal[18], which slows down sample preparation and limits the usability of acoustic trapping. In **Paper I**, a new acoustic trapping platform designed for higher throughput and capacity was developed, and it is described in more detail in the following chapter.

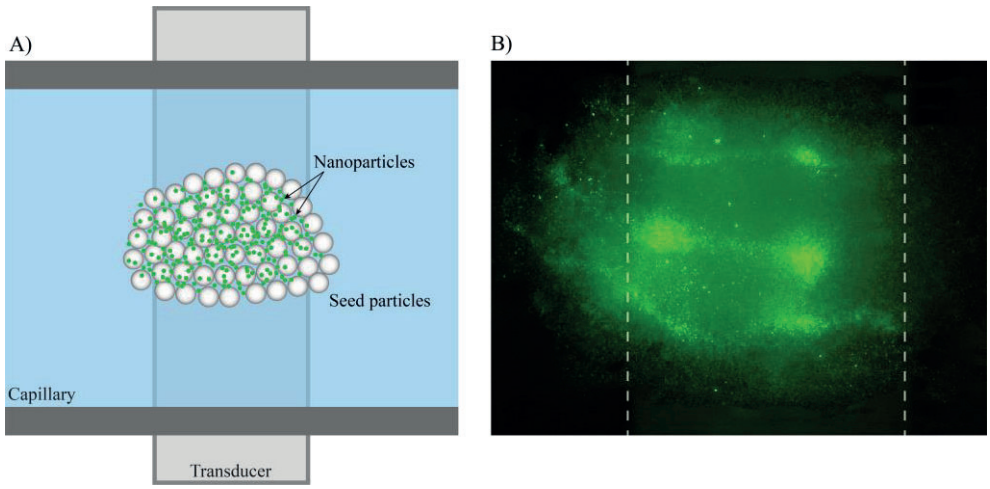

Figure 10: *A) Schematic of acoustic seed particle trapping of nanoparticles. Large seed particles are held in place in an acoustic standing wave over a transducer. Green nanoparticles are enriched in the seed particle cluster. B) Fluorescence image of acoustic seed particle trapping. Green fluorescent nanoparticles (500 nm) are enriched in a cluster of seed particles (12 µm). White dashed lines indicate the transducer area.*

4. The Multinode Acoustic Trap

The multinode acoustic trap (MAT) is a scaled-up version of an acoustic trap, designed for increased throughput and capacity. It comprises a glass capillary that has a cross-sectional area 20 times larger than previous single-node systems. Additionally, it is actuated to generate ten pressure nodes along the height of the channel, instead of one in single node systems. The multiple trapping clusters in the MAT increases the maximum capacity of the trap, and the increased area of the channel allows for higher volumetric throughput while keeping the drag force on the trapped particles lower than the acoustic retention force. This significantly shortens processing time when using the MAT. In **Paper I**, it was shown that MAT has 40 times higher seed particle capacity, as compared to conventional single-node systems. Additionally, standard operating flowrate for EV isolation in the MAT is 500 µL/min, which can be compared to the standard operating flowrate of 15 µL/min for single-node systems. Although recent advancements with silica seed particles have shown a significant improvement in throughput for single-node systems[60], the increased capacity in the MAT allows for more sample to be processed before the trap saturates, which is particularly useful when more biological material is needed for downstream analyses. The increased flow rate also makes it feasible to process larger volumes in the MAT, widening the range of applications that the technology can be used for.

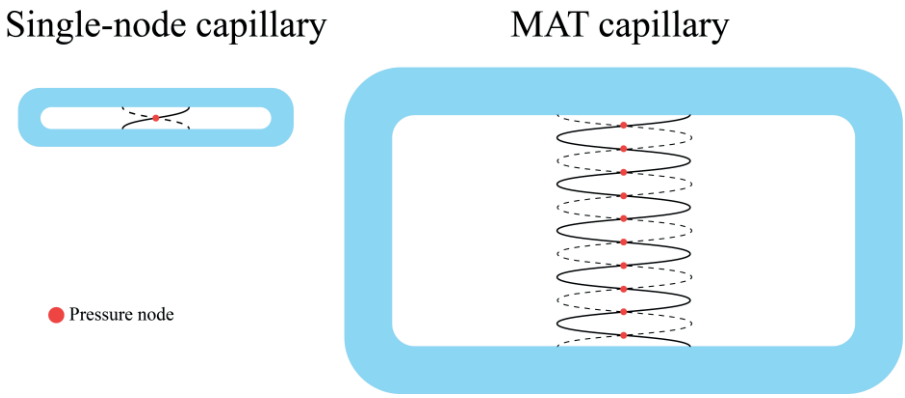

Figure 11: *Size comparison of cross section of a MAT and a conventional single-node trapping capillary. The standing wave in the MAT generates 10 pressure nodes where particles can be retained, as compared to one for single-node capillary.*

4.1 Design and Fabrication

The MAT consists of a borosilicate glass capillary (4 x 2 x 50 mm^3) mounted on a piezoelectric transducer (pz26) (2 x 7 x 0.4 mm^3) with UV-curing glue. The transducer in turn is soldered to the circuit board over a layer of air backing. The air backing provides a high mismatch in acoustic impedance, reflecting energy back into the transducer and minimizing energy dissipating into the circuit board. The capillary is further secured by gluing directly to the circuit board. This is important, since otherwise the only joint fastening the capillary in place would be the soldering joints between the transducer and circuit board, which are easy to break when handling the device. Additionally, the glue serves to dampen the acoustic field outside the transducer region, making it easier to collect particles in a single cluster above the transducer, and not collect in acoustic hotspots axially throughout the capillary. The transducer is diced from a larger piezoceramic plate and kerfed 9 times in the length direction. Kerfing the transducer has shown to improve performance through the suppression of lateral resonance modes[86], which assists in achieving an efficient resonator[87,88]. Heat-shrink tubing is used to connect to the capillary and a Luer-lock allows for easy integration with other fluidic components. A temperature sensor (PT1000) is glued next to the transducer to allow for monitoring the temperature during operation, which is especially important when handling biological samples, Figure 12.

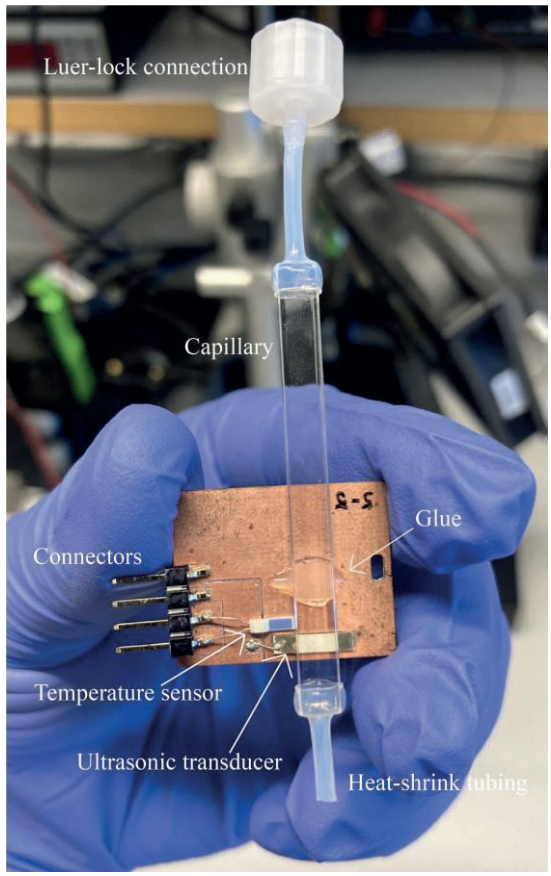

Figure 12: *Picture of a MAT. A glass capillary is mounted on a transducer. The transducer is actuated by a function generator, allowing control of the sound field above the transducer.*

During operation, the MAT is actuated with a function generator, allowing control of the sound field in the device. To retain a stable particle cluster, it is important that the transducer is actuated at the resonance frequency of the fluidic capillary. The resonance frequency will change depending on the buffer in the capillary, the temperature, and how many seed particles are being held in the field. It is therefore necessary to monitor the resonance frequency and update the actuation frequency accordingly. This is done through a tracking software developed by Hammarström et al.[86]. The frequency is periodically swept in a small range around the previous actuation frequency and the power is recorded. The actuation frequency is then set to where the maximum power was recorded, until the next frequency sweep is made. This allows for continuous and stable operation, even when biological samples such as plasma enter the trapping region.

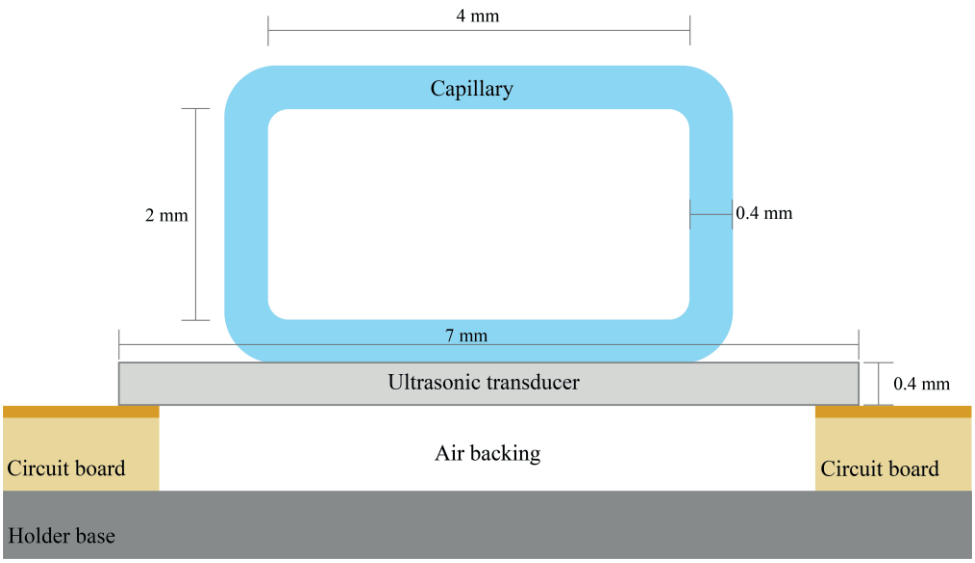

Figure 13: *Schematic cross section of the MAT over the transducer area.*

4.2 Extracellular Vesicle Isolation

A standard EV isolation protocol starts with loading polystyrene seed particles into the trap. Excess seed particles are then washed away and the biological sample containing EVs is loaded into the trap and EVs collect in the seed particle clusters. The supernatant is then washed away with clean buffer, while the EVs remain held in place in the trap. The sound is then turned off and the enriched and washed EVs can be eluted and collected together with the seed particles.

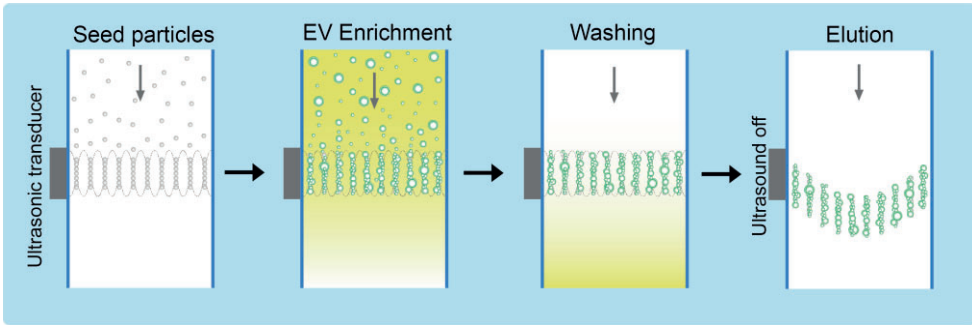

Figure 14: *Illustration of EV isolation procedure using MAT. Seed particles are first loaded into the trap. Sample containing EVs is then allowed to flow through the trap, where EVs will be enriched in the seed particle clusters. The EVs are then washed with clean buffer to remove the supernatant and proteins not associated with EVs. Finally, the sound is turned off and the EVs eluted.*

The elution volume can be reduced by letting the seed particle cluster sediment closer to the end of the tube, before being dispensed, thus reducing the volume needed to flush out the cluster. A sedimentation time of 10-15 seconds is usually enough for most particles to reach the end of the tubing. This is particularly useful when a high concentration of EVs is needed, such as for the immunoblot studies in **Paper II**, where the elution volume was reduced from 130 µL to 25 µL.

5. Proteomics

The term “proteome” was first coined by Marc Wilkins[89] as an analogue for the genome. The proteome refers to the complete set of proteins, including post-translational modifications found in an organism at a given time. Proteins drive the fundamental biology of organisms, and an understanding of protein functions and interactions is therefore crucial for understanding biology. Proteins are often studied at an individual level, which provides valuable information of the function of a specific protein. However, since proteins in an organism are involved in many interactions with other proteins, isolating proteins outside the organism may miss important interactions. A more holistic understanding can be gained by studying changes in the proteome. This could be especially valuable when trying to elucidate complex processes, such as the pathophysiology during sepsis.

5.1 Mass Spectrometry Based Proteomics

One way to measure the proteome is by mass spectrometry (MS), which is a technique for measuring the mass-to-charge ratio (m/z) of ions. Molecules, such as peptides, are ionized and accelerated in an electric field. The velocity of the ions will depend on their m/z, allowing for separation of ions based on their m/z. This in turn generates an m/z spectrum, which can be used to analyze the ions that entered the mass spectrometer. In the last decades, MS has emerged as a powerful tool for analyzing proteins samples[90]. MS can be split into two main categories, top-down and bottom-up. Top-down refers to the study of intact proteins, while bottom-up refers to the study of proteins digested into peptides. It could be assumed that measuring intact proteins would be preferable when analyzing a protein sample. However, there are several issues with measuring intact proteins. For example, proteins are large and complex molecules, making them harder to separate on a chromatographic column. Intact proteins are more difficult to ionize evenly in the mass spectrometer and they generate highly complex spectra, making data analysis harder. Additionally, the high molecular weight of proteins makes it more difficult

to accurately measure them, as instruments often perform better at measuring smaller units. As a result, bottom-up proteomics has become the most commonly used method for complex samples. For all studies in this thesis, bottom-up proteomics through liquid chromatography tandem mass spectrometry (LC-MS/MS) has been used.

5.1.1 Preparing Protein Samples Before Entering the Mass Spectrometer

Before entering the mass spectrometer, the proteins in a sample are first cleaved into peptides by enzymatic digestion. A common enzyme to use for this end is trypsin, as it generates easily ionized peptides of a suitable length. Trypsin has been used for protein digestion throughout all studies in this thesis. After digestion, the peptides are separated on a reverse phase liquid chromatography (RP-LC) column, coupled directly to the mass spectrometer. Peptides are loaded on the column and subsequently eluted based on the hydrophobicity of the peptides by perfusing the column with a gradient of hydrophilic/hydrophobic solvent[91]. The separation has two main benefits. First, it reduces the number of analytes entering the MS at any given time. Second, the retention time on the column provides information about the hydrophobicity of the peptide which may aid in its identification. Once the peptides reach the end of the column, they are ionized using electrospray ionization (ESI), a technique which received the Nobel prize in chemistry 2002[92]. Finally, the ionized peptides enter the mass spectrometer where their m/z is measured. The peptides can be measured using data-dependent acquisition or data-independent acquisition, which are outlined below.

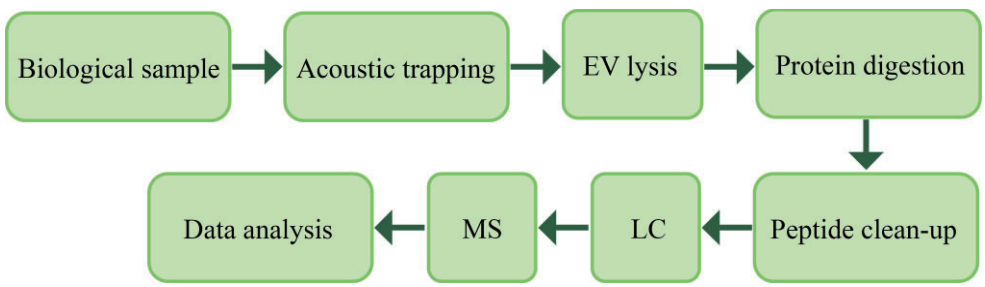

Figure 15: *Flow chart of the main sample processing steps for MS analysis used throughout this thesis.*

5.1.2 Data-dependent Acquisition

In data-dependent acquisition (DDA), also known as shotgun MS, the injected peptides are scanned by the mass analyzer in full scans (MS1). However, the MS1 spectrum is not sufficient for confident identification of a peptide sequence, as there are usually many possible amino acid combinations for each detected m/z peak. Therefore, it is necessary to further fragment the peptides and measure m/z of the fragments, generating an MS2 spectrum. Fragmentation is done in a collision cell, where the sample is collided with an inert gas, a process known as higher-energy collisional dissociation (HCD)[93]. In DDA, the top number of precursor ions (typically 15) detected for a given MS1 scan will be selected for fragmentation and MS2 acquisition. Peptide detection in DDA is therefore relatively stochastic and there is a chance that low abundant ions will not be detected. It also makes quantification more difficult. The acquired spectra are compared against an in-silico digestion of a FASTA file to generate possible peptide sequences. A FASTA file is a text-based format to store biological sequence data, such as amino-acid sequences of proteins. Any protein sequence present in the FASTA file can therefore be digested in-silico and theoretically detected. In order to assess the false discovery rate (FDR), a decoy sequence is also included, which typically consists of the peptides sequences in reverse. If a peptide from the decoy sequence is detected, it is known to be a false positive. By counting the number of peptides from the decoy sequence that are detected and comparing it to the number of peptides detected with the original sequence, the FDR can be estimated[94].

5.1.3 Data-independent Acquisition

Data-independent acquisition (DIA) is a technique designed to provide more comprehensive and unbiased analyses of complex biological samples[95]. In DIA, all peptides are fragmented, collecting data on all detectable peptides. This can be done through the selection of a mass window, typically around 25 m/z, and fragmenting all precursor ions within this mass range to create MS2 spectra for all ions[96]. The mass window then shifts sequentially to cover a pre-determined mass range e.g. 400 – 1200 m/z, often with a small overlap between windows. In this way the entire mass range is scanned systematically, and all ions fragmented. The result is a more unbiased detection of peptides and more accurate quantification. DIA generates highly complex MS2 spectra, as it contains spectra from all precursor ions within the mass range, which can make interpretation challenging. Sequential Window

Acquisition of all Theoretical Mass Spectra (SWATH-MS) is a DIA technique that utilizes targeted data analysis to achieve higher reproducibility and quantification accuracy from DIA data[97]. This is done through the use of a pre-recorded spectral library, which contains fragmentation patterns for peptides[98]. Spectral libraries are traditionally generated from the ion spectra of multiple DDA runs. The spectral library can then be used to deconvolute information from a DIA run. The implication is then that a peptide must first be detected using DDA to be included in a spectral library, before the peptide can be measured using DIA. This could be an issue if certain peptides are in low abundance or otherwise difficult to measure using DDA. However, deep learning algorithms have recently been used to predict spectral libraries from a FASTA file, removing the need for DDA runs to create spectral libraries. These predicted libraries have been shown to perform as well as experimentally validated libraries[99–101]. This also comes with the added benefit of being able to detect any peptide belonging to a protein provided in the FASTA file, at least theoretically.

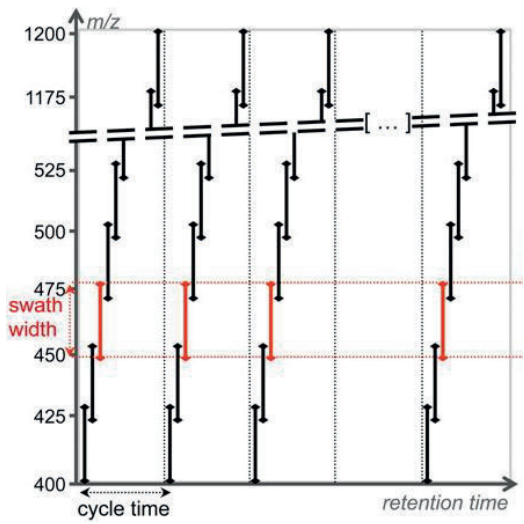

Figure 16: *Overview of the SWATH-MS method. All precursors with m/z within the given isolation window will be fragmented. The isolation window is systematically swept across the entire mass range. Reprinted from Gillet et al. 2012*[97].

6. Sepsis

Sepsis is defined as a life-threatening condition caused by a dysregulated host response to infection leading to organ dysfunction[102]. It is currently a major cause of mortality and is estimated to contribute to 19% of deaths worldwide[103]. Sepsis can be caused by a variety of different pathogens[104], among them gram-negative bacteria, such as *E. coli*, and gram-positive bacteria, such as *S. pyogenes*. Hallmarks of sepsis include dysregulated systemic inflammation, dysregulated hemostasis and organ damage. Quick diagnosis and treatment are important for improving outcome, with mortality increasing for every hour without treatment[105,106]. The severity of sepsis is assessed using the Sequential Organ Failure Assessment (SOFA) score, which evaluates different organ systems on a 0-4 point scale[102,107]. An increase in the sofa score of 2 or more in the context of an infection indicates sepsis. Calculating a SOFA score relies on several laboratory measurements and can therefore be challenging in an emergency care setting. Over the past four decades, more than 120 treatment trials for sepsis have been unsuccessful[108]. One reason is the heterogenous nature of the condition, caused by the complex and systemic host response. The host response is highly variable and depends on several factors such as pathogen, site of infection, and time elapsed since infection[109,110]. Preclinical studies in infection models have shown that sepsis causes systems-wide changes in the proteome of several organs and cell systems[108]. These changes also depend on the type of treatment administered, in addition to previously mentioned factors[108,111,112]. The variability of the disease, combined with lack of markers to accurately predict if an infection will progress to sepsis or categorize patients into homogeneous subgroups, makes performing clinical intervention trials difficult. As a consequence, national efforts have been initiated to coordinate the collection and annotation of clinical samples[113].

6.1 Platelets in Sepsis

Platelets are relatively small (~1.7 μm) cell fragments that are produced by fragmentation of megakaryocytes[114,115]. They circulate the blood stream in numbers between 150 000 to 400 000 per μL[116], and one of their main functions is to maintain hemostasis by preventing bleeding in case of vascular damage. In addition to hemostasis, platelets also play a role in inflammation and immune response and are therefore key players during sepsis. For example, platelets bind lipopolysaccharide (LPS) from gram negative bacteria such as *E. coli*, and activated platelets can trap bacteria in fibrin-rich clots as well as kill them directly[117–120]. Additionally, platelets can modulate inflammatory response and mediate leukocyte recruitment[121]. The excessive inflammatory response during sepsis mediates systemic activation of the endothelium, increasing vascular permeability and vascular leakage, which result in hypotension and decreased oxygen supply to organs[122]. The activated endothelium promotes systemic platelet activation and aggregation, which can result in disseminated intravascular coagulation (DIC) and the consumption of platelets[123]. The consumption of platelets can lead to low platelet count, known as thrombocytopenia, and is correlated with poor prognosis in sepsis patients[124].

Platelets are a major source of circulating EVs, and studies have shown that platelet-derived microvesicles make up 70-90% of circulating microvesicles[125]. Interestingly, platelet-derived EVs (PEVs) have shown immunomodulatory effects by transfer of bioactive cargo to leukocytes and endothelial cells[126]. Levels of circulating PEVs have also been shown to increase during sepsis[127]. Lower levels of circulating PEVs have been correlated with thrombocytopenia and mortality during sepsis, indicating that PEVs play a protective role during sepsis[128]. In **Paper II** we study PEVs released from platelets activated by either thrombin or bacterial protein to investigate changes in PEV function that might occur during bacterial infection.

6.2 Extracellular Vesicles in Sepsis

Sepsis has been shown to induce large changes in the EV population, which have been associated with inflammation, bacterial clearance, organ damage and apoptosis[10]. The exact role of EVs during sepsis is however complex, with both pro- and anti-inflammatory effects and pro- and anti-apoptotic effects. This indicates that the role of EVs changes throughout the course of sepsis and depends on patient

heterogeneity, pathogen, and what cell type the EV originated from. Therefore, EVs may contain so far unexplored molecular signals relevant for disease progression, that is normally not detectable when analyzing only the raw plasma. Notably, EVs can be extracted from biobanked plasma samples, which allows opportunities to extract new molecular information from already collected samples, which would otherwise be obscured by the large dynamic range in the plasma proteome. To make this feasible, there is a need for EV isolation techniques that are fast, simple, can handle small sample volumes and can be interfaced with proteomics, transcriptomics and metabolomics. Acoustic trapping lends itself as an excellent candidate to fulfill these needs, which is demonstrated in **Paper III**, where acoustic trapping is used to isolate EVs from small volumes of septic mouse plasma. Increasing the understanding of EVs would in turn increase the understanding of the biological processes occurring during sepsis, which may ultimately lead to better treatments and better outcomes for patients.

7. Immuno-acoustic Trapping

Acoustic trapping is a non-specific method and will isolate EVs from the entire population of a sample. Since the majority of circulating EVs in plasma originate from platelets[125], a large portion of the isolated EVs in an acoustic trap will be platelet derived. This might obscure the role of less abundant EVs from different cell types and hinder the study of their role in immune response and disease progression during sepsis. Immunoaffinity based isolation can be used to add specificity to EV isolation. In immunoaffinity isolation, antibodies targeting specific proteins are coupled to large beads or surfaces. EVs possessing the target protein can bind to the antibody and be separated from the rest of the sample[129–131]. This can also be used to isolate EVs originating from a specific cell type, since EVs often express the same surface protein as their parent cell[132].

In **Paper IV**, immunoaffinity isolation is combined with acoustic isolation by using antibody coated particles as seed particles in an acoustic trap, a technique referred to as immuno-acoustic trapping. After isolation of the general EV population in the acoustic trap, EVs that are bound to the antibodies can be separated from non-specific EVs through sedimentation of the seed particles. One trapping run therefore generates two fractions of EVs, one based on antibody isolation, and one based on acoustic isolation. In addition, many positive aspects of the acoustic trap are retained, such as rapid processing, small volume requirements and gentle handling. Immuno-acoustic trapping can therefore be used to isolate specific EVs and facilitate the study of EVs from specific cell types and less abundant EVs. The antibody used for isolation could easily be changed to target a specific marker of interest, allowing researchers to tailor the isolation to their needs. This broadens the possibilities of acoustic trapping as an EV isolation tool and facilitates further studies of EVs.

Conclusions and Outlook

This thesis broadens the application area of acoustic trapping as an EV isolation tool. The higher throughput in the MAT shortens processing times and allows for effective processing of dilute samples. The higher capacity allows for more sample volume to be processed effectively, which is particularly useful for less sensitive assays. The feasibility and usefulness of acoustic trapping as an EV isolation tool is demonstrated in the included papers, through numerous successful downstream analyses. The integration of acoustic trapping with MS-based proteomics demonstrated easy access to the EV proteome, and thus provided information that was not available from the original sample alone. This expands the information that is available from a biological sample by analyzing both the original sample, and the isolated EVs. Additionally, the combination of immunoaffinity-based isolation with acoustic trapping gives the option of specificity in the isolation of EVs. The small volume requirements of acoustic trapping make it suitable for processing biobanked samples, enabling further studies on large cohorts where samples have already been collected.

New insights into the function of EVs provided by advancements in EV isolation techniques may open new research possibilities for complex conditions such as sepsis. This could be achieved through the processing of biobanked plasma samples from sepsis patient cohorts to further map out the effects and the function that EVs play during disease progression. If clinically relevant signals for diagnosis of sepsis and categorization of patients into subgroups can be found in EVs, one could envision a future where acoustic traps are present at emergency departments of hospitals. A plasma sample could then be collected and processed in the acoustic trap to provide access to isolated patient EVs within minutes, allowing earlier diagnosis and saving precious time.

Studies on EVs are of course not limited to sepsis and could be applied to the study of other diseases, such as cancer and Alzheimer's disease, or studying biological processes in healthy organisms. Combined, the results outlined in this thesis will

hopefully facilitate such further studies on EVs and their role in health and disease. Ultimately, this may benefit society by leading to better treatments and outcomes for patients.

Summary of Papers

The papers included in this thesis investigate the development and use of acoustic trapping as a tool for isolating extracellular vesicles. **Paper I** describes the development of the MAT and shows it is suitable for MS analysis. **Paper II** utilizes the MAT to investigate differences in platelet-derived EVs depending on the mode of activation. **Paper III** utilizes the MAT to study EVs during gram-positive and gram-negative sepsis. Finally, **Paper IV** combines the use of immunoaffinity-based isolation with acoustic trapping, to allow specificity in EV isolation in an acoustic trap. This chapter provides a brief summary of the included papers, in chronological order.

Paper I - Multinodal acoustic trapping enables high capacity and high throughput enrichment of extracellular vesicles and microparticles in miRNA and MS proteomics studies

Paper I investigated the feasibility of scaling up an acoustic trapping platform in order to increase capacity and sample throughput. A new acoustic trap, referred to as a Multinode Acoustic Trap (MAT) was fabricated and studies examining its performance were carried out. We demonstrated that the MAT displayed a 40-fold increase in seed particle capacity compared to conventional acoustic trapping systems. We also demonstrated that the trap could enrich 500 nm polystyrene particles at flowrates up to 2000 μL/min. The MAT was then used to isolate EVs from urine samples at 500 μL/min, which can be compared to the typical flowrates of 15-25 μL/min for previous acoustic traps. We demonstrate that the MAT has capacity for enough material for downstream RNA analysis from a single run, and there is no need to pool several trapping runs, as has been done in previous studies. Further, we showed that MS analysis produced clear distinction between the protein content of the isolated EVs and the original urine sample, and that the MAT did not induce large variations in the samples. The MAT could therefore facilitate further research into EVs, by providing a relatively simple and rapid method of isolating EVs from urine.

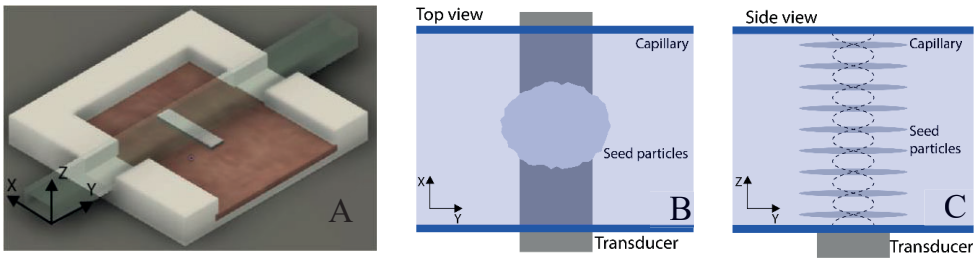

Figure 17: *A) Schematic of the MAT. A glass capillary is glued to an ultrasonic transducer to generate a standing wave inside the capillary. B) Schematic of seed particle clusters in the MAT as viewed from above. C) Schematic of seed particle clusters as viewed from the side. Reprinted from* [82].

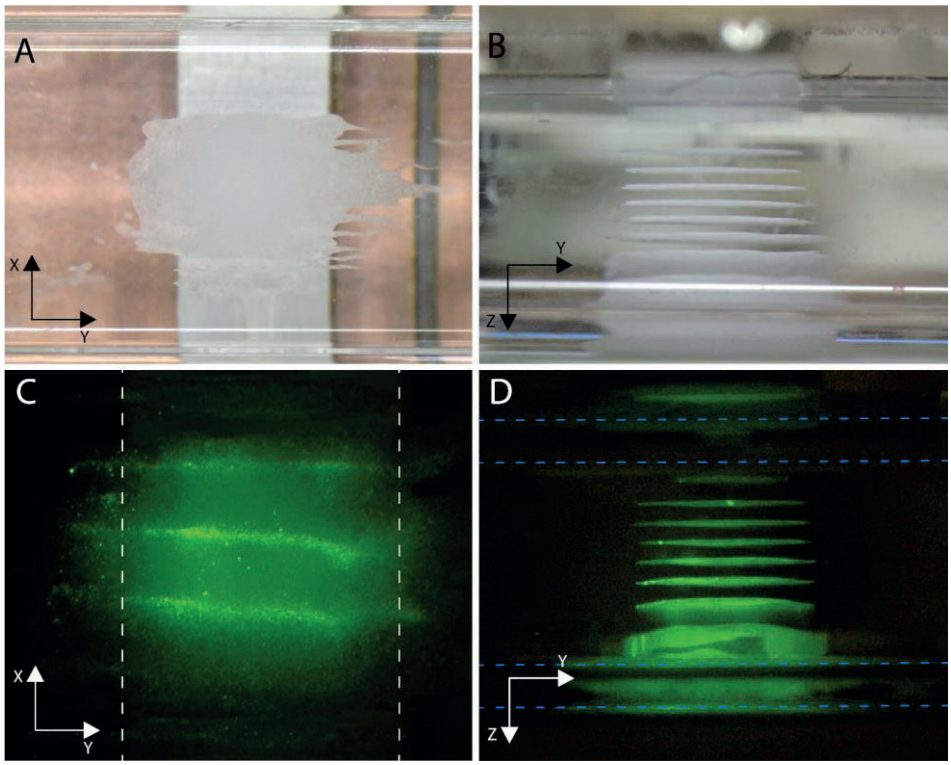

Figure 18: *Photographs of particles in the trap. The seed particles used were 12 µm polystyrene. A) Brightfield image of seed particle clusters viewed from the top. B) Brightfield image of seed particle clusters viewed from the side. C) Fluorescence image of seed particle clusters enriched with 500 nm fluorescent polystyrene particles viewed from top. White dashed lines indicate the transducer area. D) Fluorescence image of seed particle clusters enriched with 500 nm fluorescent polystyrene particles viewed from the side. Blue dashed lines indicate capillary walls. The transducer is at the top of the picture. The curved edges of the capillary make the clusters appear more smeared close to the walls. Reprinted from* [82].

Paper II - Phenotypic characterization of acoustically enriched extracellular vesicles from pathogen activated platelets

In Paper II, platelet derived EVs were isolated from plasma, using the MAT, and characterized. Platelets were stimulated with either thrombin, M1 protein from *S. pyogenes* or negative control (HEPES buffer) to study differences in EVs depending on the mode of platelet activation. The protein content of the EVs was assessed using MS proteomics. It was demonstrated that EVs derived from pathogen-activated platelets contained similar cargo to physiologically activated platelets, both containing platelet membrane proteins, granule proteins, cytoskeletal proteins, coagulation factors and immune mediators. However, complement proteins and IgG3 were significantly enriched in EVs from pathogen-activated platelets. Additionally, bacterial M1 protein was found to adhere to or be packaged within platelet derived EVs and transported with them. This mechanism was previously unknown and could contribute to systemic inflammation and platelet activation observed during infectious diseases such as sepsis. Finally, the acoustically isolated EVs were functionally intact and upon addition to whole blood exhibited pro-inflammatory effects and stimulated formation of platelet-neutrophil complexes, neutrophil activation and cytokine release. Collectively, this revealed novel aspects of pathogen-mediated platelet activation and demonstrated that the MAT was suitable for isolating EVs from plasma samples.

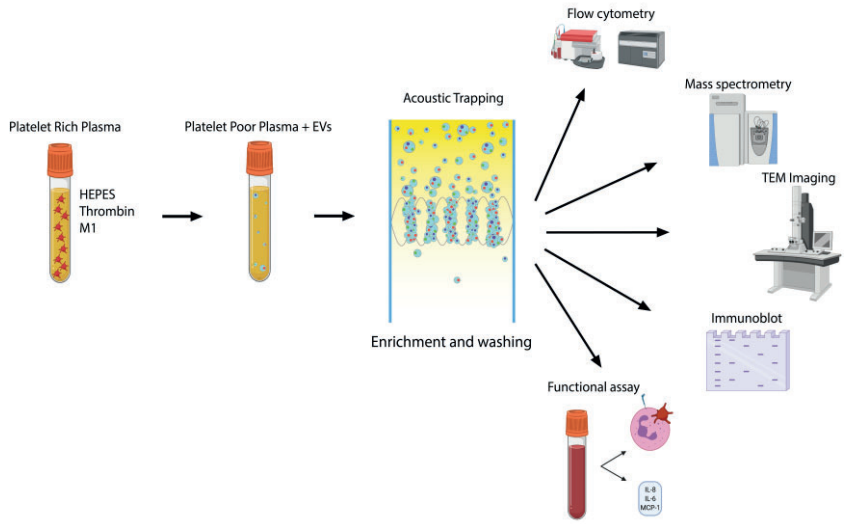

Figure 19: *Illustration of sample processing steps. Platelet rich plasma from healthy donors was stimulated with either HEPES buffer, Thrombin or M1 protein. The platelets were then removed by centrifugation and the released platelet derived EVs were isolated using acoustic trapping. The EVs were analyzed using high-sensitivity flow cytometry, mass spectrometry, transmission electron microscopy (TEM), immunoblots and functional assay by stimulation of whole blood. Reprinted from* [84].

Paper III – Proteomic profiling of acoustically isolated extracellular vesicles from blood plasma during murine bacterial sepsis

In Paper III, the MAT is used to isolate EVs from small volumes of plasma from experimental sepsis mouse models infected with either gram-positive pathogen (*S. pyogenes*) or gram-negative pathogen (*E. coli*). The proteomes of EVs and the plasma are characterized using MS-based proteomics. It was demonstrated that analyzing the EVs expanded the observable proteome in plasma, and that EVs displayed an emphasis on cellular processes and signalling compared to plasma. We showed that systemic bacterial infection altered EV and plasma proteomes differently, with a predominant effect on leukocyte migration in EVs and metabolism in plasma. Additionally, comparing the two bacteria showed a stronger effect on inflammation and neutrophil degranulation in *S. pyogenes* infection and a stronger effect on metabolism in *E. coli* infection. In summary, we show that the MAT gives easy access to the plasma EV proteome, which provides additional information of ongoing biological processes not observed in plasma alone. Additionally, the small volumes required makes it suitable for handling biobanked samples and therefore make use of already collected samples.

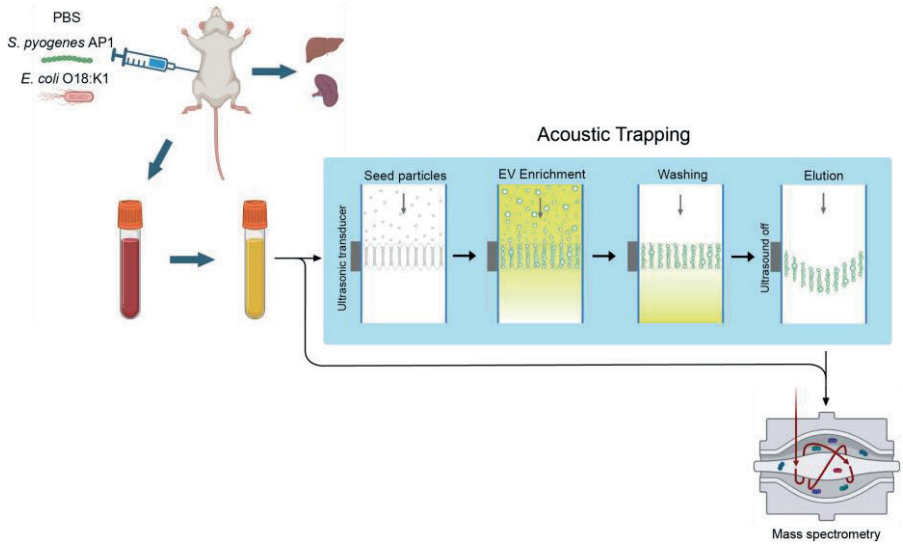

Figure 20: *Illustration of sample collection and processing steps. Mice were infected with S. pyogenes or E. coli, and control mice were administered PBS. 18 hours post infection, mice were sacrificed and blood, liver and spleen collected. EVs were isolated from the plasma using acoustic trapping.*

Paper IV – Immunoaffinity coupled acoustic trapping: Towards extracellular vesicle subpopulation

In paper IV, we investigated the feasibility of combining immunoaffinity-based isolation of EVs with acoustic trapping, in order to enable selective isolation of EVs within an acoustic trap. Silica microparticles were functionalized with anti-CD9, to target the very common EV surface marker CD9. The silica particles were subsequently used as seed particles in an acoustic trap, to isolate EVs from plasma. After elution from the trap, acoustically enriched EVs could be separated from EVs bound to the seed particles through a quick centrifugation. This generated two EV subpopulations, acoustically isolated and immuno-acoustically isolated EVs. Nanoparticle tracking analysis (NTA) confirmed particles in the exosome size range. TEM images showed EVs in both subpopulations, with the immuno-acoustically isolated population containing almost exclusively CD9-positive EVs. Proteomic profiling showed a large overlap in the protein content between the subpopulations. Protein interaction networks of uniquely detected and significantly abundant proteins between the groups showed clear interaction with CD9 in the immuno-acoustically isolated group, and no interaction with CD9 in the acoustically isolated group. Comparing immuno-acoustic isolation with standard immunoaffinity isolation through incubation with functionalized beads showed that the immuno-acoustic group had more and stronger interactions with CD9. Processing in the acoustic trap was performed in 8 minutes, while the functionalized beads were incubated 90 minutes for immunoaffinity isolation. This paper demonstrated that selectivity can be achieved in an acoustic trap through functionalized seed particles, while retaining positive aspects of using acoustic trapping for EV isolation, such as fast processing, small volume requirements, and gentle forces.

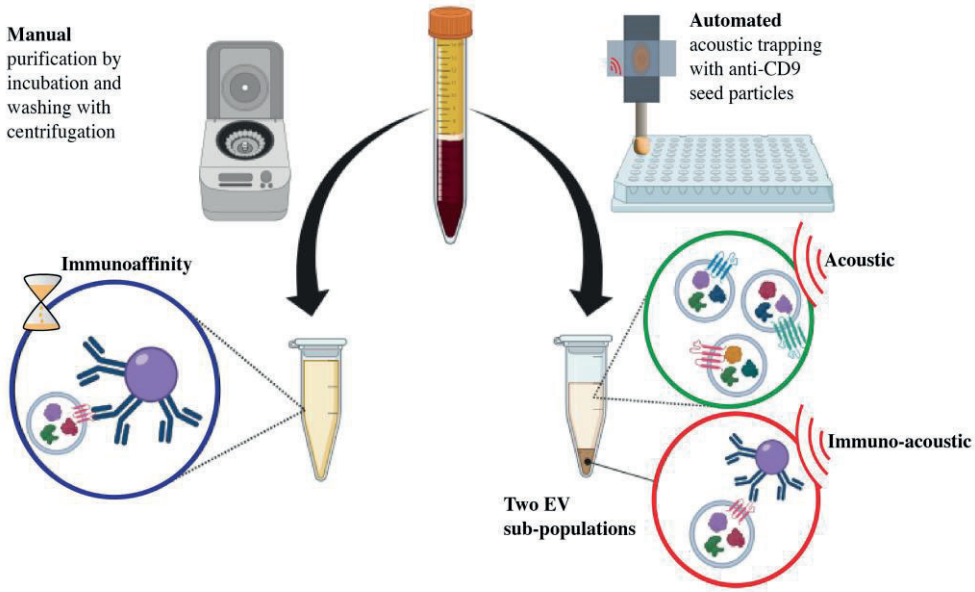

Figure 21: *Illustration of immunoaffinity-based EV isolation methods used. In immunoaffinity isolation, functionalized beads are incubated with a plasma sample and then separated through centrifugation. In immuno-acoustic isolation, functionalized beads are used as seed particles in an acoustic trap. EVs from the entire population are enriched in the acoustic trap, and after elution they can be separated into two subpopulations through sedimentation of the seed particles.*

Acknowledgements

And suddenly this day is here. It's funny how things you know are coming can still sneak up on you. I still remember sitting in Thomas' office and discussing an idea for a MSc project. This has been an incredible journey. I've learned so much and met so many fantastic people, many of whom this thesis would not have happened without.

I would like to express my deep gratitude to my supervisor, **Thomas**, for giving me the chance to join the research group and pursue this project. Thank you for letting me entertain my curiosity and explore things on my own in the lab. Thank you for all your valuable guidance and insights and all the hour-long discussions we've had. Your positivity and unwillingness to give up are inspiring.

I would like to thank my co-supervisor, **Andreas**, for supervising my MSc project that started this whole journey, and his continued supervision during my PhD. Thank you for always being available when I needed assistance or had questions, it has been of great help. You are the cornerstone of the acoustics lab, thank you.

My co-supervisor, **Johan**, thank you for taking me into your group and making me feel welcome in a research setting which I had next to no experience in. Thank you for all valuable discussions about infection and proteomics and always being very encouraging. Your enthusiasm for science and research is truly infectious.

I would like to give a big thank you to **Mikael,** for many discussions on acoustic trapping and teaching me many tricks on how to build acoustic traps. It has been really helpful, thank you.

I would like to express my gratitude to my excellent collaborators who made a lot of the research in this thesis possible. **Megan**, thank you for fantastic collaboration in both the review article and the immuno-acoustic trapping paper. Thank you for sharing some of the joys and woes of acoustic trapping when we were the only people working with it. You have been a great office mate and friend. **Frida**, thank you for excellent collaboration in putting together the paper on platelet EVs. It was really great working with you. **Yosh**, thank you for helping with mouse models in the sepsis paper, and thank you **Oonagh**, for your all your help and insights into platelets, infections and immunology. It has been lovely working with you both.

I would like to thank my colleagues in the acoustics lab at BMC, past and present, for creating such an excellent working environment. My office mates over the years, **Alex**, **Anke**, **Franzi O** and **Eva**, you guys have been great. Thank you for your company and making d1316c the best office in the building. The rest of the acoustics group, **Cecilia**, **Klara**, **Thierry**, **Amal** and **Michael**. It has been wonderful working alongside you. Thank you for good conversations and much needed coffee breaks.

I would also like to thank the brilliant people in the IMP and BioMS groups for being so welcoming and helpful. Thank you, **Anahita**, for showing me around the lab and MS sample preparation for the first time. Thank you for letting me use your lab bench and being an exceptionally helpful person. Thank you to **Lotta H**, for helping a confused PhD student navigate OpenBIS and his first MS-injections. I want to thank **Tommaso** and **CK** for their great work in keeping Minerva and Pythia running. Sorry for the times I clogged the column. Thank you to **Aaron** for discussions on protein quantification and **Erik** for helping me with DPKS. Thank you to **Filip** for assistance with unexpected OpenBIS behaviour. Thank you to **Tirthankar** for discussions on bacterial sepsis and teaching an engineer some biology. **Simon**, thank you for your insights on everything from mass spectrometry to surface chemistry. To **Sounak**, **Ale**, **Di**, **Joel**, **Elizabeth**, **Carlos**, **Marc**, **Lotta W** and anyone I might have missed, thank you for creating a fantastic research environment.

Thank you to my colleagues in the acoustics lab over at BME. Thank you to **Per** and **Pelle**, for introducing me to acoustofluidics in the first place. Thank you, **Wei**, for discussions on modelling and always being incredibly quick to respond. Thank you to **Ola** for wanting to automate everything and making me question the efficiency of my setup. **Qing**, thank you for always being friendly and positive. To the other past and present PhD students, **Mahdi**, **Enrico**, **Richard**, **Franzi M** and **Oskar**, thank you for sharing your research and giving me new insights and perspectives in acoustofluidics.

Thank you to **Ulrika** and **Desirée** for always being friendly and helping with administration. Thank you to **Axel** for teaching me how to use the milling machine and 3D printer, and **Martin** for lessons in dicing saw and clean room fabrication.

I would also like to express gratitude towards my collaborators over at DTU, although unfortunately none of these projects made it into this thesis. Thank you, **William** and **Henrik**, for all your modelling of acoustic trapping capillaries. Thank you **Ada-Ioana** and **Radu** for your efforts in fabricating 3D structures inside capillaries. It is a shame they did not function as we had hoped.

Lastly, my family, **Malin**, **Fredrik**, **Erik**, **Finn**, **Marita**, **Loke** and **Leo**, thank you for being a wonderful and supportive family. I love you guys so much. To my second family, **Salam**, **Manal** and **Dahlia**, thank you for always being there and supporting us. To my daughter, **Mira**, thank you for putting everything in life in perspective. You are amazing in the truest sense of the word. Finally, **Nora**, my partner-in-life, thank you for everything. Every challenge is easier with you by my side. I love you.

References

1. Colombo, M., Raposo, G. & Théry, C. Biogenesis, secretion, and intercellular interactions of exosomes and other extracellular vesicles. *Annual review of cell and developmental biology* vol. 30 255–289 Preprint at https://doi.org/10.1146/annurev-cellbio-101512-122326 (2014).
2. Couch, Y. *et al.* A brief history of nearly EV-erything-The rise and rise of extracellular vesicles. *J. Extracell. Vesicles* (2021) doi:10.1002/jev2.12144.
3. Raposo, G. & Stoorvogel, W. Extracellular vesicles: Exosomes, microvesicles, and friends. *Journal of Cell Biology* vol. 200 373–383 Preprint at https://doi.org/10.1083/jcb.201211138 (2013).
4. Alzahrani, F. A. & Saadeldin, I. M. *Role of Exosomes in Biological Communication Systems*. *Role of Exosomes in Biological Communication Systems* (Springer Singapore, 2021). doi:10.1007/978-981-15-6599-1.
5. Welsh, J. A. *et al.* Minimal information for studies of extracellular vesicles (MISEV2023): From basic to advanced approaches. *J Extracell Vesicles* **13**, (2024).
6. Contreras-Naranjo, J. C., Wu, H. J. & Ugaz, V. M. Microfluidics for exosome isolation and analysis: Enabling liquid biopsy for personalized medicine. *Lab on a Chip* vol. 17 3558–3577 Preprint at https://doi.org/10.1039/c7lc00592j (2017).
7. Li, G., Tang, W. & Yang, F. Cancer Liquid Biopsy Using Integrated Microfluidic Exosome Analysis Platforms. *Biotechnol J* **15**, (2020).
8. Asleh, K. *et al.* Extracellular vesicle-based liquid biopsy biomarkers and their application in precision immuno-oncology. *Biomarker Research* vol. 11 Preprint at https://doi.org/10.1186/s40364-023-00540-2 (2023).
9. Buzas, E. I. The roles of extracellular vesicles in the immune system. *Nature Reviews Immunology* vol. 23 236–250 Preprint at https://doi.org/10.1038/s41577-022-00763-8 (2023).
10. Burgelman, M., Vandendriessche, C. & Vandenbroucke, R. E. Extracellular Vesicles: A Double-Edged Sword in Sepsis. *Pharmaceuticals* **14**, (2021).

11. Vlassov, A. V., Magdaleno, S., Setterquist, R. & Conrad, R. Exosomes: Current knowledge of their composition, biological functions, and diagnostic and therapeutic potentials. *Biochimica et Biophysica Acta - General Subjects* vol. 1820 940–948 Preprint at https://doi.org/10.1016/j.bbagen.2012.03.017 (2012).

12. Erdbrügger, U. *et al.* Urinary extracellular vesicles: A position paper by the Urine Task Force of the International Society for Extracellular Vesicles. *J Extracell Vesicles* **10**, (2021).

13. Xing, Y. *et al.* Analysis of extracellular vesicles as emerging theranostic nanoplatforms. *Coord Chem Rev* (2020).

14. Viaud, S. *et al.* Dendritic Cell-Derived Exosomes for Cancer Immunotherapy: What's Next? *Cancer Res* **70**, (2010).

15. Escudier, B. *et al.* Vaccination of metastatic melanoma patients with autologous dendritic cell (DC) derived-exosomes: Results of the first phase 1 clinical trial. *J Transl Med* **3**, (2005).

16. Witwer, K. W. *et al.* Standardization of sample collection, isolation and analysis methods in extracellular vesicle research. *J. Extracell. Vesicles* **2**, (2013).

17. Linares, R., Tan, S., Gounou, C., Arraud, N. & Brisson, A. R. High-speed centrifugation induces aggregation of extracellular vesicles. *Journal of Extracellular Vesicles* vol. 4 Preprint at https://doi.org/10.3402/jev.v4.29509 (2015).

18. Ku, A. *et al.* Acoustic Enrichment of Extracellular Vesicles from Biological Fluids. *Anal Chem* **90**, 8011–8019 (2018).

19. Ding, M. *et al.* Comparison of commercial exosome isolation kits for circulating exosomal microRNA profiling. *Anal Bioanal Chem* **410**, 3805–3814 (2018).

20. Royo, F. *et al.* Comparative miRNA analysis of urine extracellular vesicles isolated through five different methods. *Cancers (Basel)* **8**, (2016).

21. Gámez-Valero, A. *et al.* Size-Exclusion Chromatography-based isolation minimally alters Extracellular Vesicles' characteristics compared to precipitating agents. *Sci Rep* **6**, (2016).

22. Rifes, P. *et al.* Modeling neural tube development by differentiation of human embryonic stem cells in a microfluidic WNT gradient. *Nat Biotechnol* **38**, 1265–1273 (2020).

23. Undvall, E. *et al.* Inertia-Induced Breakdown of Acoustic Sorting Efficiency at High Flow Rates. *Phys Rev Appl* **17**, (2022).

24. Reynolds, O. An experimental investigation of the circumstances which determine whether the motion of water shall be direct or sinuous, and of the law of resistance in parallel channels. *Phil. Trans. R. Soc.* **174**, 935–982 (1883).

25. Stokes, G. G. On the Effect of the Internal Friction of Fluids on the Motion of Pendulums. *Transactions of the Cambridge Philosophical Society* **9**, 8–106 (1851).

26. Squires, T. M. & Quake, S. R. Microfluidics: Fluid physics at the nanoliter scale. *Rev Mod Phys* **77**, 977–1026 (2005).

27. Bruus, H. Acoustofluidics 1: Governing equations in microfluidics. *Lab Chip* **11**, 3742–3751 (2011).

28. Poiseuille, J. L. M. *Recherches Experimentales Sur Ie Mouvement Des Liquides Dans Les Tubes de Tres-Petits Diametres, In Memoires Presentes Par Divers Savants a l'Academie Royale Des Sciences de l'Institut de France*. vol. 9 (1846).

29. Woo, H. K. *et al.* Exodisc for Rapid, Size-Selective, and Efficient Isolation and Analysis of Nanoscale Extracellular Vesicles from Biological Samples. *ACS Nano* **11**, 1360–1370 (2017).

30. Liang, L. G. *et al.* An integrated double-filtration microfluidic device for isolation, enrichment and quantification of urinary extracellular vesicles for detection of bladder cancer. *Sci Rep* **7**, 1–10 (2017).

31. Liu, F. *et al.* The Exosome Total Isolation Chip. *ACS Nano* **11**, 10712–10723 (2017).

32. Lo, T. W. *et al.* Microfluidic device for high-throughput affinity-based isolation of extracellular vesicles. *Lab Chip* **20**, 1762–1770 (2020).

33. Chen, C. *et al.* Microfluidic isolation and transcriptome analysis of serum microvesicles. *Lab Chip* **10**, 505–511 (2010).

34. Kanwar, S. S., Dunlay, C. J., Simeone, D. M. & Nagrath, S. Microfluidic device (ExoChip) for on-chip isolation, quantification and characterization of circulating exosomes. *Lab Chip* **14**, 1891–1900 (2014).

35. Shin, S. *et al.* Separation of extracellular nanovesicles and apoptotic bodies from cancer cell culture broth using tunable microfluidic systems. *Sci Rep* **7**, (2017).

36. Multia, E. *et al.* Automated On-Line Isolation and Fractionation System for Nanosized Biomacromolecules from Human Plasma. *Anal Chem* **92**, 13058–13065 (2020).

37. Wunsch, B. H. *et al.* Nanoscale lateral displacement arrays for the separation of exosomes and colloids down to 20nm. *Nat Nanotechnol* **11**, 936–940 (2016).

38. Smith, J. T. *et al.* Integrated nanoscale deterministic lateral displacement arrays for separation of extracellular vesicles from clinically-relevant volumes of biological samples. *Lab Chip* **18**, 3913–3925 (2018).

39. Liu, C. *et al.* Field-Free Isolation of Exosomes from Extracellular Vesicles by Microfluidic Viscoelastic Flows. *ACS Nano* **11**, 6968–6976 (2017).

40. Asghari, M. *et al.* Oscillatory Viscoelastic Microfluidics for Efficient Focusing and Separation of Nanoscale Species. *ACS Nano* **14**, 422–433 (2020).

41. Zhao, Z., Yang, Y., Zeng, Y. & He, M. A microfluidic ExoSearch chip for multiplexed exosome detection towards blood-based ovarian cancer diagnosis. *Lab Chip* **16**, 489–496 (2016).

42. Yang, J. *et al.* Magnetic Colloid Antibodies Accelerate Small Extracellular Vesicles Isolation for Point-of-Care Diagnostics. *Nano Lett* **21**, 2001–2009 (2021).

43. Wu, M. *et al.* Isolation of exosomes from whole blood by integrating acoustics and microfluidics. *Proc Natl Acad Sci U S A* **114**, 10584–10589 (2017).

44. Dao, T. N. T. *et al.* Chimeric nanocomposites for the rapid and simple isolation of urinary extracellular vesicles. *J. Extracell. Vesicles* **11**, (2022).

45. Marczak, S. *et al.* Simultaneous isolation and preconcentration of exosomes by ion concentration polarization. *Electrophoresis* **39**, 2029–2038 (2018).

46. Ayala-Mar, S., Perez-Gonzalez, V. H., Mata-Gómez, M. A., Gallo-Villanueva, R. C. & González-Valdez, J. Electrokinetically Driven Exosome Separation and Concentration Using Dielectrophoretic-Enhanced PDMS-Based Microfluidics. *Anal Chem* **91**, 14975–14982 (2019).

47. Evander, M., Gidlöf, O., Olde, B., Erlinge, D. & Laurell, T. Non-contact acoustic capture of microparticles from small plasma volumes. *Lab Chip* **15**, 2588–2596 (2015).

48. Gidlöf, O. *et al.* Proteomic profiling of extracellular vesicles reveals additional diagnostic biomarkers for myocardial infarction compared to plasma alone. *Sci Rep* **9**, (2019).

49. Rezeli, M. *et al.* Comparative Proteomic Analysis of Extracellular Vesicles Isolated by Acoustic Trapping or Differential Centrifugation. *Anal Chem* **88**, 8577–8586 (2016).

50. Havers, M., Broman, A., Lenshof, A. & Laurell, T. Advancement and obstacles in microfluidics-based isolation of extracellular vesicles. *Analytical and Bioanalytical Chemistry* vol. 415 1265–1285 Preprint at https://doi.org/10.1007/s00216-022-04362-3 (2023).

51. Yeh, Y. T. *et al.* Rapid Size-Based Isolation of Extracellular Vesicles by Three-Dimensional Carbon Nanotube Arrays. *ACS Appl Mater Interfaces* **12**, 13134–13139 (2020).

52. Kundt, A. Ueber eine neue Art akustischer Staubfiguren und Anwendung derselben zur Bestimmung der Schallgeschwindigkeit in festen Körpern und Gasen. *Pogg. Ann. der Physik und Chemie* **127**, 497–523 (1866).

53. Laurell, T. & Lenshof, A. Microscale Acoustofluidics. *Royal Society of Chemistry* (2015).

54. King, L. V. On the Acoustic Radiation Pressure on Spheres. *Proc. R. Soc. Lond. A* **147**, 212–240 (1934).

55. Yosioka, K. & Kawasima, Y. Acoustic radiation pressure on a compressible sphere. *Acustica* **5**, 167–173 (1955).

56. Gor'Kov, L. P. On the Forces Acting on a Small Particle in an Acoustical Field in an Ideal Fluid. *Sov. Phys. Doklady* **6**, 88–91 (1962).

57. Bruus, H. Acoustofluidics 7: The acoustic radiation force on small particles. *Lab on a Chip* vol. 12 1014–1021 Preprint at https://doi.org/10.1039/c2lc21068a (2012).

58. Woodside, S. M., Bowen, B. D. & Piret, J. M. Measurement of ultrasonic forces for partile-liquid separations. *Aiche J* **43**, 1727–1736 (1997).

59. Fornell, A., Baasch, T., Johannesson, C., Nilsson, J. & Tenje, M. Binary acoustic trapping in a glass capillary. *J Phys D Appl Phys* **54**, (2021).

60. Havers, M., Baasch, T., Lenshof, A., Evander, M. & Laurell, T. Silica seed particles improve the efficiency and throughput of nanoparticle acoustic trapping. *Phys Rev Appl* **21**, 34016 (2024).

61. Bjerknes, V. F. K. Fields of force. *The Columbia University Press* (1906).

62. Crum, L. A. Acoustic Force on a Liquid Droplet in an Acoustic Stationary Wave. *Journal of the Acoustical Society of America* **50**, (1971).

63. Weiser, M. A. H., Apfel, R. E. & Neppiras, E. A. Interparticle Forces on Red-Cells in a Standing Wave Field. *Acustica* **56**, 114–119 (1984).

64. Groschl, M. Ultrasonic Separation of Suspended Particles - Part I: Fundamentals. *Acustica* **84**, 432–447 (1998).

65. Silva, G. T. & Bruus, H. Acoustic interaction forces between small particles in an ideal fluid. *Phys Rev E Stat Nonlin Soft Matter Phys* **90**, (2014).

66. Baasch, T., Qiu, W. & Laurell, T. Gap Distance Between Pearl Chains in Acoustic Manipulation. *Phys Rev Appl* **10**, 14021 (2022).

67. Schlichting, H. Calculation of even periodic barrier currents. *Physikalische Zeitschrift* **33**, 327–335 (1932).

68. Rayleigh, L. On the Circulation of Air Observed in Kundt's Tubes, and on Some Allied Acoustical Problems. *Philos Trans R Soc Lond* **175**, 1–21 (1884).

69. Eckart, C. Vortices and streams caused by sound waves. *Physical Review* **73**, (1947).

70. Wiklund, M., Green, R. & Ohlin, M. Acoustofluidics 14: Applications of acoustic streaming in microfluidic devices. *Lab on a Chip* vol. 12 2438–2451 Preprint at https://doi.org/10.1039/c2lc40203c (2012).

71. Qiu, W., Joergensen, J. H., Corato, E., Bruus, H. & Augustsson, P. Fast Microscale Acoustic Streaming Driven by a Temperature-Gradient-Induced Nondissipative Acoustic Body Force. *Phys Rev Lett* **127**, (2021).

72. Joergensen, J. H., Qiu, W. & Bruus, H. Transition from Boundary-Driven to Bulk-Driven Acoustic Streaming Due to Nonlinear Thermoviscous Effects at High Acoustic Energy Densities. *Phys Rev Lett* **130**, (2023).

73. Joergensen, J. H. & Bruus, H. Theory of pressure acoustics with thermoviscous boundary layers and streaming in elastic cavities. *J Acoust Soc Am* **149**, 3599–3610 (2021).

74. Hammarström, B., Laurell, T. & Nilsson, J. Seed particle-enabled acoustic trapping of bacteria and nanoparticles in continuous flow systems. *Lab Chip* **12**, 4296–4304 (2012).

75. Lilliehorn, T. *et al.* Trapping of microparticles in the near field of an ultrasonic transducer. *Ultrasonics* **43**, 293–303 (2005).

76. Congiu, J. Automated staining and washing of cells and microvesicles using acoustic trapping. (Lund University, 2018).

77. Fornell, A. *et al.* An acoustofluidic platform for non-contact trapping of cell-laden hydrogel droplets compatible with optical microscopy. *Biomicrofluidics* **13**, 44101 (2019).

78. Evander, M. *et al.* Noninvasive acoustic cell trapping in a microfluidic perfusion system for online bioassays. *Anal Chem* **79**, 2984–2991 (2007).

79. Barnkob, R., Augustsson, P., Laurell, T. & Bruus, H. Acoustic radiation- and streaming-induced microparticle velocities determined by microparticle image velocimetry in an ultrasound symmetry plane. *Phys Rev E Stat Nonlin Soft Matter Phys* **86**, (2012).

80. Ohlsson, P. *et al.* Integrated Acoustic Separation, Enrichment, and Microchip Polymerase Chain Reaction Detection of Bacteria from Blood for Rapid Sepsis Diagnostics. *Anal Chem* **88**, 9403–9411 (2016).

81. Ku, A. *et al.* High-Throughput and Automated Acoustic Trapping of Extracellular Vesicles to Identify microRNAs With Diagnostic Potential for Prostate Cancer. *Front. Oncol.* **11**, 1 (2021).

82. Broman, A. *et al.* Multinodal Acoustic Trapping Enables High Capacity and High Throughput Enrichment of Extracellular Vesicles and Microparticles in miRNA and MS Proteomics Studies. *Anal Chem* **93**, 3929–3937 (2021).

83. Sattarov, R. *et al.* Phosphorylated tau in cerebrospinal fluid-derived extracellular vesicles in Alzheimer's disease: a pilot study. *Sci Rep* **14**, 25419 (2024).

84. Palm, F. *et al.* Phenotypic Characterization of Acoustically Enriched Extracellular Vesicles from Pathogen-Activated Platelets. *J Innate Immun* **15**, 599–613 (2023).

85. Bryl-Górecka, P. *et al.* Effect of exercise on the plasma vesicular proteome: A methodological study comparing acoustic trapping and centrifugation. *Lab Chip* **18**, 3101–3111 (2018).

86. Hammarström, B., Evander, M., Wahlström, J. & Nilsson, J. Frequency tracking in acoustic trapping for improved performance stability and system surveillance. *Lab Chip* **14**, 1005–1013 (2014).

87. Kaitila, J., Ylilammi, M., Ellä, J. & Aigner, R. Spurious resonance free bulk acoustic wave resonators. *IEEE Symposium on Ultrasonics* **1**, 84–87 (2003).

88. Thalhammer, R. & Aigner, R. Energy loss mechanisms in SMR-type BAW devices. *IEEE* 225–228 (2005) doi:10.1109/MTT67880.2005.9387932.

89. Wilkins, M. R. *et al.* Progress with proteome projects: Why all proteins expressed by a genome should be identified and how to do it. *Biotechnol Genet Eng Rev* **13**, 19–50 (1996).

90. Birhanu, A. G. Mass spectrometry-based proteomics as an emerging tool in clinical laboratories. *Clinical Proteomics* vol. 20 Preprint at https://doi.org/10.1186/s12014-023-09424-x (2023).

91. Aebersold, R. & Mann, M. Mass spectrometry-based proteomics. *Nature* **422**, 198–207 (2003).

92. Fenn, J., Mann, M., Meng, C. & Whitehouse, C. Electrospray ionization for mass spectrometry of large biomolecules. *Science (1979)* **246**, 64–71 (1989).

93. Olsen, J. *et al.* Higher-energy C-trap dissociation for peptide modification analysis. *Nat Methods* **4**, 709–712 (2007).

94. Elias, J. E. & Gygi, S. P. Target-decoy search strategy for increased confidence in large-scale protein identifications by mass spectrometry. *Nat Methods* (2007) doi:10.1038/NMETH1019.

95. Venable, J. D., Dong, M. Q., Wohlschlegel, J., Dillin, A. & Yates, J. R. Automated approach for quantitative analysis of complex peptide mixtures from tandem mass spectra. *Nat Methods* **1**, 39–45 (2004).

96. Panchaud, A. *et al.* Precursor acquisition independent from ion count: How to dive deeper into the proteomics ocean. *Anal Chem* **81**, 6481–6488 (2009).

97. Gillet, L. C. *et al.* Targeted data extraction of the MS/MS spectra generated by data-independent acquisition: A new concept for consistent and accurate proteome analysis. *Molecular and Cellular Proteomics* **11**, (2012).

98. Röst, H. L. *et al.* OpenSWATH enables automated, targeted analysis of data-independent acquisition MS data. *Nat Biotechnol* **32**, 219–223 (2014).

99. Demichev, V., Messner, C. B., Vernardis, S. I., Lilley, K. S. & Ralser, M. DIA-NN: neural networks and interference correction enable deep proteome coverage in high throughput. *Nat Methods* **17**, 41–44 (2020).

100. Isaksson, M., Karlsson, C., Laurell, T., Kirkeby, A. & Heusel, M. MSLibrarian: Optimized Predicted Spectral Libraries for Data-Independent Acquisition Proteomics. *J Proteome Res* **21**, 535–546 (2022).

101. Yang, Y. *et al.* In silico spectral libraries by deep learning facilitate data-independent acquisition proteomics. *Nat Commun* **11**, (2020).

102. Singer, M. *et al.* The Third International Consensus Definitions for Sepsis and Septic Shock (Sepsis-3). *JAMA* **315**, 801–810 (2016).

103. Rudd, K. E. *et al.* Global, regional, and national sepsis incidence and mortality, 1990–2017: analysis for the Global Burden of Disease Study. *The Lancet* **395**, 200–211 (2020).

104. Mayr, F. B., Yende, S. & Angus, D. C. Epidemiology of severe sepsis. *Virulence* vol. 5 4–11 Preprint at https://doi.org/10.4161/viru.27372 (2014).

105. Kumar, A. *et al.* Duration of hypotension before initiation of effective antimicrobial therapy is the critical determinant of survival in human septic shock. *Crit Care Med* **34**, 1589–1596 (2006).

106. Ferrer, R. *et al.* Empiric antibiotic treatment reduces mortality in severe sepsis and septic shock from the first hour: Results from a guideline-based performance improvement program. *Crit Care Med* **42**, 1749–1755 (2014).

107. Vincent, J. L. *et al.* The SOFA (Sepsis-related Organ Failure Assessment) score to describe organ dysfunction/failure. *Intensive Care Med* 707–710 (1996).

108. Mohanty, T. *et al.* A pharmacoproteomic landscape of organotypic intervention responses in Gram-negative sepsis. *Nat Commun* **14**, (2023).

109. Lelubre, C. & Vincent, J.-L. Mechanisms and treatment of organ failure in sepsis. *Nat Rev Nephrol* (2018) doi:10.1038/s41581-018-0005-7.

110. Marshall, J. C. Why have clinical trials in sepsis failed? *Trends in Molecular Medicine* vol. 20 195–203 Preprint at https://doi.org/10.1016/j.molmed.2014.01.007 (2014).

111. Gómez Toledo, A. *et al.* Proteomic atlas of organ vasculopathies triggered by Staphylococcus aureus sepsis. *Nat Commun* **10**, (2019).

112. Golden, G. J. *et al.* Endothelial Heparan Sulfate Mediates Hepatic Neutrophil Trafficking and Injury during Staphylococcus aureus Sepsis. *mBio* **12**, (2021).

113. Strålin, K. *et al.* Design of a national patient-centred clinical pathway for sepsis in Sweden. *Infect Dis* **55**, 716–724 (2023).

114. Handtke, S. & Thiele, T. Large and small platelets—(When) do they differ? *Journal of Thrombosis and Haemostasis* vol. 18 1256–1267 Preprint at https://doi.org/10.1111/jth.14788 (2020).

115. Branehög, I., Kutti, J., Ridell, B., Swolin, B. & Weinfeld, A. The Relation of Thrombokinetics to Bone Marrow Megakaryocytes in Idiopathic Thrombocytopenic Purpura (ITP)). *Blood* **45**, 551–562 (1975).

116. Daly, M. E. Determinants of platelet count in humans. *Haematologica* vol. 96 10–13 Preprint at https://doi.org/10.3324/haematol.2010.035287 (2011).

117. Riaz, A. H., Tasma, B. E., Woodman, M. E., Wooten, R. M. & Worth, R. G. Human platelets efficiently kill IgG-opsonized E. coli. *FEMS Immunol Med Microbiol* **65**, 78–83 (2012).

118. Yeaman, M. R., Norman, D. C. & Bayer', A. S. *Platelet Microbicidal Protein Enhances Antibiotic-Induced Killing of and Postantibiotic Effect in Staphylococcus Aureus*. *ANTIMICROBIAL AGENTS AND CHEMOTHERAPY* https://journals.asm.org/journal/aac (1992).

119. Gaertner, F. *et al.* Migrating Platelets Are Mechano-scavengers that Collect and Bundle Bacteria. *Cell* **171**, 1368-1382.e23 (2017).

120. Hamzeh-Cognasse, H. *et al.* Platelet toll-like receptors are crucial sensors of infectious danger moieties. *Platelets* **29**, 533–540 (2018).

121. Maouia, A., Rebetz, J., Kapur, R. & Semple, J. W. The Immune Nature of Platelets Revisited. *Transfusion Medicine Reviews* vol. 34 209–220 Preprint at https://doi.org/10.1016/j.tmrv.2020.09.005 (2020).

122. Opal, S. M. & van der Poll, T. Endothelial barrier dysfunction in septic shock. *Journal of Internal Medicine* vol. 277 277–293 Preprint at https://doi.org/10.1111/joim.12331 (2015).

123. Levi, M. Hemostasis and Thrombosis in Critically Ill Patients. *Semin Thromb Hemost* **34**, (2008).

124. Vardon-Bounes, F. *et al.* Platelets are critical key players in sepsis. *International Journal of Molecular Sciences* vol. 20 Preprint at https://doi.org/10.3390/ijms20143494 (2019).

125. Horstman, L. L. & Ahn, Y. S. *Platelet Microparticles: A Wide-Angle Perspective*. *Critical Reviews in Oncology/Hematology* vol. 30 (1999).

126. Forlow, S. B., McEver, R. P. & Nollert, M. U. Leukocyte-leukocyte interactions mediated by platelet microparticles under flow. *Blood* **95**, 1317–1323 (2000).

127. Woth, G. *et al.* Activated platelet-derived microparticle numbers are elevated in patients with severe fungal (Candida albicans) sepsis. *Ann Clin Biochem* **49**, 554–560 (2012).

128. Puskarich, M. A. *et al.* Phosphatidylserine expressing platelet microparticle levels at hospital presentation are decreased in sepsis non-survivors and correlate with thrombocytopenia. *Thromb Res* **168**, 138–144 (2018).

129. Abdelmohsen, K. *et al.* Survey of organ-derived small extracellular vesicles and particles (sEVPs) to identify selective protein markers in mouse serum. *Journal of Extracellular Biology* **2**, (2023).

130. Khanabdali, R. *et al.* High throughput Surface Epitope Immunoaffinity Isolation of Extracellular Vesicles and Downstream Analysis. *Biol Methods Protoc* (2024) doi:10.1093/biomethods/bpae032.

131. Mcilvenna, L. C. *et al.* Single vesicle analysis reveals the release of tetraspanin positive extracellular vesicles into circulation with high intensity intermittent exercise Key points. *J Physiol* **601**, 5093–5106 (2023).

132. Li, J. *et al.* Characterization of Cellular Sources and Circulating Levels of Extracellular Vesicles in a Dietary Murine Model of Nonalcoholic Steatohepatitis. *Hepatol Commun* **3**, 1235–1249 (2019).

Paper I

analytical chemistry

pubs.acs.org/ac Article

Multinodal Acoustic Trapping Enables High Capacity and High Throughput Enrichment of Extracellular Vesicles and Microparticles in miRNA and MS Proteomics Studies

Axel Broman,* Andreas Lenshof, Mikael Evander, Lotta Happonen, Anson Ku, Johan Malmström, and Thomas Laurell

Cite This: *Anal. Chem.* 2021, 93, 3929−3937 Read Online

ACCESS | Metrics & More | Article Recommendations | Supporting Information

ABSTRACT: We report a new design of an acoustophoretic trapping device with significantly increased capacity and throughput, compared to current commercial acoustic trapping systems. Acoustic trapping enables nanoparticle and extracellular vesicle (EV) enrichment without ultracentrifugation. Current commercial acoustic trapping technology uses an acoustic single-node resonance and typically operates at flow rates <50 μL/min, which limits the processing of the larger samples. Here, we use a larger capillary that supports an acoustic multinode resonance, which increased the seed particle capacity 40 times and throughput 25−40 times compared to single-node systems. The resulting increase in capacity and throughput was demonstrated by isolation of nanogram amounts of microRNA from acoustically trapped urinary EVs within 10 min. Additionally, the improved trapping performance enabled isolation of extracellular vesicles for downstream mass spectrometry analysis. This was demonstrated by the differential protein abundance profiling of urine samples (1−3 mL), derived from the non-trapped versus trapped urine samples.

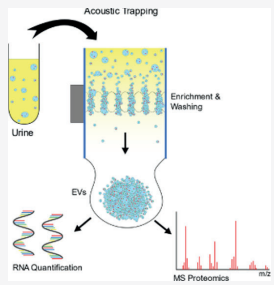

INTRODUCTION

Extracellular vesicles (EVs) are small, membrane-enclosed particles that are released by cells and contain a wide range of bioactive molecules. These include proteins, lipids, and genetic information, often in the form of mRNA and non-coding RNA. EVs act as cell−cell messengers, shuttling around these bioactive molecules and help in regulating cellular function.[1] Additionally, the content in EVs reflects the state of the parent cell and can therefore be used to assess the health and disease of the organism as a whole.[2,3] As such, there is great interest in the study of EVs, which requires improved methods for isolating and enriching these vesicles.

The current gold standard for EV isolation is differential ultracentrifugation (UC), which is a laborious and time-consuming method that often requires large sample volumes. Additionally, ultracentrifugation frequently gives inconsistent results across studies due to the use of different rotors and variations in the protocols.[4−8] Finally, the very large forces involved in UC may coalesce vesicles and form vesicle aggregates[9] as well as coprecipitate larger protein complexes, e.g., Tamm−Horsfall proteins in urine.[10]

To overcome the problems with ultracentrifugation, many microfluidic devices for EV isolation and enrichment have been developed. These include nanoscale deterministic lateral displacement (nano-DLD),[11] immunoaffinity-functionalized microstructures or beads,[12,13] dielectrophoresis (DEP),[14] viscoelastic separation,[15] surface acoustic waves (SAW),[16] and acoustic trapping.[17] Microfluidic approaches rely on the deterministic laminar flow profile and have the benefit of working with much smaller sample volumes as compared to UC. Microfluidic devices have by nature a low throughput compared to conventional techniques. In the aforementioned methods for EV isolation, the flow rate is typically a few microliters per minute, without including any potential labeling or incubation time. This is inherently not a problem, as the volumes required for analysis can be quite small. It does however put an upper limit to the sample volume due to processing time. In the case of dilute samples like urine or cell culture medium, where larger volume needs to be processed, microfluidic approaches commonly fail.

Acoustic trapping is a promising technology for isolating and enriching EVs. It offers a gentle, label-free, non-contact way of capturing and retaining particles against a flow by generating a strong localized ultrasonic standing wave inside a microfluidic channel. The standing wave creates a stationary pressure node in the center of the channel, which can capture particles down to a few microns by the primary acoustic radiation force.[18,19] The first demonstration to capture particles in the 100 nm range was

Received: November 12, 2020
Accepted: February 1, 2021
Published: February 16, 2021

https://dx.doi.org/10.1021/acs.analchem.0c04772
Anal. Chem. 2021, 93, 3929−3937

reported by Hammarström et al.,[20] utilizing scattered sound interaction from preloaded seed particles. Isolation of extracellular vesicles from blood plasma using acoustic seed particle trapping was first demonstrated by Evander et al.[17] Numerous mass spectrometry-based proteomics studies have investigated EVs,[21] and recently, Rezeli et al. were the first to demonstrate mass spectrometry-based proteomics data derived from microparticles isolated by acoustic trapping, although limited by the minute analyte amounts isolated by the trapping unit.[22] Later, Ku et al. demonstrated the use of acoustic trapping to enrich EVs from biological fluids such as plasma, urine, and conditioned media for microRNA analysis. TEM images also verified an intact EV morphology after the acoustic processing.[23] More recently, a SAW-based approach has also demonstrated the trapping of nanoparticles by means of scattered sound interaction with particles in a packed bed.[24] Later, this system also reported EV isolation from cell culture supernatant at a throughput of 100 nL/min, indicating potential for significant scalability.[25]

In this paper, we present a novel, scaled-up acoustic trapping device with significantly increased throughput and capacity as compared to previously reported systems. The new device comprises a piezoelectric transducer and a glass capillary with a cross-sectional area 20 times larger than the capillary in the acoustic trapping system in the aforementioned studies. The capillary is actuated at a multinode resonance instead of the standard single-node resonance, generating nine trapping nodes instead of one. This enables more particles to be retained in the trapping zone, thus increasing the capacity of the device. Furthermore, since the ability to retain particles in the trap is dependent on the shear stress induced by the fluid flow, the larger capillary cross section allows for higher flow rates without the increased shear stress on the trapped particles. This now enables rapid, label-free processing of milliliter-sized samples, facilitating the acoustic isolation of EVs from dilute biological samples. In this paper, we therefore demonstrate that acoustic trapping using bulk actuation is scalable. Quantitative proteomics analysis revealed enrichment of distinct proteome patterns associated with the trapped urine samples compared to non-trapped urine, paving the way for future studies interfaced to MS-based proteomics or RNA sequencing analysis.

THEORY

Radiation Forces. The theory behind acoustic radiation forces has been described by Gorkov,[26] Whitworth et al.,[27] Crum,[28] Weiser et al.,[29] and Groschl.[30] Briefly, in acoustic trapping, a standing ultrasonic wave is generated inside a channel and will exert radiation forces on particles in proportion to the energy density in the resonator and the size of the particles as well as the particle density and compressibility relative to the surrounding medium. For a spherical particle in an ideal fluid, and if the wavelength is much larger than the particle, the magnitude of the force is equal to the average impulse flux through any closed surface of the sphere.[26] The primary radiation force (PRF) of a plane standing wave on a particle with a radius much smaller than the wavelength is given by[31]

$$F_{\mathrm{rad}} = -\nabla\frac{4\pi}{3}a^3\left[f_1\frac{1}{2}\kappa_0 p_{\mathrm{in}}^2 - f_2\frac{3}{4}\rho_0 v_{\mathrm{in}}^2\right]$$
$$f_1(\tilde{\kappa}) = 1 - \tilde{\kappa} \text{ and } \tilde{\kappa} = \frac{\kappa_{\mathrm{p}}}{\kappa_{\mathrm{m}}}$$
$$f_2(\tilde{\rho}) = \frac{2(\tilde{\rho}-1)}{2\rho+1} \text{ and } \tilde{\rho} = \frac{\rho_{\mathrm{p}}}{\rho_0} \quad (1)$$

where a is the radius of the particle, f_1 and f_2 are the monopole and dipole scattering coefficients, respectively, κ_{p} and κ_0 are the compressibilities, ρ_{p} and ρ_0 are the densities of the particle and the medium, respectively, and p_{in} and v_{in} are the pressure and velocity field time averages. For a one-dimensional planar wave, the expression is simplified to

$$F_z^{\mathrm{rad}} = 4\pi\Phi(\tilde{\kappa},\tilde{\rho})ka^3E_{\mathrm{ac}}\sin(2kz)$$
$$\Phi(\tilde{\kappa},\tilde{\rho}) = \frac{1}{3}\left[\frac{5\tilde{\rho}-2}{2\tilde{\rho}+1} - \tilde{\kappa}\right] \quad (2)$$

where E_{ac} is the acoustic energy density, k is the wavenumber, and Φ is the acoustic contrast factor. The acoustic contrast factor indicates how a given particle behaves in a sound field. If the contrast factor has a positive value, the particle migrates toward the pressure node. If the factor has a negative value, the particle migrates toward the pressure antinode (Figure 1).

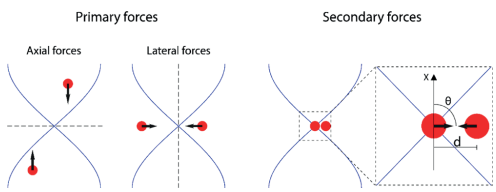

Figure 1. Summary of the acoustic radiation forces on particles with the positive acoustic contrast factor in an acoustic trap. The axial forces push particles into the nodal plane. Lateral forces, caused by the acoustic energy density gradient, push particles toward the center of the acoustic field and enable particle retention against the flow. Secondary forces become relevant when particle distances are small and cause particle aggregation. Illustration inspired by Hammarström et al.[20]

As part of the PRF, particles will also experience a lateral radiation force due to the fact that the sound wave is localized to the transducer region and the acoustic energy density diminishes rapidly outside the transducer area.[32] The acoustic energy density gradient in the lateral direction (axial direction of the capillary) is perpendicular to the standing wave direction.[33] The lateral radiation force is given by

$$F_{\mathrm{L}} = \frac{4\pi}{3}a^3\nabla E_{\mathrm{ac}}\left(\frac{3(\rho_{\mathrm{p}}-\rho_0)}{\rho_0+2\rho_{\mathrm{p}}}\cos^2(kx) - \frac{\kappa_0-\kappa_{\mathrm{p}}}{\kappa_0}\sin^2(kx)\right) \quad (3)$$

Lastly, particles will also experience an interparticle radiation force that arises from sound scattering between particles in solution, commonly called secondary force.[30] If the incident wave is a plane wave, the secondary radiation force on two identical particles at a distance d in a pressure field p is given as

https://dx.doi.org/10.1021/acs.analchem.0c04772
Anal. Chem. 2021, 93, 3929−3937

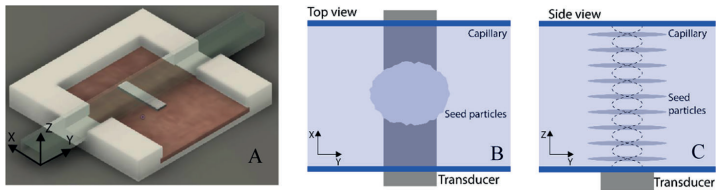

Figure 2. (A) Three-dimensional schematic of the acoustic trapping device. A glass capillary is attached to a piezoelectric transducer. The transducer is soldered to a circuit board for electronic interfacing and controlling the sound wave. (B) Model of the trapping device viewed from the top. Particles are trapped over the transducer. (C) Model of the standing acoustic wave inside the channel viewed from the side. Particle clusters are shown, collected in the nine nodes created by the standing wave.

$$F_s = 4\pi a^6 \left(\frac{(\rho_p - \rho_m)^2 (3\cos^2\theta - 1)}{6\rho_m d^4} v^2(x) - \frac{\omega^2 \rho_m (\kappa_p - \kappa_0)^2}{9d^2} p^2(x) \right) \quad (4)$$

Trapping Unit. The trapping unit consists of a borosilicate glass capillary ($2 \times 4 \times 50$ mm^3) (Vitrocom) with connecting tubings, glued to an ultrasonic transducer (Pz26, Meggitt) and a temperature sensor (Pt100, Jumo) mounted on a printed circuit board (PCB), see Figure 2a. The sample is run through the capillary and a localized ultrasonic standing wave is generated inside the capillary in the region of the ultrasonic transducer.

The transducer is actuated at a channel resonance of 4.4 MHz. This results in a standing wave with nine trapping nodes along the height of the channel (Figure 2b,c). Particles are collected in these nodes and retained against the flow in the channel, enabling isolation, enrichment, buffer switching, and washing of the particles. Submicron particles can also be enriched in the trap by the secondary acoustic force by first loading the trap with large seed particles that interact with nanoparticles in close proximity. Using this method, particles of around 100 nm have been captured.[20]

The resonance frequency is dependent on the speed of sound in the medium and is therefore sensitive to temperature fluctuations and particles collecting in the trap. To compensate for small changes in the resonance frequency, a frequency tracking software developed by Hammarström et al.[34] was used to continually update the signal generator frequency to match the resonance frequency of the trapping capillary. Briefly, the software periodically scans a frequency range around the resonance peak and measures the transducer impedance spectra. The software subsequently sets the output frequency to match the impedance minimum until a new scan is made.

EXPERIMENTAL SECTION

Measuring Trapping Capacity. The capacity of the trap was measured for five different actuating voltages (7, 9, 11, 13, and 15 V_{pp}). A solution containing 12 μm polystyrene particles (Sigma-Aldrich) was run through the trap at 500 μL/min until the trap was saturated with particles. The capillary was then washed with 2 mL of Milli-Q water to remove any non-trapped particles. The retained particle cluster was then extracted by turning off the ultrasound and flushing the channel with 3.5 mL of Milli-Q at 5000 μL/min. Triton-X (0.1%) was added to the solution to mitigate particles sticking to the wall. Following vortexing and sonication, the solution was transferred to a BD Trucount tube and run through a cytometer (BD FACS Canto II) to count the number of particles.

Measuring Throughput and Trapping Efficiency. The trapping efficiency of 500 nm polystyrene particles (PS) was measured at five different flow rates (100, 200, 500, 1000, and 2000 μL/min). The trap was first loaded with a seed particle cluster containing 12 μm polystyrene beads, and excess particles were washed away with 2 mL of Milli-Q at a flow rate matching the sample flow rate. Five hundred microliters of a solution containing fluorescent nanoparticles (Fluoro-Max 500 nm, polystyrene, Thermo Scientific) was then aspirated through the trap, followed by rinsing with 2 mL of Milli-Q to remove untrapped nanoparticles. The seed cluster, along with trapped fluorescent nanoparticles, was collected by turning off the ultrasound and flushing with 3.5 mL of Milli-Q at a flow rate of 5000 μL/min. The fluorescence intensity of the collected sample was then measured as the average reading from the trapped sample, aliquoted in four wells, using a 96-well plate reader (FLUOstar Omega, BMG Labtech, Germany) and compared to the input sample to calculate the trapping efficiency.

Capturing Extracellular Vesicles from Urine Samples. We investigated the device's capability of capturing EVs from urine samples. Urine from a healthy donor was centrifuged at 2000g for 10 min (Eppendorf Centrifuge 5702) to remove cellular debris, to prevent clogging the trap, and the supernatant was collected. The trap was mounted vertically, with the outlet pointing downward. The system was primed with Dulbecco's phosphate-buffered saline (PBS), followed by loading the trap with seed particles (12 μm polystyrene). Different volumes of urine (1, 2, or 3 mL) were run through the trap at a flow rate of 500 μL/min to capture EVs. The trap was then rinsed with 1 mL of PBS to wash away the urine supernatant. Finally, the ultrasound was turned off and the cluster was allowed to sediment for 5 s to get closer to the exit before it was recovered in a volume of 250 μL of PBS at a flow rate of 5000 μL/min.

The samples were then analyzed either by nanoparticle tracking (NTA) (NanoSight LM14C, Malvern Panalytical, U.K.) or by chip-based capillary electrophoresis (Agilent 2100 Bioanalyzer System, Agilent). The NTA measurements assessed the size distribution and concentration of particles in the samples. The samples that were analyzed in the bioanalyzer were first treated with 0.5 μg/μL ribonuclease (RNase) to remove any free RNA, thus ensuring that any detected RNA originated from inside vesicles. Vesicle-borne RNA was then extracted using Norgen's Single Cell RNA Purification Kit, following the protocol for "Total RNA purification from Plasma or Serum". The RNA was eluted with 10 μL of elution buffer provided in the kit. One microliter of this solution was then loaded into an

https://dx.doi.org/10.1021/acs.analchem.0c04772
Anal. Chem. 2021, 93, 3929−3937

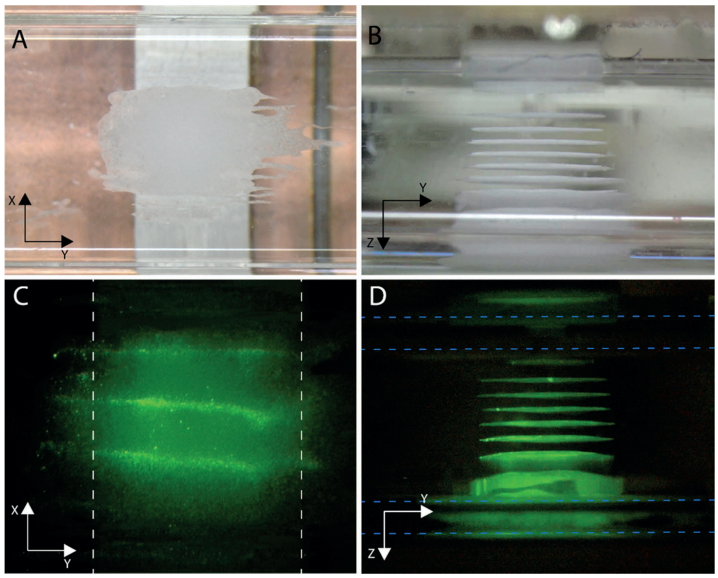

Figure 3. Pictures of particle clusters captured and retained in the multinodal acoustic trap. The flow rate in all pictures is 500 μL/min. (A) Bright-field image of the seed particle clusters viewed from the top. (B) Seed particle cluster viewed from the side. (C) Fluorescence image of a seed particle cluster enriched with 500 nm fluorescent polystyrene particles, viewed from the top. White dashed lines indicate the transducer. (D) Seed particle cluster enriched with 500 nm fluorescent polystyrene particles, viewed from the side. Blue dashed lines indicate the capillary wall. In both (B) and (D), nine clusters of particles can be seen stacked vertically above the transducer. The transducer is located at the top of the picture. The curved edges of the capillary cause optical distortions close to the wall, making the clusters appear more smeared.

mRNA Pico Chip and analyzed in the bioanalyzer to give the length distribution and concentration of RNA in the sample.

Capturing Extracellular Vesicles for Mass Spectrometry. To further assess the trap and to observe if there are clear differences in protein content between the trapped and non-trapped samples, the urine samples were analyzed using mass spectrometry. One, two, or three milliliters of urine was processed in the acoustic trapping unit following the protocol as above. The trapped and washed EVs from the acoustic trap, along with a triplicate of the non-trapped sample were lysed using a Bioruptor Plus (Diagenode) using 20 cycles (30 s on and 30 s off) using the low setting. The proteins in the samples were then prepared for quantitative data-independent acquisition mass spectrometry (DIA-MS) using trypsin double digestion. One hundred μL of each sample, along with 4.6 μL of a 10 M urea and 50 mM ammonium bicarbonate (ABC) solution and 2 μL of 0.5 μg/μL sequencing grade trypsin, (Promega) was mixed and incubated at 37 °C for 30 min. The urea-ABC solution (45.4 μL) was added and the samples were incubated at room temperature for 30 min. The cysteine bonds were reduced with 0.5 μL of 500 mM tris(2-carboxyethyl)phosphine (TCEP) (at 37 °C for 60 min) and then alkylated with 1 μL of 500 mM iodoacetamide (at room temperature for 30 min). The samples were diluted with 250 μL of 100 mM ABC to a urea concentration below 1.5 M, and 2 μL of trypsin was added for protein digestion (at 37 °C for 16 h). The samples were acidified to a pH of 2−3 using 10% formic acid and the peptides were purified using SOLAμ HRP reverse phase columns (Thermo Scientific). The peptides were dried in a SpeedVac (miVAC DUO) and reconstituted in 2% acetonitrile and 0.2% formic acid. The peptide content in each sample was measured using a spectrophotometer (DeNovix, DS-11 FX+) to ensure an equal amount of peptides from each sample (0.5 μg) was injected into the mass spectrometer.

Liquid Chromatography Tandem Mass Spectrometry (LC-MS/MS). The peptides were analyzed using data-dependent mass spectrometry analysis (DDA-MS) and data-independent mass spectrometry analysis (DIA-MS) on a Q Exactive HFX (Thermo Scientific) connected to an EASY-nLC 1200 (Thermo Scientific). The peptides were separated on a Thermo EASY-Spray column (Thermo Scientific 50 cm column, column temperature 45 °C) operated at a maximum pressure of 800 bar. A linear gradient of 4−45% acetonitrile in aqueous 0.1% formic acid was run for 50 min for both DDA and DIA. For DDA analysis, one full MS scan (resolution 60 000 for a mass range of 390−1210 m/z) was followed by MS/MS scans (resolution 15 000) of the 15 most abundant ion signals. The precursor ions with 2 m/z isolation width were isolated and fragmented using higher-energy collisional-induced dissociation at a normalized collision energy of 30. The automatic gain control was set as 3e6 for full MS scan and 1e5 for MS/MS. For DIA, a full MS scan (resolution 60 000 for a mass range of 390−1210 m/z) was followed by 32 MS/MS full fragmentation scans (resolution 30 000) using an isolation window of 26 m/z (including 0.5 m/z overlap between the previous and next window). The precursor ions within each isolation window were fragmented using higher-energy collisional-induced dissociation at a normalized collision energy of 30. The automatic gain control was set to 3e6 for MS and 1e6 for MS/MS.

https://dx.doi.org/10.1021/acs.analchem.0c04772
Anal. Chem. 2021, 93, 3929−3937

Mass Spectrometry Data Analysis. MS raw data were converted to gzipped and Numpressed mzML using[35] the tool MSconvert from the ProteoWizard, v3.0.5930 suite.[36] All data analyses were stored and managed using openBIS.[37] DDA data acquired spectra were analyzed using the search engine X! Tandem (2013.06.15.1-LabKey, Insilicos, ISB),[38] OMSSA (version 2.1.8),[39] and COMET (version 2014.02 rev.2)[40] against an in-house compiled database containing the *Homo sapiens* and *S. pyogenes* serotype M1 reference proteomes (UniProt proteome IDs UP000005640 and UP000000750, respectively), yielding a total of 22 155 protein entries and an equal amount of reverse decoy sequences. Fully tryptic digestion was used allowing two missed cleavages. Carbamidomethylation (C) was set to static and oxidation (M) to variable modifications, respectively. Mass tolerance for precursor ions was set to 0.2 Da, and for fragment ions to 0.02 Da. Identified peptides were processed and analyzed through the Trans-Proteomic Pipeline (TPP v4.7 POLAR VORTEX rev 0, Build 201403121010) using PeptideProphet.[41] The false discovery rate (FDR) was estimated with Mayu (v1.7) and peptide spectrum matches (PSMs) were filtered with protein FDR set to 1% resulting in a peptide FDR > 1%.

The DIA data were processed using the OpenSWATH pipeline.[42] For DIA data analysis, spectral libraries from the above DDA data set were created in openBIS using SpectraST (version 5.0, TPP v4.8.0 PHILAE, build 201506301157-exported (Ubuntu-x86_64)) in TPP.[43] For DIA data analysis, raw data files were converted to mzXML using msconvert and analyzed using OpenSWATH (version 2.0.1revision: c23217e). The retention time (RT) extraction window was ±300 s, and *m*/*z* extraction was set at 0.05 Da tolerance. RT was calibrated using iRT peptides. Peptide precursors were identified by OpenSWATH (2.0.1) and PyProphet (2.0.1), using a false discovery rate of 1% at the peptide precursor level and 1% at the protein level, and TRIC[44] for reducing the identification error. The resulting DIA data sets were analyzed using Jupyter Notebooks (version 3.1.1).

RESULTS AND DISCUSSION

Multinode Acoustic Trapping. The multinodal trapping unit can be seen in Figure 3. The trap showed nine distinct trapping nodes where seed particles (12 μm polystyrene) were enriched and retained against the flow (Figure 3a,b). Fluorescence imaging showed that it was also possible to capture and enrich smaller fluorescent particles (500 nm) (Figure 3c,d). It should be mentioned that pictures A, B, C, and D in Figure 3 were all taken of different clusters.

Performance Testing with Polystyrene Beads. To assess the trapping capacity of the device for different levels of input power, the ability of the multinode trap to retain seed particles at different actuation voltages was investigated. Increased power should increase the strength of the acoustic field but can also introduce problems with overheating. The system displayed increased trapping capacity with increasing voltage over the transducer (Figure 4), which is in agreement with the higher acoustic energy density in the trapping region at elevated voltage. However, the system saturated at around 860 000 seed particles (12 μm polystyrene) while operating at a flow rate of 500 μL/min (Figure 4). Compared to the commercial single-node AcouTrap system, which has a maximum capacity of 20 000 identical particles (data provided by AcouSort AB),[45] this corresponded approximately to a 40-fold increase in the seed particle capacity of the system.

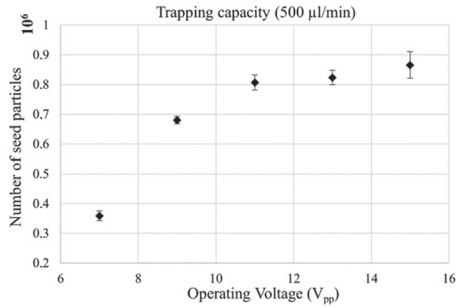

Figure 4. Capacity of the acoustic trap (actuated at voltages ranging from 7 to 15 V_{PP}) as measured by the amount of 12 μm polystyrene seed particles that could be retained simultaneously at a flow rate of 500 μL/min. The standard deviation is displayed as error bars (N = 3).

The throughput and trapping efficiency of the trap was evaluated by trapping fluorescent 500 nm particles at varying flow rates, with the trapping efficiency being defined as the percentage of input particles that are caught in the trap. The results from the throughput and trapping efficiency measurements can be seen in Figure 5. The large capillary allows for

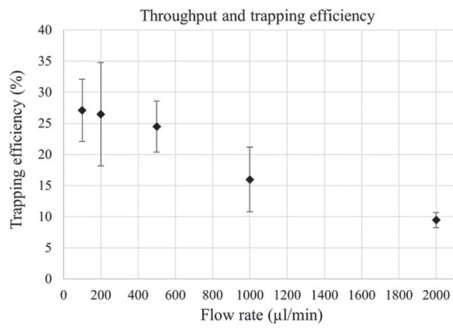

Figure 5. Trapping efficiency of the acoustic trap, as measured by the recovery of 500 nm fluorescent polystyrene particles, over a range of flow rates. The voltage was kept constant at 11 V_{PP} for all flow rates. The standard deviation is displayed as error bars (N = 3). The increasing flow rate decreases the trapping efficiency.

faster flow rates without increasing the drag force on the trapped particle clusters and without decreasing the time for the particle to migrate to the pressure nodes compared to a smaller capillary. The device was able to hold a stable seed particle cluster and trap submicron particles by the particle scattered sound interaction at flow rates of up to 2000 μL/min. The trapping efficiency decreased with the increase of the flow rate, with the highest average efficiency of 28% at 100 μL/min and the lowest of 9.5% at 2000 μL/min. The drop in trapping efficiency was expected as an increased flow rate increases the flow velocity of the particles and therefore decreases the time window for a given particle to be caught in the trap.

A high flow rate is a major advantage, as it allows for the rapid enrichment of particles and vesicles from larger sample volumes. It is clear that even though the multinode trap did not display a trapping efficiency higher than 28%, the high throughput still

https://dx.doi.org/10.1021/acs.analchem.0c04772
Anal. Chem. 2021, 93, 3929−3937

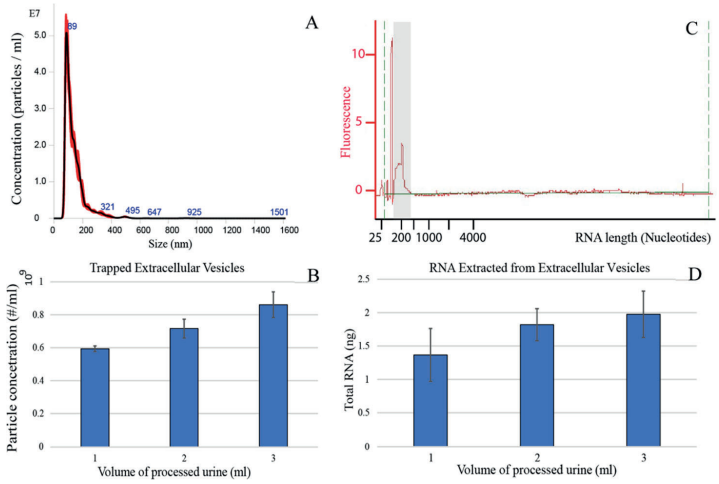

Figure 6. Extracellular vesicle trapping from 1, 2, and 3 mL of the urine samples. The flow rate was fixed at 500 μL/min for all samples. (A) The size distribution of particles from 3 mL of trapped urine with a vesicle peak at 89 nm. (B) Particle concentration in the eluted fraction of EVs from the NTA measurements for varying volumes of the input sample. Background from PBS has been subtracted. (C) The length distribution of intravesicle RNA from trapped vesicles expressed in the number of nucleotides. The first and the highest peaks represent the nucleotide reference ladder that was added to calibrate the system and should be ignored. The vesicle-derived RNA is seen in the peak around 200 nucleotides in length, highlighted in the gray zone. (D) The average total amount of RNA extracted for each input volume of urine.

enables a rapid capture of particles/vesicles per unit time. This is highly useful for samples with a more dilute concentration of particles, for example, urine. An alternative to the multinode system presented herein could be multiple single-node trapping regions in series; however, the benefits of using a larger single trapping zone with multiple nodes become evident in the vastly increased flow rate offered. Furthermore, a system with multiple parallel trapping capillaries could possibly match the throughput of the multinode system, but the increased complexity in terms of driving electronics and associated costs of multiple trapping units as well as electronic circuitry makes it a less attractive alternative.

A flow rate of 500 μL/min was considered a good compromise between throughput and trapping efficiency and was chosen as the operating flow rate for further experiments with biological fluids.

Extracellular Vesicles from Urine Samples. After the trapping performance had been evaluated with 500 nm PS beads, we investigated the potential for trapping extracellular vesicles from the urine samples, using the optimized settings from above. Urine from a healthy donor (1, 2, and 3 mL) was processed in the trap and the particle content was evaluated using nanoparticle tracking analysis (NTA; Figure 6a,b), and the vesicle RNA content was measured using an Agilent mRNA Pico Chip in a bioanalyzer (Agilent 2100 Bioanalyzer System) (Figure 6c,d).

The NTA measurements showed a clear peak of EVs at 89 nm (Figure 6a), and the amount of trapped EVs increased with increasing input sample volume (Figure 6b). On average, 0.86×10^9 EVs were trapped from 3 mL of urine. It can be observed that the sizes of the captured EVs were within the exosomal size range. The increase in trapped EVs was however not proportional to the input volume. Increasing the input sample from 1 to 3 mL only yielded a 45% increase in trapped EVs. An explanation for this could be that the trapping efficiency of particles might not be constant over time and we hypothesize that the system displays a higher trapping efficiency for the first fraction of a sample passing through the trap and as the seed trapping cluster fills with particles, the trapping efficiency drops correspondingly.

Further, Figure 6c illustrates the results of the bioanalyzer, with a peak in EV-derived RNA sequences at about 200 nucleotides in length, and Figure 6d gives the total amount of extracted RNA. As expected, processing a larger sample yielded an increased amount of intravesicular RNA. It should be noted that the samples were treated with RNase before the vesicles were lysed to eliminate any free-floating RNA from the samples. This ensured that all of the detected RNA originated from the internal vesicle cargo. On average, 3 mL of urine yielded 2 ng of purified intravesicular RNA. Similar to Figure 6b, the amount of recovered RNA did not increase proportionally with the increased input volume. Here, it is also seen that the increase in the input sample volume from 1 to 3 mL increased the RNA yield by 45%.

Our multinodal device trapped extracellular vesicles from urine at a flow rate of 500 μL/min. The total processing time for 3 mL of urine, including loading of seed particles, washing, and eluting, was 12 min and yielded 2 ng of intravesicular RNA. This can be compared with results from Ku et al.,[10] who in a similar study, using a single-node system, isolated extracellular vesicles from the urine samples. They managed to isolate 0.79 ng of RNA from 9.75 mL of urine in approximately 20 h, operating at a flow rate of 15 μL/min and pooling EVs from 11 trapping rounds.

Capturing Extracellular Vesicles for Mass Spectrometry. To evaluate how the enriched population of EVs differed in the protein content compared to non-trapped urine, we subjected the trapped and non-trapped samples to quantitative mass spectrometry analysis (Figure 7).

https://dx.doi.org/10.1021/acs.analchem.0c04772
Anal. Chem. 2021, 93, 3929−3937

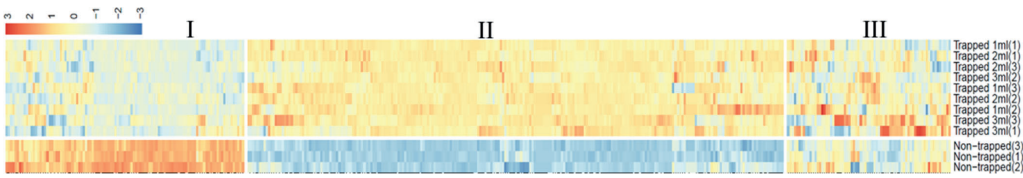

Figure 7. Heatmap of proteins found in trapped urine samples versus non-trapped urine samples. Keratin proteins have been removed. The heatmap is column-normalized and the legend gives the *z*-score of each sample. Cluster I shows weaker signals in the trapped fraction, suggesting that these are solute proteins that have been washed away from the trap during the washing step. Cluster II shows stronger signals in the trapped fraction, suggesting that these are proteins originating from vesicles that have been enriched during the trapping step. Cluster III shows highly fluctuating signals, indicating that these are proteins that are close to the limit of detection.

The subsequent MS analysis revealed substantial differences between the trapped samples and the non-trapped samples (Figure 7). In contrast, there were only minor differences in the protein content between the varying sample volumes. Visualizing the relative protein quantities in a column-normalized heatmap reveals three distinct protein clusters. Protein cluster I contains proteins found in higher abundance in the non-trapped samples, suggesting that these proteins are not associated with EVs and are washed away during the washing step of the trapping sequence. Proteins with stronger intensities in the trapped samples are found in cluster II and represent proteins that are associated with the EVs that have been enriched during the trapping step. Cluster III contains proteins with a higher degree of variability, due to partial or weak association with the EVs. The limited differences in the protein content for the different volumes of trapped urine are expected since the same amount of the starting material (0.5 μg) was injected for mass spectrometry analysis. Additionally, the data for each injection has been TIC-normalized (total ion current) to account for any differences in the amount of the peptide injected. Trapping more of the same urine sample should not change the type or ratio of the protein being captured; it should only change the amount of the protein captured. For a detailed heatmap where individual proteins can be seen, please see Supporting Information.

An important parameter for quantitative proteomics analysis is reproducible sample preparation. To investigate the degree of reproducibility, we plotted the relative standard deviation (RSD) for all proteins (Figure 8). The trapping resulted in a slight increase of the mean RSD from 10 and 20%. Importantly, the vast majority of the proteins have an RSD below 50%, which shows that the trapping only has a minor impact on reproducibility. We conclude that the sample preparation does not introduce a large increase in RSD, which is an important aspect for future quantitative proteomics comparisons for trapped EVs.

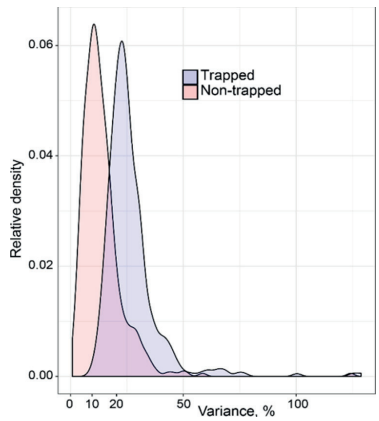

Figure 8. Variance of the content of individual proteins for the trapped samples and the non-trapped samples.

CONCLUSIONS

In this study, we have presented a novel acoustic trapping device that supports a multinode resonance mode. Our results showed that the multinodal acoustic trap had significantly increased trapping capacity and throughput as compared to existing single-node systems. The multinode trap was able to capture extracellular vesicles in the exosome size range and could process 1−3 mL samples in the order of 8−12 min. The amount of isolated intravesicular RNA was in the low ng range. The MS proteomic analysis of proteins derived from the acoustically trapped samples displayed a significantly different protein expression profile as compared to the corresponding protein profile derived from the non-trapped urine samples. In comparison to other reports on microfluidic EV isolation, the throughput reported using multinodal acoustic trapping stands out. When comparing to more conventional EV isolation techniques, such as density gradient centrifugation, ultracentrifugation, ultrafiltration, immunoaffinity isolation, precipitation, and field flow fractionation, these fall short in the many hour-long processing times. An effort to present the performance of different EV isolation techniques was given by Wu et al.[46] The new multinodal trapping system opens up for rapid, noncontact, and label-free EV isolation from biofluids that may pave the way for automated biomarker profiling in clinical samples.

ASSOCIATED CONTENT

Supporting Information

The Supporting Information is available free of charge at https://pubs.acs.org/doi/10.1021/acs.analchem.0c04772.

Detailed heatmap comparing protein profiles in urine samples versus urinary EVs isolated by the new trapping platform (PDF)

Original MS data and a list of all identified proteins (XLSX)

AUTHOR INFORMATION

Corresponding Author

Axel Broman − *Department of Biomedical Engineering, Faculty of Engineering, Lund University, 221 84 Lund, Sweden;*

https://dx.doi.org/10.1021/acs.analchem.0c04772
Anal. Chem. 2021, 93, 3929−3937

orcid.org/0000-0002-2500-701X; Email: axel.broman@bme.lth.se

Authors

Andreas Lenshof − *Department of Biomedical Engineering, Faculty of Engineering, Lund University, 221 84 Lund, Sweden*

Mikael Evander − *Department of Biomedical Engineering, Faculty of Engineering, Lund University, 221 84 Lund, Sweden*

Lotta Happonen − *Department of Clinical Sciences, Infection Medicine, Faculty of Medicine, Lund University, 221 84 Lund, Sweden*

Anson Ku − *Department of Laboratory Medicine, Faculty of Medicine, Lund University, 222 42 Lund, Sweden;* orcid.org/0000-0002-6471-5502

Johan Malmström − *Department of Clinical Sciences, Infection Medicine, Faculty of Medicine, Lund University, 221 84 Lund, Sweden*

Thomas Laurell − *Department of Biomedical Engineering, Faculty of Engineering, Lund University, 221 84 Lund, Sweden*

Complete contact information is available at: https://pubs.acs.org/10.1021/acs.analchem.0c04772

Notes

The authors declare the following competing financial interest(s): Thomas Laurell is a founder and owns stock in AcouSort AB, and Mikael Evander and Andreas Lenshof own stock in AcouSort AB. AcouSort AB is a spin-off company from Lund University that manufactures and markets acoustofluidic technology.

■ ACKNOWLEDGMENTS

This paper was supported by the Swedish Research Council (Grant Nos. 2019-00795 and 2018-03672), the Swedish Research Council (project 2018-05795), and the Swedish Foundation for Strategic Research (Grant No. SBE13-0049).

■ REFERENCES

(1) Vlassov, A. V.; Magdaleno, S.; Setterquist, R.; Conrad, R. *Biochim. Biophys. Acta, Gen. Subj.* **2012**, *1820*, 940−948.
(2) Théry, C. *F1000 Biol. Rep.* **2011**, *3*, 15.
(3) Raposo, G.; Stoorvogel, W. *J. Cell Biol.* **2013**, *200*, 373−383.
(4) Lobb, R. J.; Becker, M.; Wen, S. W.; Wong, C. S. F.; Wiegmans, A. P.; Leimgruber, A.; Moller, A. *J. Extracell. Vesicles* **2015**, *4*, No. 27031.
(5) Cvjetkovic, A.; Lotvall, J.; Lasser, C. *J. Extracell. Vesicles* **2014**, *3*, No. 23111.
(6) Campoy, I.; Lanau, L.; Altadill, T.; Sequeiros, T.; Cabrera, S.; Cubo-Abert, M.; Perez-Benavente, A.; Garcia, A.; Borros, S.; Santamaria, A.; Ponce, J.; Matias-Guiu, X.; Reventos, J.; Gil-Moreno, A.; Rigau, M.; Colas, E. *J. Transl. Med.* **2016**, *14*, No. 180.
(7) Van Deun, J.; Mestdagh, P.; Sormunen, R.; Cocquyt, V.; Vermaelen, K.; Vandesompele, J.; Bracke, M.; De Wever, O.; Hendrix, A. *J. Extracell. Vesicles* **2014**, *3*, No. 24858.
(8) Sunkara, V.; Woo, H. K.; Cho, Y. K. *Analyst* **2016**, *141*, 371−381.
(9) Linares, R.; Tan, S.; Gounou, C.; Arraud, N.; Brisson, A. R. *J. Extracell. Vesicles* **2015**, *4*, No. 29509.
(10) Ku, A.; Ravi, N.; Yang, M. J.; Evander, M.; Laurell, T.; Lilja, H.; Ceder, Y. *PLoS One* **2019**, *14*, No. e0224604.
(11) Wunsch, B. H.; Smith, J. T.; Gifford, S. M.; Wang, C.; Brink, M.; Bruce, R. L.; Austin, R. H.; Stolovitzky, G.; Astier, Y. *Nat. Nanotechnol.* **2016**, *11*, 936−940.
(12) Wang, J.; Li, W.; Zhang, L.; Ban, L.; Chen, P.; Du, W.; Feng, X.; Liu, B. F. *ACS Appl. Mater. Interfaces* **2017**, *9*, 27441−27452.
(13) Zhao, Z.; Yang, Y.; Zeng, Y.; He, M. *Lab Chip* **2016**, *16*, 489−496.
(14) Ayala-Mar, S.; Perez-Gonzalez, V. H.; Mata-Gomez, M. A.; Gallo-Villanueva, R. C.; Gonzalez-Valdez, J. *Anal. Chem.* **2019**, *91*, 14975−14982.
(15) Liu, C.; Guo, J. Y.; Tian, F.; Yang, N.; Yan, F. S.; Ding, Y. P.; Wei, J. Y.; Hu, G. Q.; Nie, G. J.; Sun, J. S. *ACS Nano* **2017**, *11*, 6968−6976.
(16) Wang, Z. Y.; Li, F.; Rufo, J.; Chen, C. Y.; Yang, S. J.; Li, L.; Zhang, J. X.; Cheng, J.; Kim, Y.; Wu, M. X.; Abemayor, E.; Tu, M.; Chia, D.; Spruce, R.; Batis, N.; Mehanna, H.; Wong, D. T. W.; Huang, T. J. *J. Mol. Diagn.* **2020**, *22*, 50−59.
(17) Evander, M.; Gidlof, O.; Olde, B.; Erlinge, D.; Laurell, T. *Lab Chip* **2015**, *15*, 2588−2596.
(18) Evander, M.; Johansson, L.; Lilliehorn, T.; Piskur, J.; Lindvall, M.; Johansson, S.; Almqvist, M.; Laurell, T.; Nilsson, J. *Anal. Chem.* **2007**, *79*, 2984−2991.
(19) Lilliehorn, T.; Simu, U.; Nilsson, M.; Almqvist, M.; Stepinski, T.; Laurell, T.; Nilsson, J.; Johansson, S. *Ultrasonics* **2005**, *43*, 293−303.
(20) Hammarström, B.; Laurell, T.; Nilsson, J. *Lab Chip* **2012**, *12*, 4296−4304.
(21) Rosa-Fernandes, L.; Rocha, V. B.; Carregari, V. C.; Urbani, A.; Palmisano, G. *Front. Chem.* **2017**, *5*, 102.
(22) Rezeli, M.; Gidlof, O.; Evander, M.; Bryl-Gorecka, P.; Sathanoori, R.; Gilje, P.; Pawlowski, K.; Horvatovich, P.; Erlinge, D.; Marko-Varga, G.; Laurell, T. *Anal. Chem.* **2016**, *88*, 8577−8586.
(23) Ku, A.; Lim, H. C.; Evander, M.; Lilja, H.; Laurell, T.; Scheding, S.; Ceder, Y. *Anal. Chem.* **2018**, *90*, 8011−8019.
(24) Habibi, R.; Neild, A. *Lab Chip* **2019**, *19*, 3032−3044.
(25) Habibi, R.; He, V.; Ghavamian, S.; de Marco, A.; Lee, T. H.; Aguilar, M. I.; Zhu, D. D.; Lim, R.; Neild, A. *Lab Chip* **2020**, *20*, 3633−3643.
(26) Gorkov, L. P. *Dokl. Akad. Nauk SSSR* **1961**, *140*, 88−91.
(27) Whitworth, G.; Grundy, M. A.; Coakley, W. T. *Ultrasonics* **1991**, *29*, 439−444.
(28) Crum, L. A. *J. Acoust. Soc. Am.* **1975**, *57*, 1363−1370.
(29) Weiser, M. A. H.; Apfel, R. E.; Neppiras, E. A. *Acustica* **1984**, *56*, 114−119.
(30) Groschl, M. *Acustica* **1998**, *84*, 432−447.
(31) Laurell, T.; Lenshof, A. *Microscale Acoustofluidics*; Royal Society of Chemistry, 2015; pp 72−73.
(32) Ley, M. W. H.; Bruus, H. *Phys. Rev. Appl.* **2017**, *8*, No. 024020.
(33) Woodside, S. M.; Bowen, B. D.; Piret, J. M. *AIChE J.* **1997**, *43*, 1727−1736.
(34) Hammarström, B.; Evander, M.; Wahlstrom, J.; Nilsson, J. *Lab Chip* **2014**, *14*, 1005−1013.
(35) Teleman, J.; Dowsey, A. W.; Gonzalez-Galarza, F. F.; Perkins, S.; Pratt, B.; Rost, H. L.; Malmstrom, L.; Malmstrom, J.; Jones, A. R.; Deutsch, E. W.; Levander, F. *Mol. Cell. Proteomics* **2014**, *13*, 1537−1542.
(36) Chambers, M. C.; Maclean, B.; Burke, R.; Amodei, D.; Ruderman, D. L.; Neumann, S.; Gatto, L.; Fischer, B.; Pratt, B.; Egertson, J.; Hoff, K.; Kessner, D.; Tasman, N.; Shulman, N.; Frewen, B.; Baker, T. A.; Brusniak, M. Y.; Paulse, C.; Creasy, D.; Flashner, L.; Kani, K.; Moulding, C.; Seymour, S. L.; Nuwaysir, L. M.; Lefebvre, B.; Kuhlmann, F.; Roark, J.; Rainer, P.; Detlev, S.; Hemenway, T.; Huhmer, A.; Langridge, J.; Connolly, B.; Chadick, T.; Holly, K.; Eckels, J.; Deutsch, E. W.; Moritz, R. L.; Katz, J. E.; Agus, D. B.; MacCoss, M.; Tabb, D. L.; Mallick, P. *Nat. Biotechnol.* **2012**, *30*, 918−920.
(37) Bauch, A.; Adamczyk, I.; Buczek, P.; Elmer, F. J.; Enimanev, K.; Glyzewski, P.; Kohler, M.; Pylak, T.; Quandt, A.; Ramakrishnan, C.; Beisel, C.; Malmstrom, L.; Aebersold, R.; Rinn, B. *BMC Bioinf.* **2011**, *12*, 468.
(38) Craig, R.; Beavis, R. C. *Rapid Commun. Mass Spectrom.* **2003**, *17*, 2310−2316.
(39) Geer, L. Y.; Markey, S. P.; Kowalak, J. A.; Wagner, L.; Xu, M.; Maynard, D. M.; Yang, X.; Shi, W.; Bryant, S. H. *J. Proteome Res.* **2004**, *3*, 958−964.
(40) Eng, J. K.; Jahan, T. A.; Hoopmann, M. R. *Proteomics* **2013**, *13*, 22−24.
(41) Keller, A.; Nesvizhskii, A. I.; Kolker, E.; Aebersold, R. *Anal. Chem.* **2002**, *74*, 5383−5392.

(42) Röst, H. L.; Rosenberger, G.; Navarro, P.; Gillet, L.; Miladinovic, S. M.; Schubert, O. T.; Wolski, W.; Collins, B. C.; Malmstrom, J.; Malmstrom, L.; Aebersold, R. *Nat. Biotechnol.* **2014**, *32*, 219−223.
(43) Lam, H.; Deutsch, E. W.; Eddes, J. S.; Eng, J. K.; Stein, S. E.; Aebersold, R. *Nat. Methods* **2008**, *5*, 873−875.
(44) Röst, H. L.; Liu, Y.; D'Agostino, G.; Zanella, M.; Navarro, P.; Rosenberger, G.; Collins, B. C.; Gillet, L.; Testa, G.; Malmstrom, L.; Aebersold, R. *Nat. Methods* **2016**, *13*, 777−783.
(45) Personal communication with AcouSort AB. 2020.
(46) Wu, M.; Ozcelik, A.; Rufo, J.; Wang, Z.; Fang, R.; Jun Huang, T. *Microsyst. Nanoeng.* **2019**, *5*, 32.

https://dx.doi.org/10.1021/acs.analchem.0c04772
Anal. Chem. 2021, 93, 3929−3937

Supporting Information

Multinodal acoustic trapping enables high capacity and high throughput enrichment of extracellular vesicles and microparticles in miRNA and MS proteomics studies

Axel Broman[1*], Andreas Lenshof[1], Mikael Evander[1], Lotta Happonen[2], Anson Ku[3], Johan Malmström[2] and Thomas Laurell[1]

[1] *Lund University, Faculty of Engineering, Department of Biomedical Engineering, Sweden*

[2] *Lund University, Faculty of Medicine, Department of Clinical Sciences, Infection Medicine, Sweden*

[3] *Lund University, Faculty of Medicine, Department Laboratory Medicine, Sweden*

**Corresponding author: axel.broman@bme.lth.se*

Table of Contents

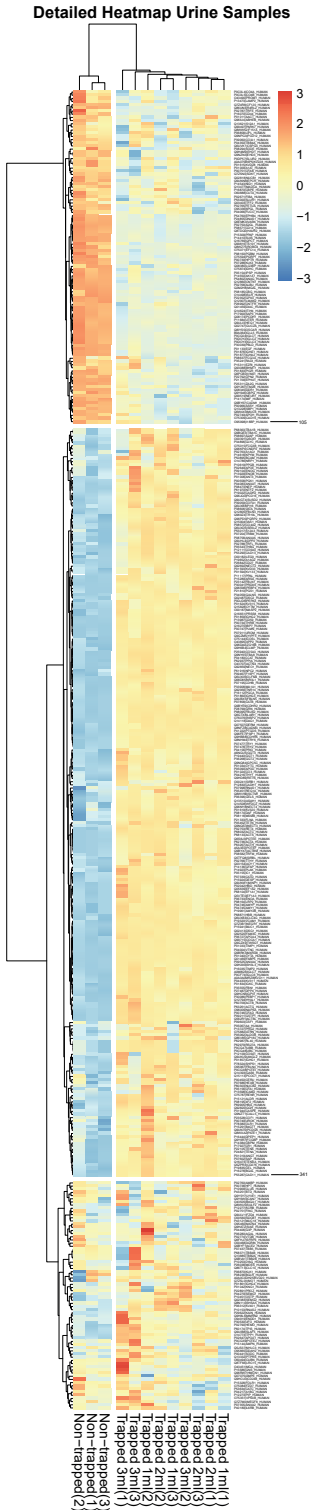

Figure S1: Detailed version of figure 7. Heatmap of proteins found in trapped urine samples versus non-trapped. Keratin proteins have been removed. The heatmap is row-normalized and the legend gives the z-score of each sample.

Table S1. List of proteins from heatmap in order from top to bottom.

Number	Uniprot ID	Uniprot Entry name
1	P0C0L4	CO4A_HUMAN
2	P0C0L5	CO4B_HUMAN
3	O43490	PROM1_HUMAN
4	P13473	LAMP2_HUMAN
5	Q7Z4R8	CF120_HUMAN
6	Q86UN3	R4RL2_HUMAN
7	P02787	TRFE_HUMAN
8	P16070	CD44_HUMAN
9	P01011	AACT_HUMAN
10	Q96IU4	ABHEB_HUMAN
11	Q13621	S12A1_HUMAN
12	Q99497	PARK7_HUMAN
13	Q8WW52	F151A_HUMAN
14	P06858	LIPL_HUMAN
15	Q9NPG4	PCD12_HUMAN
16	P39060	COIA1_HUMAN
17	P04350	TBB4A_HUMAN
18	Q6UVK1	CSPG4_HUMAN
19	P08294	SODE_HUMAN
20	Q9H4M9	EHD1_HUMAN
21	Q9NZN3	EHD3_HUMAN
22	P0DP57	SLUR2_HUMAN
23	A0A075B6P5	KV228_HUMAN
24	P01615	KVD28_HUMAN
25	P01009	A1AT_HUMAN
26	P00751	CFAB_HUMAN
27	Q7Z5N4	SDK1_HUMAN
28	Q02818	NUCB1_HUMAN
29	Q9UNN8	EPCR_HUMAN
30	P14543	NID1_HUMAN
31	Q13477	MADCA_HUMAN
32	P16870	CBPE_HUMAN
33	O60888	CUTA_HUMAN
34	P02671	FIBA_HUMAN
35	P55000	SLUR1_HUMAN
36	Q03403	TFF2_HUMAN
37	P02765	FETUA_HUMAN
38	O95336	6PGL_HUMAN
39	P04066	FUCO_HUMAN
40	P54760	EPHB4_HUMAN
41	P24855	DNAS1_HUMAN
42	Q6EMK4	VASN_HUMAN
43	P02750	A2GL_HUMAN
44	P08571	CD14_HUMAN
45	Q8TDQ0	HAVR2_HUMAN
46	P15309	PPAP_HUMAN
47	P14410	SUIS_HUMAN
48	Q16769	QPCT_HUMAN
49	Q99816	TS101_HUMAN
50	Q8WZ75	ROBO4_HUMAN
51	O75071	EFC14_HUMAN
52	P98160	PGBM_HUMAN
53	O75594	PGRP1_HUMAN
54	P00739	HPTR_HUMAN
55	P07288	KLK3_HUMAN
56	Q08380	LG3BP_HUMAN
57	O75874	IDHC_HUMAN
58	P05154	IPSP_HUMAN
59	P14550	AK1A1_HUMAN
60	P54802	ANAG_HUMAN
61	Q12860	CNTN1_HUMAN
62	P02768	ALBU_HUMAN
63	Q2M2H8	MGAL_HUMAN
64	P08185	CBG_HUMAN
65	O14498	ISLR_HUMAN
66	P22352	GPX3_HUMAN
67	Q12907	LMAN2_HUMAN

68	P26992	CNTFR_HUMAN
69	Q01459	DIAC_HUMAN
70	Q14624	ITIH4_HUMAN
71	P17900	SAP3_HUMAN
72	Q08174	PCDH1_HUMAN
73	P11684	UTER_HUMAN
74	Q9ULI3	HEG1_HUMAN
75	Q02747	GUC2A_HUMAN
76	Q8IYS5	OSCAR_HUMAN
77	B9A064	IGLL5_HUMAN
78	P0CG04	IGLC1_HUMAN
79	P0DOY2	IGLC2_HUMAN
80	P0DOY3	IGLC3_HUMAN
81	P30039	PBLD_HUMAN
82	P01133	EGF_HUMAN
83	P01876	IGHA1_HUMAN
84	P01877	IGHA2_HUMAN
85	P08637	FCG3A_HUMAN
86	P35241	RADI_HUMAN
87	P15311	EZRI_HUMAN
88	Q93088	BHMT1_HUMAN
89	P01833	PIGR_HUMAN
90	Q6PCB0	VWA1_HUMAN
91	P22792	CPN2_HUMAN
92	P21709	EPHA1_HUMAN
93	P25311	ZA2G_HUMAN
94	Q9Y287	ITM2B_HUMAN
95	Q08345	DDR1_HUMAN
96	Q9Y646	CBPQ_HUMAN
97	Q99519	NEUR1_HUMAN
98	P14174	MIF_HUMAN
99	Q9BY67	CADM1_HUMAN
100	P00966	ASSY_HUMAN
101	Q13228	SBP1_HUMAN
102	Q6W4X9	MUC6_HUMAN
103	P02749	APOH_HUMAN

104	O75309	CAD16_HUMAN
105	O95998	I18BP_HUMAN
106	P68363	TBA1B_HUMAN
107	Q9BQE3	TBA1C_HUMAN
108	P08697	A2AP_HUMAN
109	O00391	QSOX1_HUMAN
110	P34896	GLYC_HUMAN
111	O75015	FCG3B_HUMAN
112	Q96KP4	CNDP2_HUMAN
113	P02763	A1AG1_HUMAN
114	P14618	KPYM_HUMAN
115	P50895	BCAM_HUMAN
116	O14786	NRP1_HUMAN
117	P10619	PPGB_HUMAN
118	P02649	APOE_HUMAN
119	P09104	ENOG_HUMAN
120	P13929	ENOB_HUMAN
121	P01008	ANT3_HUMAN
122	P00558	PGK1_HUMAN
123	P04083	ANXA1_HUMAN
124	P08473	NEP_HUMAN
125	P61970	NTF2_HUMAN
126	P19022	CADH2_HUMAN
127	Q96JQ0	PCD16_HUMAN
128	Q9UGT4	SUSD2_HUMAN
129	P39059	COFA1_HUMAN
130	Q6UXB8	PI16_HUMAN
131	P38606	VATA_HUMAN
132	Q12805	FBLN3_HUMAN
133	Q969Z4	TR19L_HUMAN
134	Q96PD5	PGRP2_HUMAN
135	Q15904	VAS1_HUMAN
136	P08572	CO4A2_HUMAN
137	Q6UXD5	SE6L2_HUMAN
138	P55017	S12A3_HUMAN
139	P07204	TRBM_HUMAN

140	P08758	ANXA5_HUMAN
141	Q9UHL4	DPP2_HUMAN
142	P02788	TRFL_HUMAN
143	P05543	THBG_HUMAN
144	P12111	CO6A3_HUMAN
145	P55290	CAD13_HUMAN
146	O00182	LEG9_HUMAN
147	P19652	A1AG2_HUMAN
148	P26842	CD27_HUMAN
149	Q92692	NECT2_HUMAN
150	P01593	KVD33_HUMAN
151	P01594	KV133_HUMAN
152	P11117	PPAL_HUMAN
153	P15289	ARSA_HUMAN
154	P23142	FBLN1_HUMAN
155	P30041	PRDX6_HUMAN
156	Q96S96	PEBP4_HUMAN
157	P21810	PGS1_HUMAN
158	P34059	GALNS_HUMAN
159	Q02487	DSC2_HUMAN
160	P0DJD8	PEPA3_HUMAN
161	P01624	KV315_HUMAN
162	Q15828	CYTM_HUMAN
163	O00187	MASP2_HUMAN
164	Q16651	PRSS8_HUMAN
165	P01859	IGHG2_HUMAN
166	P13987	CD59_HUMAN
167	P00734	THRB_HUMAN
168	Q16270	IBP7_HUMAN
169	P00747	PLMN_HUMAN
170	P07911	UROM_HUMAN
171	Q9GZM5	YIPF3_HUMAN
172	O75144	ICOSL_HUMAN
173	O43895	XPP2_HUMAN
174	Q96DA0	ZG16B_HUMAN
175	Q9H6B4	CLMP_HUMAN

176	P25940	CO5A3_HUMAN
177	Q9NY65	TBA8_HUMAN
178	P04180	LCAT_HUMAN
179	P62937	PPIA_HUMAN
180	O43707	ACTN4_HUMAN
181	Q92859	NEO1_HUMAN
182	P61916	NPC2_HUMAN
183	P09467	F16P1_HUMAN
184	Q6UX06	OLFM4_HUMAN
185	Q68D85	NR3L1_HUMAN
186	P07195	LDHB_HUMAN
187	P33908	MA1A1_HUMAN
188	Q92956	TNR14_HUMAN
189	P16112	PGCA_HUMAN
190	P01860	IGHG3_HUMAN
191	Q9UBX5	FBLN5_HUMAN
192	P07858	CATB_HUMAN
193	Q9BYE9	CDHR2_HUMAN
194	P28799	GRN_HUMAN
195	P98095	FBLN2_HUMAN
196	Q6GTX8	LAIR1_HUMAN
197	O76076	WISP2_HUMAN
198	Q14118	DAG1_HUMAN
199	Q07507	DERM_HUMAN
200	Q8NFZ8	CADM4_HUMAN
201	P41222	PTGDS_HUMAN
202	Q96FE7	P3IP1_HUMAN
203	Q9HBB8	CDHR5_HUMAN
204	Q8NHM4	TRY6_HUMAN
205	P07477	TRY1_HUMAN
206	P07478	TRY2_HUMAN
207	P04156	PRIO_HUMAN
208	A6NGU5	GGT3_HUMAN
209	P19440	GGT1_HUMAN
210	P36268	GGT2_HUMAN
211	Q9NQ84	GPC5C_HUMAN

212	P01034	CYTC_HUMAN
213	P05090	APOD_HUMAN
214	P01024	CO3_HUMAN
215	P04216	THY1_HUMAN
216	Q9HD89	RETN_HUMAN
217	O00241	SIRB1_HUMAN
218	P12830	CADH1_HUMAN
219	P07998	RNAS1_HUMAN
220	P05451	REG1A_HUMAN
221	Q8WVN6	SCTM1_HUMAN
222	P06396	GELS_HUMAN
223	Q13510	ASAH1_HUMAN
224	Q14508	WFDC2_HUMAN
225	Q96NY8	NECT4_HUMAN
226	P01619	KV320_HUMAN
227	P08174	DAF_HUMAN
228	P08118	MSMB_HUMAN
229	P21333	FLNA_HUMAN
230	P05452	TETN_HUMAN
231	Q9NQS3	NECT3_HUMAN
232	P02753	RET4_HUMAN
233	P68032	ACTC_HUMAN
234	P68133	ACTS_HUMAN
235	Q6S8J3	POTEE_HUMAN
236	P62736	ACTA_HUMAN
237	P63267	ACTH_HUMAN
238	A5A3E0	POTEF_HUMAN
239	Q9BYX7	ACTBM_HUMAN
240	P08582	TRFM_HUMAN
241	Q5TFQ8	SIRBL_HUMAN
242	P02766	TTHY_HUMAN
243	Q03154	ACY1_HUMAN
244	P14136	GFAP_HUMAN
245	P14923	PLAK_HUMAN
246	P05155	IC1_HUMAN
247	P07339	CATD_HUMAN

248	P15924	DESP_HUMAN
249	Q9UNW1	MINP1_HUMAN
250	P02042	HBD_HUMAN
251	Q05639	EF1A2_HUMAN
252	P68104	EF1A1_HUMAN
253	Q5VTE0	EF1A3_HUMAN
254	P06733	ENOA_HUMAN
255	P98164	LRP2_HUMAN
256	P04746	AMYP_HUMAN
257	P04745	AMY1_HUMAN
258	P19961	AMY2B_HUMAN
259	P68871	HBB_HUMAN
260	Q6UXB4	CLC4G_HUMAN
261	P19320	VCAM1_HUMAN
262	Q7Z3B1	NEGR1_HUMAN
263	P15941	MUC1_HUMAN
264	Q02413	DSG1_HUMAN
265	Q92520	FAM3C_HUMAN
266	P06727	APOA4_HUMAN
267	Q99715	COCA1_HUMAN
268	Q9GZX9	TWSG1_HUMAN
269	P01033	TIMP1_HUMAN
270	P04004	VTNC_HUMAN
271	Q9BRK3	MXRA8_HUMAN
272	P01040	CYTA_HUMAN
273	Q01469	FABP5_HUMAN
274	P09525	ANXA4_HUMAN
275	Q9H299	SH3L3_HUMAN
276	P16035	TIMP2_HUMAN
277	A0M8Q6	IGLC7_HUMAN
278	P0CF74	IGLC6_HUMAN
279	A0A0A0MRZ8	KVD11_HUMAN
280	P04433	KV311_HUMAN
281	P01834	IGKC_HUMAN
282	P35555	FBN1_HUMAN
283	P27487	DPP4_HUMAN

284	Q9HCN6	GPVI_HUMAN
285	P30086	PEBP1_HUMAN
286	Q12794	HYAL1_HUMAN
287	P60709	ACTB_HUMAN
288	P63261	ACTG_HUMAN
289	O96009	NAPSA_HUMAN
290	P00746	CFAD_HUMAN
291	P09211	GSTP1_HUMAN
292	Q562R1	ACTBL_HUMAN
293	P09603	CSF1_HUMAN
294	P05067	A4_HUMAN
295	P13727	PRG2_HUMAN
296	O75882	ATRN_HUMAN
297	P05062	ALDOB_HUMAN
298	Q86V85	GP180_HUMAN
299	P62987	RL40_HUMAN
300	P62979	RS27A_HUMAN
301	P0CG47	UBB_HUMAN
302	P0CG48	UBC_HUMAN
303	P12109	CO6A1_HUMAN
304	Q9UKU9	ANGL2_HUMAN
305	P01857	IGHG1_HUMAN
306	P78324	SHPS1_HUMAN
307	O95967	FBLN4_HUMAN
308	P0CG38	POTEI_HUMAN
309	Q14393	GAS6_HUMAN
310	Q15113	PCOC1_HUMAN
311	P00450	CERU_HUMAN
312	P07686	HEXB_HUMAN
313	P80303	NUCB2_HUMAN
314	P05156	CFAI_HUMAN
315	P13598	ICAM2_HUMAN
316	O75787	RENR_HUMAN
317	P15121	ALDR_HUMAN
318	P08195	4F2_HUMAN
319	P69905	HBA_HUMAN

320	Q92820	GGH_HUMAN
321	P31944	CASPE_HUMAN
322	Q9NZT1	CALL5_HUMAN
323	P23528	COF1_HUMAN
324	P00749	UROK_HUMAN
325	P78380	OLR1_HUMAN
326	P15291	B4GT1_HUMAN
327	Q9UN70	PCDGK_HUMAN
328	Q8WXA2	PATE1_HUMAN
329	P16444	DPEP1_HUMAN
330	Q9Y6R7	FCGBP_HUMAN
331	P14384	CBPM_HUMAN
332	P17927	CR1_HUMAN
333	P22105	TENX_HUMAN
334	P24821	TENA_HUMAN
335	P01019	ANGT_HUMAN
336	P07602	SAP_HUMAN
337	Q16473	TENXA_HUMAN
338	Q5ZPR3	CD276_HUMAN
339	P19835	CEL_HUMAN
340	P16278	BGAL_HUMAN
341	P55287	CAD11_HUMAN
342	P02760	AMBP_HUMAN
343	P00738	HPT_HUMAN
344	P10909	CLUS_HUMAN
345	P43251	BTD_HUMAN
346	Q9Y5Y7	LYVE1_HUMAN
347	Q9Y6W3	CAN7_HUMAN
348	O43505	B4GA1_HUMAN
349	Q8IWU5	SULF2_HUMAN
350	P12277	KCRB_HUMAN
351	P02751	FINC_HUMAN
352	Q9ULV1	FZD4_HUMAN
353	O00560	SDCB1_HUMAN
354	P43121	MUC18_HUMAN
355	O95460	MATN4_HUMAN

356	Q9HAT2	SIAE_HUMAN
357	P04406	G3P_HUMAN
358	P06280	AGAL_HUMAN
359	P02774	VTDB_HUMAN
360	Q6FHJ7	SFRP4_HUMAN
361	O00468	AGRIN_HUMAN
362	Q9BYF1	ACE2_HUMAN
363	P07437	TBB5_HUMAN
364	P68371	TBB4B_HUMAN
365	Q13885	TBB2A_HUMAN
366	Q9BVA1	TBB2B_HUMAN
367	P10253	LYAG_HUMAN
368	P26038	MOES_HUMAN
369	Q86T13	CLC14_HUMAN
370	P06870	KLK1_HUMAN
371	P08236	BGLR_HUMAN
372	A0A0C4DH25	KVD20_HUMAN
373	Q7Z5L0	VMO1_HUMAN
374	P01861	IGHG4_HUMAN
375	P01042	KNG1_HUMAN
376	P22891	PROZ_HUMAN
377	P04279	SEMG1_HUMAN
378	P10451	OSTP_HUMAN
379	Q02383	SEMG2_HUMAN
380	Q8N114	SHSA5_HUMAN
381	P06312	KV401_HUMAN
382	P10153	RNAS2_HUMAN
383	P29622	KAIN_HUMAN
384	Q9H8L6	MMRN2_HUMAN
385	O94919	ENDD1_HUMAN
386	P30530	UFO_HUMAN
387	P02790	HEMO_HUMAN
388	P60174	TPIS_HUMAN
389	Q9UIB8	SLAF5_HUMAN
390	O14773	TPP1_HUMAN
391	P02647	APOA1_HUMAN
392	P0CG39	POTEJ_HUMAN
393	P15144	AMPN_HUMAN
394	Q5JS37	NHLC3_HUMAN
395	O95865	DDAH2_HUMAN
396	P00441	SODC_HUMAN
397	Q13332	PTPRS_HUMAN
398	O60494	CUBN_HUMAN
399	Q8TF66	LRC15_HUMAN
400	O43451	MGA_HUMAN
401	P15586	GNS_HUMAN
402	Q96RW7	HMCN1_HUMAN
403	Q07075	AMPE_HUMAN
404	Q9HCU0	CD248_HUMAN
405	P15328	FOLR1_HUMAN
406	O75084	FZD7_HUMAN
407	P53634	CATC_HUMAN
408	P04217	A1BG_HUMAN
409	P12273	PIP_HUMAN
410	O75351	VPS4B_HUMAN
411	Q7Z7M0	MEGF8_HUMAN
412	P07355	ANXA2_HUMAN
413	P40189	IL6RB_HUMAN

Paper II

Journal of Innate Immunity

Research Article

J Innate Immun 2023;15:599–613
DOI: 10.1159/000531266

Received: January 13, 2023
Accepted: May 23, 2023
Published online: May 27, 2023

Phenotypic Characterization of Acoustically Enriched Extracellular Vesicles from Pathogen-Activated Platelets

Frida Palm[a] Axel Broman[b] Genevieve Marcoux[c] John W. Semple[c, d, e] Thomas L. Laurell[b] Johan Malmström[a] Oonagh Shannon[a, f]

[a]Division of Infection Medicine, Department of Clinical Sciences, Lund, Lund University, Lund, Sweden; [b]Department of Biomedical Engineering, Lund University, Lund, Sweden; [c]Division of Hematology and Transfusion Medicine, Department of Laboratory Medicine, Lund University, Lund, Sweden; [d]Clinical Immunology and Transfusion Medicine, Office of Medical Services, Region Skåne, Lund, Sweden; [e]Department of Pharmacology and Toxicology, University of Toronto, Toronto, ON, Canada; [f]Section for Oral Biology and Pathology, Faculty of Odontology, Malmö University, Malmö, Sweden

Keywords
Platelets · Extracellular vesicles · Sepsis · Streptococcus

Abstract
Extracellular vesicles (EVs) are derived from the membrane of platelets and released into the circulation upon activation or injury. Analogous to the parent cell, platelet-derived EVs play an important role in hemostasis and immune responses by transfer of bioactive cargo from the parent cells. Platelet activation and release of EVs increase in several pathological inflammatory diseases, such as sepsis. We have previously reported that the M1 protein released from the bacterial pathogen *Streptococcus pyogenes* directly mediates platelet activation. In this study, EVs were isolated from these pathogen-activated platelets using acoustic trapping, and their inflammation phenotype was characterized using quantitative mass spectrometry-based proteomics and cell-based models of inflammation. We determined that M1 protein mediated release of platelet-derived EVs that contained the M1 protein. The isolated EVs derived from pathogen-activated platelets contained a similar protein cargo to those from physiologically activated platelets (thrombin) and included platelet membrane proteins, granule proteins, cytoskeletal proteins, coagulation factors, and immune mediators. Immunomodulatory cargo, complement proteins, and IgG3 were significantly enriched in EVs isolated from M1 protein-stimulated platelets. Acoustically enriched EVs were functionally intact and exhibited pro-inflammatory effects on addition to blood, including platelet-neutrophil complex formation, neutrophil activation, and cytokine release. Collectively, our findings reveal novel aspects of pathogen-mediated platelet activation during invasive streptococcal infection.

Introduction

Extracellular vesicles (EVs) are small vesicular bodies (30 nm–1 μm) that are derived from the cell membrane of various cells upon activation or injury, such as platelets,

Frida Palm and Axel Broman contributed equally to this work.

karger@karger.com
www.karger.com/jin

Correspondence to:
Oonagh Shannon, oonagh.shannon@med.lu.se

endothelial cells, erythrocytes, and leukocytes [1]. EVs can carry numerous bioactive molecules such as RNA, lipids, and proteins and typically present cell-specific surface antigens that reflect their cell of origin [2, 3]. EVs are continuously produced and found in all fluids of the human body but are most concentrated in the blood, where the majority (70–90%) of the circulating EVs are derived from platelets [4].

Platelets are the main regulators of hemostasis by prevention of bleeding and promotion of wound healing. This is achieved through the release of proteins and bioactive products from the platelet granules and upregulation of platelet surface receptors [5, 6]. Platelets have also been shown to become activated in response to infection and inflammation. Platelets interact with inflammation mediators, such as fibrinogen, IgG, and complement proteins [7], and directly modulate the function of other immune cells, including neutrophils and monocytes [5]. Platelet-derived EVs are also attributed an important role in maintaining hemostasis by provision of a binding surface for fibrinogen and coagulation factors [8]. The immunomodulatory effects of platelet-derived EVs are less investigated, but they can transfer bioactive cargo to immune cells, such as leukocytes, resulting in either activation or inhibition of leukocyte effector function [9]. Platelet-derived EVs also contribute to innate and adaptive immunity through antigen presentation via MHC-1 molecules and have access to the lymphoid organs and the bone marrow [10]. Circulating levels of EVs increase in several pathological states, such as thrombosis, rheumatoid arthritis, cancer, and sepsis [11, 12]. For example, platelet EV-derived mitochondrial damage-associated molecular patterns have been shown to enhance pro-inflammatory adverse reactions in transfusion recipients [13, 14]. The content and biological function of EVs may differ depending upon the agonist or conditions responsible for activation in distinct physiological or pathological scenarios [15, 16]; therefore, quantitative studies on the protein cargo of platelet-derived EVs may represent an important source of biomarkers of disease. The purpose of our study was to isolate and characterize EVs that may be released from pathogen-activated platelets during bacterial sepsis.

Sepsis is a life-threatening organ dysfunction caused by a dysregulated host response to infection [17]. The dual role of platelets in hemostasis and the immune response places them as key sentinels in the response to sepsis. *S. pyogenes* more commonly causes throat and skin infections; however, invasive disease such as sepsis is associated with distinct serotypes of the bacteria. The *emm1* serotype of *S. pyogenes* is the most commonly associated with invasive disease [18]. The surface-associated M1 protein of the *emm1* serotype contributes to evasion of the complement system and phagocytosis through interaction with several host plasma proteins: fibrinogen, albumin, the Fc-domain of IgG, and complement regulatory proteins [19]. The M1 protein can also be released from the bacterial surface to mediate activation of neutrophils, monocytes, and T cells [19]. We have previously demonstrated that M1 protein can activate platelets [20, 21] and stimulate platelet-leukocyte complex formation [22] as a result of the formation of immune complexes containing specific anti-M protein IgG and fibrinogen that engage with both the Fc- and the fibrinogen receptors on platelets incubated with fibrinogen-binding serotypes of M protein [20, 23–25].

A recently developed technology for isolating EVs is acoustic trapping, which utilizes an ultrasonic standing wave generated inside a microfluidic channel. Particles in the sound field that are denser and less compressible than the surrounding fluid will move to the pressure nodes in the field, where they can be retained against a flow [26]. In this way, acoustic trapping can be used for isolation, enrichment, and washing of EVs [27]. We recently reported on an acoustic trapping platform with significant improvements in throughput and capacity that enabled processing of milliliter sample volumes in minutes [28]. The decreased processing time and ability to work with small sample volumes, in combination with gentle forces, make acoustic trapping an attractive method for EV isolation as compared to conventional techniques such as ultracentrifugation.

In this work, we have applied an acoustic trapping platform to isolate platelet-derived EVs, with the aim of characterizing the EVs derived from plasma supernatants of pathogen (M1 protein)-stimulated platelets as compared with EVs from physiologically activated (resting or thrombin-activated) platelets. We applied quantitative mass spectrometry-based proteomics to characterize the protein cargo of enriched EV populations, and the functional integrity of acoustically enriched EVs was assessed in blood cell inflammation models.

Materials and Methods

Blood Collection and Preparation

Blood was collected from healthy donors into 0.1 M Na_3 citrate as an anticoagulant and centrifuged at 150 *g* for 15 min to obtain platelet-rich plasma (PRP). Informed consent was obtained from the donors prior to blood collection, and ethical approval was obtained from the Local Ethics Committee (approval 2015/801).

M1 Protein Purification

M1 protein was purified from the *S. pyogenes* mutant strain MC25, which lacks the cell wall-anchoring domain and secretes M1 protein into the supernatant, as previously described [20]. Briefly, MC25 bacteria were grown in Todd Hewitt broth with yeast, and proteins from the supernatant were precipitated with 80% $(NH_4)_2SO_4$. The precipitate was dialyzed against PBS and purified on Sepharose coupled with human fibrinogen. The M1 protein was eluted with 0.2 M glycine (pH 2.0) and dialyzed against PBS. Purified M1 protein was confirmed using SDS-PAGE.

Flow Cytometry for Determination of Platelet Activation

Flow cytometry was used to investigate platelet activation in response to M1 protein as previously described [21]. PRP from five healthy donors was diluted 2:3 in 1 mM HEPES buffer pH 7.4 and stimulated with M1 protein (2.5 μg/mL) for 15 min at room temperature. HEPES buffer alone was used to determine the background platelet activation, and the platelet agonist thrombin (1 U/mL, Triolab) was used as a positive control for platelet activation during hemostasis. The anticoagulant peptide Gly-Pro-Arg-Pro (1.25 mg/mL; Bachem) was added prior to stimulation with thrombin to prevent fibrin polymerization and coagulation. After stimulation, the samples were incubated with anti-CD62P-PE (1:10) (BD Biosciences, clone AC1.2) for 15 min at room temperature protected from light. Platelet counts were acquired on an Accuri C6 Plus flow cytometer (BD Biosciences), and the data were analyzed using C6 Plus Software. Platelets were gated based on size and granularity in logarithmic mode, and the CD62P intensity for the gated population was analyzed in histograms.

Isolation of EVs Using Acoustic Trapping

PRP from four healthy donors was stimulated with M1 protein (2.5 μg/mL), HEPES buffer alone, or thrombin (1 U/mL, Triolab), as described for flow cytometry. The samples were centrifuged at 1,600 *g* for 5 min, and the plasma supernatants, containing platelet-derived EVs, were processed on an acoustic trapping platform as previously described [28]. We have previously demonstrated that acoustic trapping generates equivalent populations of EVs as ultracentrifugation [29]. Briefly, an ultrasonic standing wave is generated in a glass capillary, and particles in the vicinity of the trap will move toward the pressure nodes of the standing wave, where they can be captured and retained against flow. By preloading the trap with large seed particles, submicron particles can be enriched through interaction with the seed particles [26]. This allows for isolation, enrichment, and washing of submicron particles, such as EVs. Prior to trapping, 400 μL of each plasma sample was diluted with D-PBS (Sigma-Aldrich) to 2,000 μL, yielding a concentration of 20% plasma. The trap was actuated at 12 V_{PP} (peak-to-peak) and loaded with 12 μm polystyrene seed particles (Sigma-Aldrich) to establish a seed particle cluster. The cluster was then washed with 1 mL PBS in order to remove excess seed particles. Sample was then run through the trap to isolate EVs in the seed particle cluster. While being held in the trap, the EVs were washed with 5 mL of PBS to remove background plasma proteins. Unless otherwise stated, the operating flowrate for all steps was 500 μL/min. Finally, the sound was turned off, and the cluster was allowed to sediment for 5 s to get closer to the exit, before it was eluted in a volume of 130 μL PBS at 5,000 μL/min. The isolated vesicles were then analyzed using flow cytometry and mass spectrometry. Additionally, the functional aspect of isolated EVs was investigated through addition of EVs to whole blood.

High-Sensitivity Flow Cytometry

Platelet-derived EVs in plasma or enriched by acoustic trapping were characterized using flow cytometry. PRP from the same four healthy donors as above was stimulated with M1 protein, thrombin, or HEPES buffer alone; plasma was collected; and EVs were isolated as described above. Platelet-derived EVs in plasma and acoustic trap-isolated EVs were incubated with PE-Cy™5 labeled mouse anti-human CD42b (0.25 mg/mL, BD Bioscience, Clone HIP1) for 30 min at room temperature protected from light. Samples were acquired on an Amnis CellStream Flow Cytometer (Luminex). Flow cytometer performance tracking was performed daily before all analyses using the Amnis CellStream Calibration Reagent (Luminex). The assigned voltage for forward scatter, side scatter, 488 (CD62p), and 642 (CD42b) was set to 100%. Acquisition of 10 μL per sample was performed at low speed (~3 μL/min). Silica particles (Kisker Biotech GmbH & Co., Steinfurt, Germany) of known dimensions (100 nm, 200 nm, 300 nm, 500 nm, and 1,000 nm in diameter) were used for the instrument set up standardization (online suppl. Fig. 1; for all online suppl. material, see https://doi.org/10.1159/000531266). Fluorophores were chosen for distinct lasers to minimize compensation requirements.

Mass Spectrometry Sample Preparation

The proteome contents of isolated EVs from trapped samples and the non-trapped fraction of the original sample from the same four donors as above were analyzed using mass spectrometry. The vesicles were first lysed by addition of 200 μL of RIPA buffer (Sigma-Aldrich) for 10 min followed by mechanical disruption in a Bioruptor Plus (Diagenode) for 20 cycles (30 s on, 30 s off) using the low setting. Subsequently, 1,200 μL ice-cold acetone was added to each sample prior to incubation at −20°C overnight. The samples were then centrifuged at 18,200 *g* for 30 min at 4°C, and the supernatant was removed. Then, 500 μL of ice-cold 99.5% ethanol was added to each sample, and the samples were centrifuged again at 18,200 *g* for 30 min at 4°C and the supernatant removed. The samples were then dried in a SpeedVac (miVAC DUO) for 10 min and then resuspended in 100 μL of PBS.

The proteins were prepared for quantitative data-independent acquisition mass spectrometry (DIA-MS) using trypsin double digestion. A 4.6 μL solution containing 10 M urea and 50 mM ammonium bicarbonate, as well as 2 μL 0.5 μg/μL sequencing grade trypsin (Promega), for a final concentration of 432 mM urea, 2.16 mM ABC, and 9.4 ng/μL trypsin. The samples were incubated for 30 min at 37°C. Next, 45.4 μL of the urea-ABC solution were added to the samples and then incubated for 30 min at room temperature. The cysteine bonds were reduced by adding 0.5 μL of 500 mM tris (2-carboxyethyl) phosphine, resulting in final concentration of 1.64 mM tris (2-carboxyethyl) phosphine, for 60 min at 37°C. The cysteine bonds were then alkylated with 1 μL of 500 mM iodoacetamide, resulting in a final concentration of 3.26 mM iodoacetamide, for 30 min at room temperature in a dark environment. The samples were diluted using 250 μL of 100 mM ABC for a final urea concentration below 1.5 M, and, for protein digestion, 2 μL of trypsin were added, and the samples were incubated for 16 h at 37°C. The samples were acidified using 10% formic acid to a pH of 2–3, and the peptides were purified with SOLAμ HRP reverse phase columns (Thermo Scientific). The peptides were then dried in a SpeedVac and reconstituted in 2% acetonitrile and 0.2% formic acid. To ensure injection of an

equal amount of peptide (1 μg) into the mass spectrometer, the peptide content in each sample was measured using a spectrophotometer (DeNovix, DS-11 FX+).

Liquid Chromatography Tandem Mass Spectrometry

The peptides from each sample were analyzed using DIA-MS analysis on a Q Exactive HF-X (Thermo Scientific) connected to an EASY-nLC 1200 (Thermo Scientific). The peptides were separated on a Thermo EASY-Spray column (Thermo Scientific 50 cm column) operated at 45°C and a maximum pressure of 800 bar. A linear gradient of 4%–45% acetonitrile in aqueous formic acid (0.1%) was run for 50 min. A full MS scan (resolution 60,000 for a mass range of 390–1,210 m/z) was followed by 32 full fragmentation MS/MS scans (resolution 30,000) with an isolation window of 26 m/z, including a 0.5 m/z overlap between windows. The precursor ions in each isolation window were fragmented using higher energy collisional-induced dissociation with normalized collision energy of 30. The automatic gain control was set to 3e6 for MS and 1e6 for MS/MS.

Mass Spectrometry Data Analysis

Raw MS data were gzipped and Numpressed mzML [30] using msconvert from ProteoWizard [31], v3.0.5930. Data were stored and managed with openBIS [32]. For DIA data analysis, a previously described spectral library containing the *Homo sapiens* and *S. pyogenes* serotype M1 reference proteomes (UniProt proteome IDs UP000005640 and UP000000750, respectively) was used [33]. The DIA-MS data were processed using the OpenSWATH pipeline [34]. For data analysis, raw data files were converted to mzXML using the tool msconvert and analyzed using OpenSWATH (version 2.0.1 revision:c23217). The retention time (RT) was calibrated using iRT peptides, and the RT extraction window was ±300 s. The m/z extraction tolerance was set at 0.05 Da. Peptide precursors were then identified by OpenSWATH (2.0.1) and PyProphet (2.0.1), with a false discovery rate of 1% at both the peptide precursor level and at the protein level. TRIC [35] was used to reduce identification error. The resulting datasets were analyzed using Jupyter Notebooks (3.1.1). Proteins identified with only one peptide, along with keratin proteins, were discarded. Total ion current (TIC) normalized intensities were calculated for the remaining proteins, and the proteins were assessed using Metascape [36].

Immunoblotting

Isolated vesicles were eluted with 25 μL PBS, incubated with reducing SDS-PAGE sample loading buffer (Thermo Fisher Scientific) for 10 min at 85°C, and loaded onto a stain-free protein gel (Bio-Rad). Plasma containing EVs from platelets stimulated with M1 protein, HEPES buffer alone, or thrombin was prepared as described above and subsequently centrifuged at 20,000 *g* for 90 min to isolate the EVs. The EVs that were isolated with centrifugation were loaded onto the gel and used as a positive control for the M1 protein. A Prestained Protein Ladder (Thermo Fisher Scientific) was used as a reference. SDS-PAGE was carried out, and the proteins were transferred to a membrane using a Trans-Blot Turbo System (Bio-Rad). The membrane was incubated with 5% skim milk (Millipore) for 1 h to reduce nonspecific binding and incubated with rabbit anti-M1 protein (1.2 μg/mL, BioGenes GmbH) at 4°C overnight. The membrane was washed 3 × 5 min with 0.05% Tween (Merck) in PBS and incubated with HRP-conjugated goat anti-rabbit (1:3,000, Invitrogen) for 1 h. The membrane was washed as described above and incubated with Western ECL Substrate (Bio-Rad) for 5 min. The membrane was imaged using a ChemiDoc system (Bio-Rad).

Transmission Electron Microscopy

Isolated EVs were fixed by addition of 65 μL of paraformaldehyde 6% to 130 μL of isolated EVs, yielding a concentration of 2% paraformaldehyde. The samples were incubated overnight at 4°C. The surface charge of the sample grids (TED PELLA Inc., Athene Hex Grids, Cu, 400M) was modified by glow discharge treatment. 30 μL of sample was added to the grid and incubated for 20 min. Following a wash with PBS for 5 min, the samples were treated with BSA (1%) for 10 min to reduce nonspecific binding. The EVs were immunogold labeled with a dual stain for both CD42 and M1 proteins. Samples were treated with mouse anti-CD42 primary antibody (1:30, BD Pharmingen) and incubated for 60 min. Following a wash with PBS for 5 min, the samples were treated with immunogold-conjugated secondary antibody (1:20, BBI Solutions, EM. Goat anti-mouse IgG, 10 nm) for 30 min and then washed with PBS for 5 min. The staining procedure was repeated with rabbit anti-M1 primary antibody (1:500, BioGenes GmbH) and immunogold-conjugated secondary antibody (1:20, BBI Solutions, Goat anti-rabbit, 15 nm). The samples were then fixed with 1% glutaraldehyde for 5 min and washed three times with Milli-Q for 5 min each. Finally, the samples were treated with 2% uranyl acetate for 5 min to improve contrast and washed with Milli-Q for 1 min. The samples were then imaged on a transmission electron microscope (FEI Tecnai Bio-Twin 120 kV).

Flow Cytometry of Platelet-Neutrophil Complex Formation and Neutrophil Activation

Whole blood from the same four healthy donors as above was stimulated for 15 min with 50 μL of EVs isolated from platelets from the same donor stimulated with HEPES, thrombin, or M1 protein, as described above. M1 protein (2.5 μg/mL) and thrombin (1U/mL) in combination with the anticoagulant peptide Gly-Pro-Arg-Pro (1.25 mg/mL) were used as positive controls for platelet activation. HEPES buffer alone was used to determine the background platelet and leukocyte activation. After stimulation, the samples were incubated for 15 min protected from light with anti-CD61-PE (1:10) (BD Biosciences, clone VI-PL2) to detect platelets associated with neutrophils and anti-CD11b-PerCP (1:10) (BD Biosciences, clone ICRF44) to determine neutrophil activation. The samples were acquired on an Accuri C6 Plus Flow Cytometer (BD Biosciences), and the data were analyzed using C6 Plus Software. The neutrophils were gated based on size and granularity, and the CD61 and CD11b intensity within the neutrophil gate was analyzed in histograms.

Whole Blood Stimulation and Cytokine Quantification

Cytokine release in response to isolated platelet-derived EVs was measured in whole blood using commercial ELISA kits. Whole blood from five healthy donors was diluted 1:5 in RPMI medium (Gibco, Life Technologies) and stimulated with 50 μL isolated EVs from platelets stimulated with HEPES, thrombin, or M1 protein for 24 h in a CO_2 incubator (37°C, 5% CO_2, >95% relative humidity). Heparin (0.6 μg/mL, Sigma-Aldrich) was added in combination with penicillin (100 mg/mL, Gibco, Life Technologies) and streptomycin (100 mg/mL, Gibco, Life Technologies) to prevent clot formation and contamination. Lipopolysaccharide from *Escherichia coli* O111:B4 (1 μg/mL, EMD Millipore Corp.) was used as a positive control for monocyte activation, and HEPES buffer alone was used to determine the background cytokine release. The cytokine release mediated by M1 protein alone (2.5 μg/mL) was also investigated. After incubation, the samples were

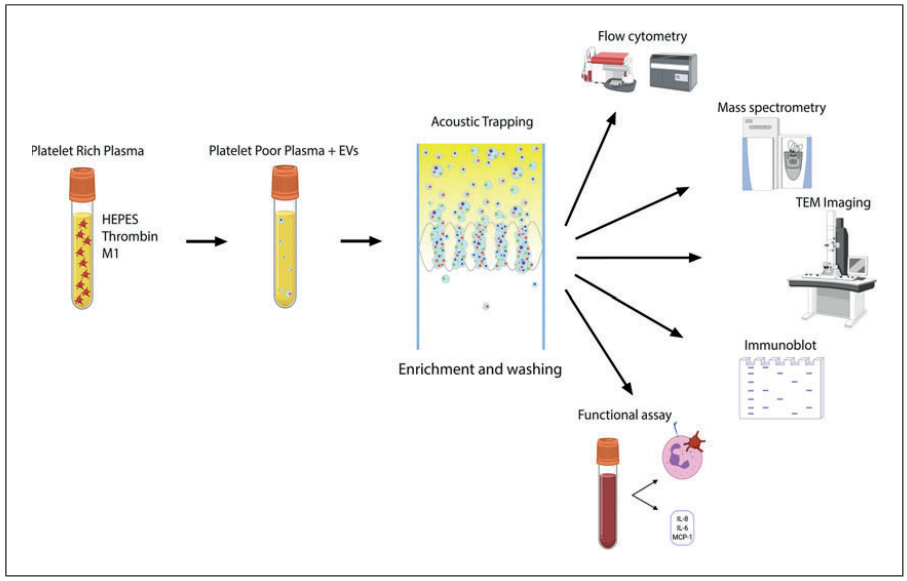

Fig. 1. Schematic illustration of the sample processing. Whole blood was collected from five healthy donors, from which platelet-rich plasma (PRP) was prepared. Platelets in PRP were stimulated with one of three stimulants to release EVs. The platelets were then centrifuged, and EVs from the platelet-poor plasma were isolated using acoustic trapping. The isolated EVs were analyzed using mass spectrometry, high-sensitivity flow cytometry, transmission electron microscopy (TEM), immunoblots, and stimulation of whole blood.

centrifuged at 500 *g* for 5 min, and cytokine and chemokine levels in the supernatants were measured using commercial ELISA kits for IL-6 (Invitrogen, Thermo Fisher Scientific), human CCL2/MCP-1 (R and D Systems), and human CXCL8/IL-8 (R and D Systems), according to manufacturer instructions.

Statistical Analyses

A Mann-Whitney U test was chosen to compare sample distribution in two groups for nonparametric data. Sample distribution was compared to background levels, unless otherwise stated. Median and individual values were used to present nonparametric data for continuous variables. Results were considered statistically significant if $p < 0.05$. Data were analyzed using Prism 9 (GraphPad Software).

Results

M1 Protein from a Bacterial Pathogen Mediated Release of EVs That Were Acoustically Enriched

The purpose of this study was to use acoustic trapping to isolate and characterize EVs derived from pathogen (M1 protein)-stimulated platelets. A schematic overview of sample processing and analysis is shown in Figure 1. Platelet activation was investigated using flow cytometry of upregulation of CD62P to the surface of platelets in PRP from healthy donors. M1 protein and thrombin mediated significant platelet activation in all donors. A median of 77% and 93% of the platelet population became activated, respectively, compared to the background level of only 3% (Fig. 2a). EVs in plasma and isolated EVs captured by acoustic trapping (Fig. 1) from the healthy donors were characterized using flow cytometry. The platelet-specific marker CD42b was used to detect platelet-derived EVs in the size range 100–1,000 nm in plasma from platelets stimulated with thrombin and M1 protein, as well as in plasma from resting platelets incubated in HEPES buffer alone. The median number of EVs detected in plasma from M1 protein-stimulated platelets was 280,000/μL, compared to 250,000/μL in plasma from resting platelets and 300,000/μL in plasma from platelets stimulated with thrombin (Fig. 2b). Acoustic trapping generated isolated platelet-derived EVs from thrombin, M1 protein, and resting platelets. The median number of isolated EVs from M1 protein-stimulated platelets was 230,000/μL, compared to 240,000/μL from

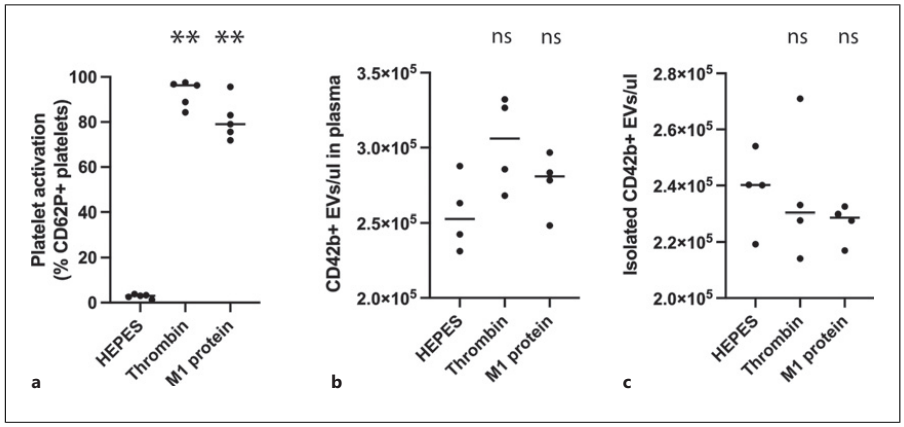

Fig. 2. M1 protein mediates platelet activation and release of EVs that are enriched by acoustic trapping. Platelet activation by the M1 protein was investigated using flow cytometry of platelet-rich plasma (PRP) from five healthy donors (n = 5) (**a**). Platelet activation is presented as percent platelets positive for CD62P. ** $p < 0.01$. Mann-Whitney test was used. Concentration of platelet-derived EVs in plasma from four healthy donors (**b**) and EVs after isolation with acoustic trapping (**c**) was determined using high-sensitivity flow cytometry. EV concentration is presented as EVs positive for CD42b/μL. Thrombin was used as a positive control for platelet activation and EV release, and HEPES buffer was used as a control for background platelet activation. Mann-Whitney test was used, sample distribution was compared to background platelet activation in resting platelets (HEPES). ns, not significant.

resting platelets and 230,000/μL from platelets stimulated with thrombin (Fig. 2c). Acoustic trapping has previously shown enrichment of EVs below 100 nm in diameter [28, 37]; however, the flow cytometer used is unable to resolve particles smaller than 100 nm. Therefore, only EVs in the size range 100–1,000 nm were included in the flow cytometry measurements, determined through the calibration particles. Size distributions of all particles found in the plasma samples, measured with nanoparticle tracking analysis, can be found in online supplementary Figure 2.

Proteome Profiling of Acoustically Enriched EVs

EVs derived from platelets stimulated with the three distinct agonists were isolated on the acoustic trapping platform and analyzed with quantitative mass spectrometry, in parallel with plasma samples of non-isolated EVs. In total, 557 proteins were identified. Proteins that were identified with only one peptide, along with all keratin proteins, were discarded, resulting in 344 remaining proteins. Protein intensities for the different samples were TIC normalized and plotted in a heatmap (Fig. 3a). Cluster I showed a weaker protein signal in the isolated EVs as compared to EVs in plasma, suggesting that these proteins were part of the background plasma signal that is washed away in the acoustic trap. Cluster II showed a stronger protein signal in the isolated EVs as compared to EVs in plasma, indicating proteins that were associated with vesicles and were enriched in the acoustic trap. It should be noted that since the protein intensities have been TIC normalized, they represent a fraction of the total signal and not an absolute value. A larger version of the heatmap where individual proteins are illustrated is available (online suppl. Fig. 3).

Metascape was used to perform gene enrichment analysis (Fig. 3b) on the 288 proteins found in cluster II. These proteins were associated with hemostasis, complement, and coagulation cascades. To further investigate the effects of thrombin or M1 protein activation on released platelet EVs compared to resting platelets, TIC normalized protein intensities for isolated EVs were plotted in a heatmap (Fig. 3c). Cluster III shows a stronger protein signal for EVs from thrombin- or M1 protein-activated platelets compared to the resting state (HEPES), suggesting these proteins are associated with platelet activation. Cluster IV shows proteins with a stronger signal for EVs from resting platelets, suggesting these proteins are normally found in platelet EVs. A gene enrichment analysis (Fig. 3d) was performed using

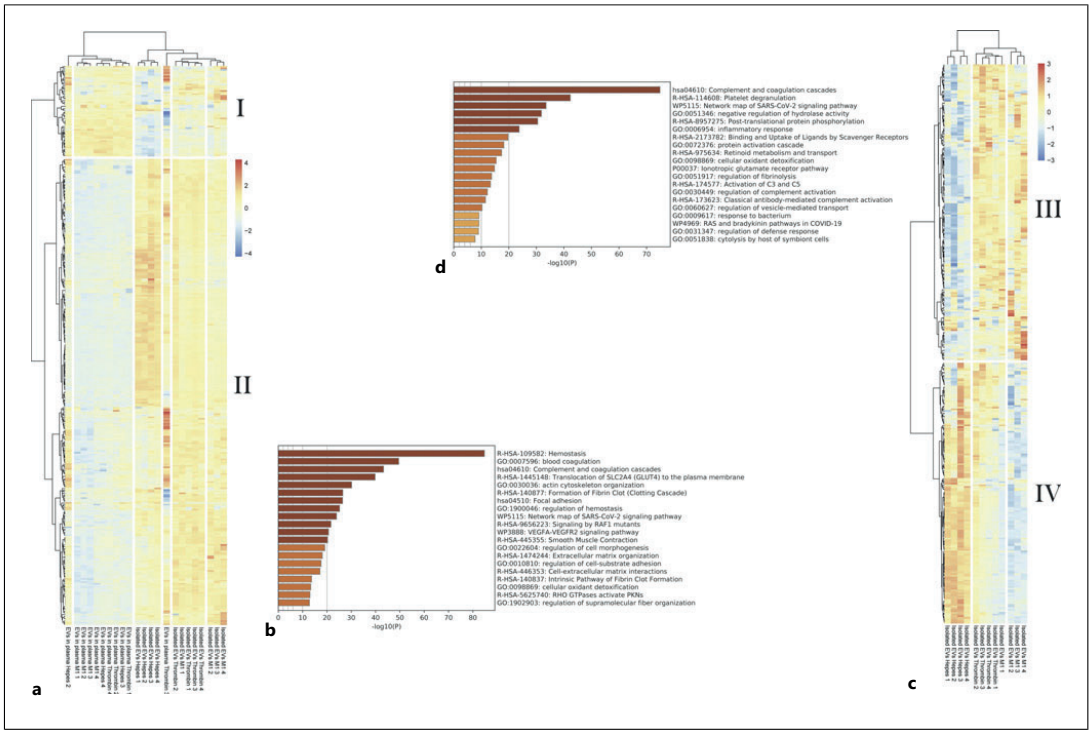

Fig. 3. Establishing a pipeline for proteome profiling of isolated EVs. EVs derived from resting platelets (HEPES), and thrombin- or M1 protein-activated platelets were isolated on the acoustic trapping platform and analyzed with quantitative mass spectrometry in parallel with plasma samples of non-isolated EVs from four healthy donors (n = 4). **a** Heatmap of protein intensities for all samples. The intensities shown are the log 10 of the TIC normalized intensities. The proteins are row normalized, and the legend gives the z-score. Cluster I indicates proteins with lower intensity in isolated EVs, compared to EVs in plasma. Cluster II indicates proteins with higher signal in isolated EVs. **b** Gene enrichment analysis of proteins in cluster II, performed using Metascape. **c** Heatmap of protein intensities for isolated EV samples. Cluster III indicates proteins with higher intensity in EVs from platelets stimulated with thrombin or M1. Cluster IV shows higher intensity in EVs from resting platelets (HEPES). **d** Gene enrichment analysis of proteins in cluster III, performed using Metascape.

Metascape software on the 183 proteins found in cluster III. The analysis showed a strong expression of proteins associated with complement, coagulation cascades, and platelet degranulation.

Distinct Proteins from Coagulation and Complement Systems Are Upregulated in EVs Derived from Pathogen-Stimulated Platelets

TIC normalized intensities of proteins associated with the groups that were revealed through the Metascape analysis were investigated further to assess differences in protein cargo of EVs derived from resting platelets, M1 protein- and thrombin-activated platelets. Several proteins associated with platelet activation and platelet aggregation were observed in platelet-derived EVs from all agonists (Fig. 4a, b). Integrin alpha-IIb (CD41), platelet glycoprotein V (GPV), integrin beta-3 (CD61), and P-selectin levels are slightly higher in EVs isolated from resting platelets compared to EVs isolated from platelets stimulated with thrombin and M1 protein. Platelet factor 4 (PF4) and platelet glycoprotein Ib (GPIb) were found at equivalent levels in all EV populations (Fig. 4a, b).

Furthermore, proteins associated with blood coagulation were also present in platelet-derived EVs (Fig. 4c). Plasminogen was found at equivalent levels in all EV populations, whereas prothrombin and von Willebrand

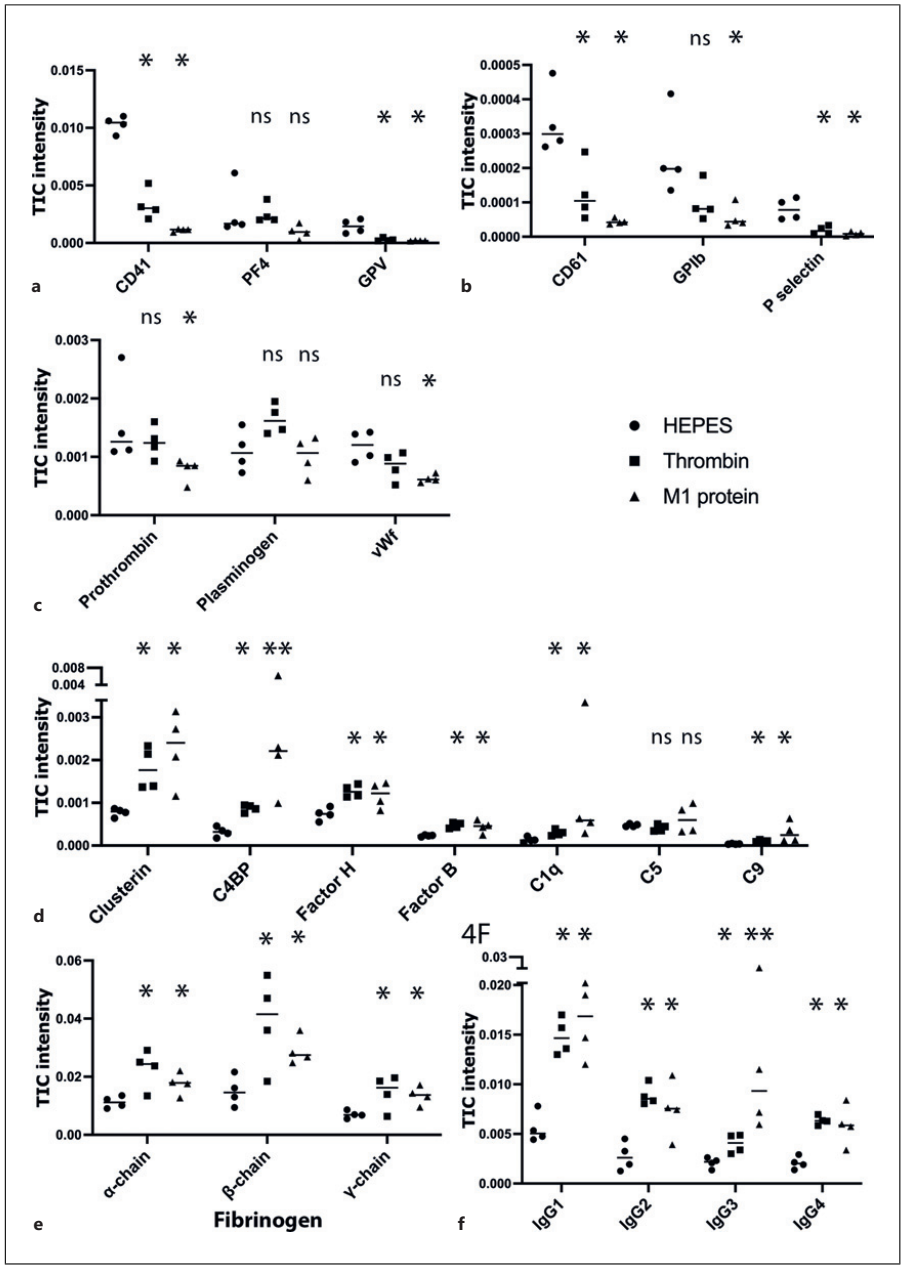

4

(For legend see next page.)

factor levels were slightly lower in EVs isolated from platelets stimulated with M1 protein compared to EVs isolated from platelets stimulated with thrombin and resting platelets (Fig. 4c).

Complement components and regulators of complement system activation were found in platelet-derived EVs (Fig. 4d). The majority of complement and complement regulatory proteins were significantly upregulated in EVs derived from platelets stimulated with M1 protein and thrombin, compared with resting platelets. Only complement component C5 was found at equivalent levels in all EV populations. Interestingly, the complement regulatory protein C4BP and the complement components C1q and C9 were significantly upregulated in EVs derived from platelets stimulated with M1 protein, as compared to both resting and thrombin-stimulated platelets.

Fibrinogen and all four subclasses of IgG were found in platelet-derived EVs (Fig. 4e, f). Fibrinogen was significantly upregulated in EVs derived from platelets stimulated with M1 protein and thrombin, compared to resting platelets (Fig. 4e). Furthermore, IgG1-2 and IgG4 were upregulated in EVs derived from platelets stimulated with M1 protein and thrombin, compared to resting platelets (Fig. 4f). Interestingly, IgG3 was significantly upregulated in EVs derived from platelets stimulated with M1 protein, as compared with both resting and thrombin-stimulated platelets (Fig. 4f). This demonstrates that the IgG3 required for platelet activation by M1 protein was also enriched in the vesicles released upon generation of EVs from activated platelets.

M1 Protein Was Packaged within EVs

In addition to human proteins associated with the groups that were revealed through the Metascape analysis, the TIC normalized intensity of M1 protein transported by EVs was investigated. The M1 protein was significantly enriched in EVs from platelets stimulated by M1 protein, as compared with non-trapped plasma samples stimulated with M1 protein (Fig. 5a). This suggests that M1 protein can be packaged into EVs during budding and transported with platelet-derived EVs in the circulation. Alternatively, M1 protein may associate directly with EVs released from activated platelets. The presence of M1 protein was confirmed using immunoblotting (Fig. 5b) and transmission electron microscopy (Fig. 5c). Both of these techniques determined that EVs from M1 protein-activated platelets contained the M1 protein (Fig. 5b, c).

Acoustically Enriched EVs Mediated Platelet-Neutrophil Complex Formation and Neutrophil Activation

Platelet activation results in platelet-neutrophil complex formation [22], which was investigated using flow cytometry. EVs were isolated from resting or stimulated platelets using acoustic trapping and added to whole blood from four healthy donors. The positive controls of thrombin and M1 protein alone mediated significant platelet-neutrophil complex formation, with a median level of 88 and 78% platelet-positive neutrophils, respectively (Fig. 6a). EVs from platelets stimulated with M1 protein and thrombin mediated significantly increased platelet-neutrophil complex formation with a median level of 55 and 51% platelet-positive neutrophils, as compared with the background level of 22%. Isolated EVs from resting platelets also mediated platelet-neutrophil complex formation, with a median level of 45% platelet-positive neutrophils. Interindividual variation was more pronounced in samples treated with platelet-derived EVs as compared with agonists alone. M1 protein alone is a more potent mediator of platelet activation and platelet-neutrophil complex formation than EVs isolated from M1 protein-activated platelets.

In parallel analyses in blood samples from the same four donors as above, neutrophil activation was investigated. The positive controls of thrombin and M1 protein alone mediated the highest neutrophil activation with a median CD11b fluorescence intensity of 82,000 and 45,000, respectively (Fig. 6b). EVs isolated from platelets stimulated with M1 protein and thrombin mediated significantly increased neutrophil activation, with a median CD11b fluorescence intensity of 27,000 and 29,000, respectively, compared to the background level of 15,000. Isolated EVs from resting platelets also mediated neutrophil activation, with a median CD11b fluorescence intensity of 24,000. Collectively, this indicates that platelet EVs derived from all three conditions mediate neutrophil activation at equivalent levels.

Fig. 4. Distinct proteins associated with blood coagulation and complement system activation are upregulated in EVs derived from platelets stimulated with M1 protein. EVs derived from resting platelets (HEPES), and thrombin- or M1 protein-activated platelets from four healthy donors ($n = 4$) were isolated on the acoustic trapping platform and analyzed with quantitative mass spectrometry. Protein intensities are presented as TIC normalized intensities of proteins associated with platelet activation (**a**, **b**), blood coagulation (**c**), complement system activation (**d**), fibrinogen (**e**) and IgG (**f**). Mann-Whitney test was used; sample distribution was compared to EVs derived from resting platelets (HEPES). * $p < 0.05$; ** $p < 0.01$; ns, not significant.

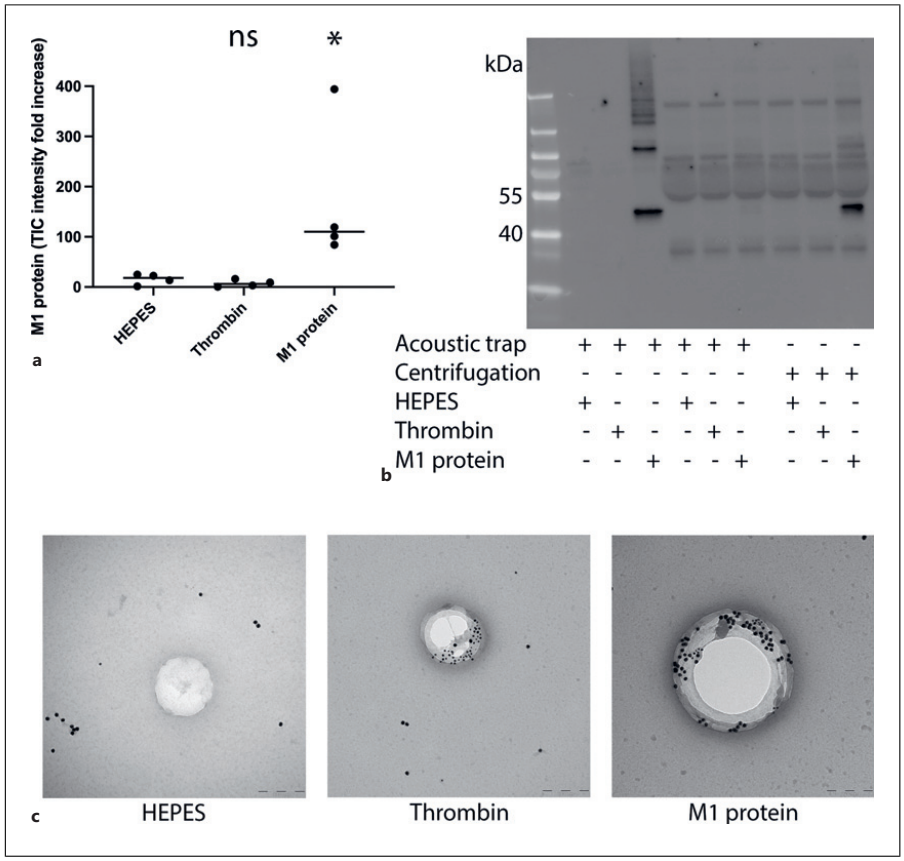

Fig. 5. M1 protein is transported in platelet-derived EVs after stimulation. EVs derived from resting platelets (HEPES), and thrombin- or M1 protein-activated platelets were isolated from four healthy donors ($n = 4$) on the acoustic trapping platform and analyzed with quantitative mass spectrometry (**a**), immunoblot (**b**), and transmission electron microscopy (**c**). **a** Protein intensity is presented as TIC normalized intensity fold increase of M1 protein in isolated EVs compared to non-trapped plasma controls. * $p < 0.05$; ns, not significant, Mann-Whitney test, sample distribution was compared to EVs derived from resting platelets (HEPES). **b** Immunoblot against the M1 protein. 1 = protein ladder, 2, 5, 8 = EVs derived from resting platelets (HEPES), 3, 6, 9 = EVs derived from thrombin-activated platelets, 4, 7, 10 = EVs derived from M1 protein-activated platelets. 2–4 = EVs isolated on the acoustic trapping platform and eluted in 25 µL PBS, 5–7 = supernatant of EVs isolated using ultracentrifugation, 8–10 = EVs isolated using ultracentrifugation. **c** Isolated EVs were stained with gold-labeled antibodies against the platelet-specific marker CD42b (10 nm) and against the M1 protein (15 nm).

Acoustically Enriched EVs Mediated Cytokine Release from Blood Cells

Cytokine release in response to isolated platelet-derived EVs was measured in whole blood using commercial ELISA kits for interleukin-8 (IL-8), interleukin-6 (IL-6), and monocyte chemoattractant protein-1 (MCP-1). These pro-inflammatory cytokines were selected as representative of early acute inflammation: IL-6 is a pleiotropic cytokine and critical mediator of the acute phase response, IL-8 is a predominant chemokine for neutrophils, and MCP-1 is a potent chemokine for monocytes. As expected, M1 protein alone significantly increased levels of IL-8, IL-6, and MCP-1 in whole blood, compared to background levels (Fig. 7a–c). Isolated EVs

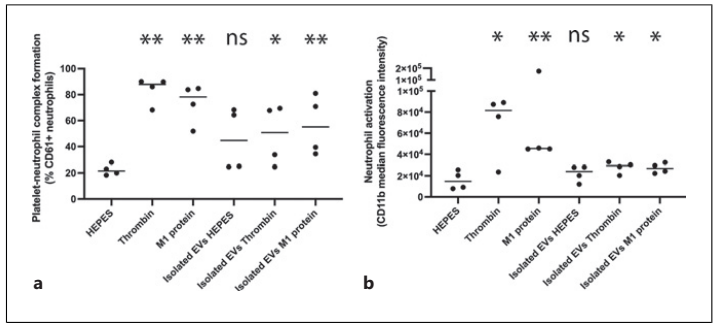

Fig. 6. Platelet-derived EVs mediate platelet-neutrophil complex formation and neutrophil activation. Flow cytometry was used to assess platelet-neutrophil complex (PNC) formation (**a**) and neutrophil activation (**b**) by the isolated EVs from resting platelets (HEPES), and from platelets activated with thrombin or M1 protein in blood from four healthy donors (n = 5). Data are presented as % neutrophils that are CD61 positive (platelet associated) (**a**) and neutrophil CD11b median fluorescence intensity (**b**). Thrombin and M1 protein are used as positive controls for platelet-neutrophil complex formation and neutrophil activation. HEPES buffer is used as a control for background PNC formation and neutrophil activation. Mann-Whitney test was used; sample distribution was compared to background levels in resting platelets (HEPES). * $p < 0.05$; ** $p < 0.01$; ns, not significant.

derived from both resting and M1 protein stimulation generated a statistically significant release of IL-8 when compared to background levels; however, the IL-8 levels generated by EVs derived from M1 protein-stimulated cells were relatively low as compared with EVs from resting platelets (Fig. 7a). Isolated EVs from resting platelets resulted in significantly increased levels of IL-6 and a tendency toward MCP-1 release in whole blood, while M1 protein- or thrombin-stimulated samples failed to mediate release of these cytokines (Fig. 7b). Collectively, our findings indicate that platelet-derived EVs mediate cytokine release in whole blood; however, the interindividual variation is high. EVs derived from M1 protein-stimulated platelets were generally weak mediators of pro-inflammatory cytokine release in whole blood, while the M1 protein alone was a potent mediator of cytokine release.

Discussion

In this study, we have determined that platelets release EVs upon stimulation with a virulence factor, M1 protein, from a significant bacterial pathogen. Intact EVs were isolated and enriched using a newly developed acoustic trapping platform, as confirmed with high-sensitivity flow cytometry, immunoblotting, and electron microscopy. Differential protein abundance profiling revealed distinct differences between intact plasma with EVs and EVs isolated from plasma using acoustic trapping, with one set of proteins washed away in the trap and one set of proteins enriched, indicating that they were specific to the EV proteome. It should be noted that the EV characterization with flow cytometry only detected EVs in the size range 100–1,000 nm, whereas the mass spectrometry measurements were derived from the entire EV population. Characterization of the protein cargo of EVs derived from pathogen-activated platelets, M1 protein, as compared with resting or thrombin-activated platelets, revealed that all three EV populations were enriched for platelet membrane proteins, granule proteins, and cytoskeletal proteins, in combination with coagulation factors and immune mediators. The functional integrity of EVs isolated using acoustic trapping was confirmed by their ability to stimulate platelet and neutrophil activation and cytokine release when incubated with blood cells.

The plasma levels of platelet-derived EVs did not increase significantly upon stimulation with thrombin or M1 protein under our experimental conditions. Previous studies have demonstrated that in vitro levels of EVs differ depending on the platelet agonist [15, 38, 39]. Thrombin is a powerful mediator of EV release, and we have determined that M1 protein generates EVs at equivalent levels in certain individuals. Under our experimental conditions, the resting platelet population also generated EVs which likely reflects in vitro activation of the platelets during centrifugation at 1,600 g in the absence of platelet inhibition. Platelets are highly reactive cells, and a heterogeneous interindividual response is to be expected upon in vitro stimulation of platelets from healthy individuals [2].

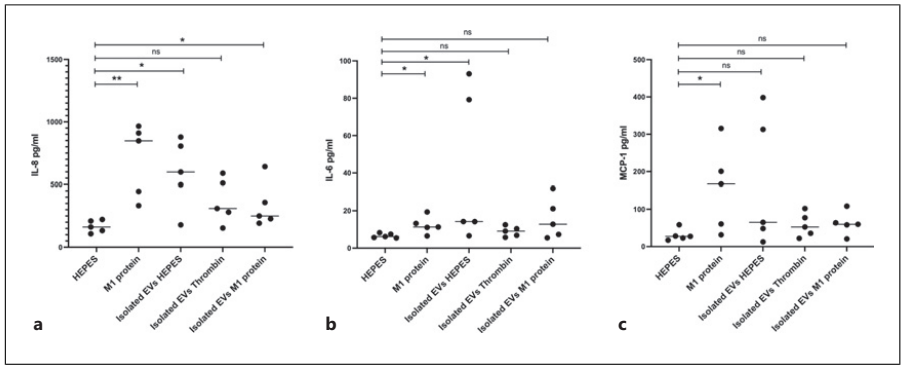

Fig. 7. Platelet-derived EVs mediate cytokine release from monocytes in whole blood. Cytokine release mediated by the EVs from resting platelets (HEPES), and from platelets activated with thrombin or M1 protein in blood from five healthy donors, was investigated using commercial IL-8 (**a**), IL-6 (**b**), and MCP-1 (**c**) kits. Cytokine levels are presented as pg/mL. M1 protein was used as a positive control for cytokine release and HEPES buffer was used as a control for background cytokine release. Mann-Whitney test was used. * $p < 0.05$; ** $p < 0.01$; ns, not significant.

It is well known that platelets constantly scan the vasculature for areas of injury or inflammation or indirectly respond to pathogen invasion through interactions with leukocytes and the endothelium [40]. Previous studies have also shown increased levels of circulating platelet-derived EVs in several pathological states, in particular as biomarkers of cardiovascular disease [11]. Sepsis is a multifactorial syndrome involving immune and coagulation dysregulation, and platelet-derived vesicles are elevated in sepsis [41, 42]. It has been reported that EVs may have a protective role during sepsis and that platelet-derived EV levels are decreased in sepsis non-survivors. For example, EVs enhance the sensitivity of contraction of mouse aorta in response to serotonin and may protect against vascular hyporeactivity accounting for hypotension in sepsis patients [43, 44]. There were significant differences in the protein cargo of EVs isolated from resting platelets, physiologically stimulated (thrombin) platelets, and pathogen (M1 protein)-stimulated platelets. The observed differences were mainly quantitative, as the protein content within the distinct EV populations was very similar, but the protein enrichment levels differed significantly in some cases. Previous studies have shown that the proteins packaged within platelet-derived EVs differ depending on the platelet stimulus [15, 16]. Our findings demonstrate an increased level of blood coagulation proteins after stimulation with thrombin and M1 protein, as compared with resting platelets. This is in line with previous studies that reported increased procoagulant activity of EVs derived from activated platelets [45, 46]. Procoagulant EVs may contribute to the coagulopathy in sepsis [47], which may be an important attribute for M1 protein during invasive streptococcal disease. Furthermore, we have previously demonstrated that other M protein serotypes that can bind fibrinogen can mediate platelet activation [23]; therefore, the findings presented herein are likely applicable to other serotypes of *S. pyogenes*.

Increased levels of complement components were also observed after stimulation with both thrombin and M1 protein; however, this was further enhanced in the case of M1 protein. All four subclasses of IgG were also increased after stimulation; however, the level of IgG3 was specifically increased after stimulation with M1 protein. We have previously demonstrated that IgG3 is particularly enriched in immune complexes formed by M1 protein, resulting in C1q-mediated complement activation on M1 protein-activated platelets [20]. Fabris and colleagues [48] have shown that platelet-derived EVs in patients with sepsis contain platelet factor 4 and anti-bacterial IgG, which may also contribute to immune complex-mediated immune responses during infection.

Platelet-derived EVs can exhibit distinct immunomodulatory properties that are dependent on the cargo incorporated within the EVs, thereby encompassing both pro- and anti-inflammatory effects. The pro-inflammatory potential of platelet-derived EVs was investigated in our study. We determined that platelet-neutrophil complex formation, neutrophil activation, and cytokine release occurred in whole blood after incubation with platelet EVs. The relatively low number of donors ($n = 5$) investigated and the

heterogenous inter-interindividual variation observed are, however, an important limitation to the study; therefore, we cannot conclude whether distinct pro-inflammatory profiles are generated for the three conditions investigated. The formation of platelet-neutrophil complexes has been previously observed in sepsis [49]. In addition, platelet-derived EVs have been reported to directly associate with leukocytes and facilitate chemotaxis of leukocytes [9, 50]. M protein stimulates platelet-neutrophil complex formation, resulting in functional impairment of these neutrophils with decreased chemotaxis and phagocytosis [22]. The present findings imply that platelet-derived EVs may also contribute to the immunomodulatory effects of M1 protein on neutrophils; however, M1 protein incorporated in EVs is a less potent pro-inflammatory mediator as compared with M1 protein alone under all conditions investigated.

Importantly, the M1 protein was itself associated with isolated EVs, which shows that M1 protein can be transported with platelet-derived EVs after stimulation. This mechanism of bacterial toxin transfer with host cell EVs has been previously described for Shiga toxin from enterohemorrhagic *E. coli* [51]. Interestingly, Shiga toxin is transported with host blood cell-derived EVs and taken up by renal cells, where it contributes to the pathogenesis of kidney failure. EVs are released from platelets stimulated with LPS from Gram-negative bacteria, and these EVs derived from LPS/TLR4 activation of platelets can stimulate further activation of endothelial cells [52], which may represent an important effector of vascular dysfunction that is a hallmark of sepsis.

Collectively, we have determined the phenotype of platelet-derived EVs that are isolated and enriched using acoustic trapping. Our subsequent proteomic profiling showed that blood coagulation proteins, complement components, and IgG were enriched in all EV populations irrespective of agonist. A specific increase in complement components and IgG3 was observed after pathogen-mediated platelet activation (M1 protein), and the bacterial virulence factor, M1 protein, was transported within platelet-derived EVs. Equivalent levels of pro-inflammatory responses were generated in blood cells exposed to the acoustically enriched EVs irrespective of agonist.

Acknowledgments

Lund University Bioimaging Centre (LBIC) is gratefully thanked for providing experimental resources. Sara Wettemark is thanked for excellent technical assistance with blood cell analyses. Figure 1 was created with BioRender.

Statement of Ethics

Blood was collected from healthy donors by trained personnel. Written informed consent was obtained from the donors prior to blood collection. This study protocol was reviewed and approved by the Regional Ethical Review Authority, Lund (approval number 2015/801).

Conflict of Interest Statement

The authors have no conflicts of interest to declare.

Funding Sources

This research was supported by grants from Knut and Alice Wallenberg Foundation: 2016.0023 (O.S. and J.M.); WAF 2017.0271 (J.M.); the Swedish Research Council: 2018-05795 (O.S. and J.M.); 2019-00795 and 2018-03672 (T.L.); and 2021-01310 (J.W.S). G.M. is the recipient of a postdoctoral fellowship from Fonds de Recherche du Québec-Santé (FRQS).

Author Contributions

F.P. and A.B. performed experiments, analyzed the data, and wrote the manuscript. G.M. and J.W.S. designed, performed, and analyzed high-sensitivity flow cytometry of extracellular vesicles and edited the manuscript. O.S., T.L.L., and J.M. designed and supervised the study and edited the manuscript. All authors read and approved the manuscript for submission.

Data Availability Statement

All data generated or analyzed during this study are included in this article and its supplementary material files. Further inquiries can be directed to the corresponding author.

References

1 Burnier L, Fontana P, Kwak BR, Angelillo-Scherrer A. Cell-derived microparticles in haemostasis and vascular medicine. Thromb Haemost. 2009;101(03):439–51.
2 Yee DL, Sun CW, Bergeron AL, Dong JF, Bray PF. Aggregometry detects platelet hyperreactivity in healthy individuals. Blood. 2005;106(8):2723–9.
3 Melki I, Tessandier N, Zufferey A, Boilard E. Platelet microvesicles in health and disease. Platelets. 2017;28(3):214–21.
4 Mause SF, Weber C. Microparticles: protagonists of a novel communication network for intercellular information exchange. Circ Res. 2010;107(9):1047–57.
5 Morrell CN, Aggrey AA, Chapman LM, Modjeski KL. Emerging roles for platelets

as immune and inflammatory cells. Blood. 2014;123(18):2759–67.
6 Maouia A, Rebetz J, Kapur R, Semple JW. The immune nature of platelets revisited. Transfus Med Rev. 2020;34(4):209–20.
7 Cox D, Kerrigan SW, Watson SP. Platelets and the innate immune system: mechanisms of bacterial-induced platelet activation. J Thromb Haemost. 2011;9(6):1097–107.
8 Solum NO, Brosstad F, Pedersen T, Kveine M, Holme PA. Microvesicles bind soluble fibrinogen, adhere to immobilized fibrinogen and coaggregate with platelets. Thromb Haemost. 1998;79(02):389–94.
9 Forlow SB, McEver RP, Nollert MU. Leukocyte-leukocyte interactions mediated by platelet microparticles under flow. Blood. 2000;95(4):1317–23.
10 Marcoux G, Laroche A, Hasse S, Bellio M, Mbarik M, Tamagne M, et al. Platelet EVs contain an active proteasome involved in protein processing for antigen presentation via MHC-I molecules. Blood. 2021;138(25):2607–20.
11 VanWijk MJ, VanBavel E, Sturk A, Nieuwland R. Microparticles in cardiovascular diseases. Cardiovasc Res. 2003;59(2):277–87.
12 Woth G, Tőkés-Füzesi M, Magyarlaki T, Kovács GL, Vermes I, Mühl D. Activated platelet-derived microparticle numbers are elevated in patients with severe fungal (Candida albicans) sepsis. Ann Clin Biochem. 2012;49(Pt 6):554–60.
13 Marcoux G, Magron A, Sut C, Laroche A, Laradi S, Hamzeh-Cognasse H, et al. Platelet-derived extracellular vesicles convey mitochondrial DAMPs in platelet concentrates and their levels are associated with adverse reactions. Transfusion. 2019;59(7):2403–14.
14 Boudreau LH, Duchez AC, Cloutier N, Soulet D, Martin N, Bollinger J, et al. Platelets release mitochondria serving as substrate for bactericidal group IIA-secreted phospholipase A2 to promote inflammation. Blood. 2014;124(14):2173–83.
15 Shai E, Rosa I, Parguiña AF, Motahedeh S, Varon D, García Á. Comparative analysis of platelet-derived microparticles reveals differences in their amount and proteome depending on the platelet stimulus. J Proteomics. 2012;76 Spec No:287–96.
16 Milioli M, Ibáñez-Vea M, Sidoli S, Palmisano G, Careri M, Larsen MR. Quantitative proteomics analysis of platelet-derived microparticles reveals distinct protein signatures when stimulated by different physiological agonists. J Proteomics. 2015;121:56–66.
17 Opal SM, Garber GE, LaRosa SP, Maki DG, Freebairn RC, Kinasewitz GT, et al. Systemic host responses in severe sepsis analyzed by causative microorganism and treatment effects of drotrecogin alfa (activated). Clin Infect Dis. 2003;37(1):50–8.
18 Gherardi G, Vitali LA, Creti R. Prevalent emm types among invasive GAS in europe and north America since year 2000. Front Public Health. 2018;6:59.
19 Ghosh P. The nonideal coiled coil of M protein and its multifarious functions in pathogenesis. Adv Exp Med Biol. 2011;715:197–211.
20 Palm F, Sjöholm K, Malmström J, Shannon O. Complement activation occurs at the surface of platelets activated by streptococcal M1 protein and this results in phagocytosis of platelets. J Immunol. 2019;202(2):503–13.
21 Shannon O, Hertzén E, Norrby-Teglund A, Mörgelin M, Sjöbring U, Björck L. Severe streptococcal infection is associated with M protein-induced platelet activation and thrombus formation. Mol Microbiol. 2007;65(5):1147–57.
22 Hurley SM, Kahn F, Nordenfelt P, Mörgelin M, Sørensen OE, Shannon O. Platelet-dependent neutrophil function is dysregulated by M protein from Streptococcus pyogenes. Infect Immun. 2015;83(9):3515–25.
23 Palm F, et al. Distinct serotypes of streptococcal M proteins mediate fibrinogen-dependent platelet activation and pro-inflammatory effects. Infect Immun. 2021;90(2):e0046221.
24 Herwald H, Cramer H, Mörgelin M, Russell W, Sollenberg U, Norrby-Teglund A, et al. M protein, a classical bacterial virulence determinant, forms complexes with fibrinogen that induce vascular leakage. Cell. 2004;116(3):367–79.
25 Kahn F, Mörgelin M, Shannon O, Norrby-Teglund A, Herwald H, Olin AI, et al. Antibodies against a surface protein of Streptococcus pyogenes promote a pathological inflammatory response. PLoS Pathog. 2008;4(9):e1000149.
26 Hammarström B, Laurell T, Nilsson J. Seed particle-enabled acoustic trapping of bacteria and nanoparticles in continuous flow systems. Lab Chip. 2012;12(21):4296–304.
27 Evander M, Gidlöf O, Olde B, Erlinge D, Laurell T. Non-contact acoustic capture of microparticles from small plasma volumes. Lab Chip. 2015;15(12):2588–96.
28 Broman A, Lenshof A, Evander M, Happonen L, Ku A, Malmström J, et al. Multinodal acoustic trapping enables high capacity and high throughput enrichment of extracellular vesicles and microparticles in miRNA and MS proteomics studies. Anal Chem. 2021;93(8):3929–37.
29 Rezeli M, Gidlöf O, Evander M, Bryl-Górecka P, Sathanoori R, Gilje P, et al. Comparative proteomic analysis of extracellular vesicles isolated by acoustic trapping or differential centrifugation. Anal Chem. 2016;88(17):8577–86.
30 Teleman J, Dowsey AW, Gonzalez-Galarza FF, Perkins S, Pratt B, Röst HL, et al. Numerical compression schemes for proteomics mass spectrometry data. Mol Cell Proteomics. 2014;13(6):1537–42.
31 Chambers MC, Maclean B, Burke R, Amodei D, Ruderman DL, Neumann S, et al. A cross-platform toolkit for mass spectrometry and proteomics. Nat Biotechnol. 2012;30(10):918–20.
32 Bauch A, Adamczyk I, Buczek P, Elmer FJ, Enimanev K, Glyzewski P, et al. openBIS: a flexible framework for managing and analyzing complex data in biology research. BMC Bioinformatics. 2011;12:468.
33 Chowdhury S, Khakzad H, Bergdahl GE, Lood R, Ekstrom S, Linke D, et al. Streptococcus pyogenes forms serotype- and local environment-dependent interspecies protein complexes. mSystems. 2021;6(5):e0027121.
34 Rost HL, Rosenberger G, Navarro P, Gillet L, Miladinović SM, Schubert OT, et al. OpenSWATH enables automated, targeted analysis of data-independent acquisition MS data. Nat Biotechnol. 2014;32(3):219–23.
35 Rost HL, Liu Y, D'Agostino G, Zanella M, Navarro P, Rosenberger G, et al. TRIC: an automated alignment strategy for reproducible protein quantification in targeted proteomics. Nat Methods. 2016;13(9):777–83.
36 Zhou Y, Zhou B, Pache L, Chang M, Khodabakhshi AH, Tanaseichuk O, et al. Metascape provides a biologist-oriented resource for the analysis of systems-level datasets. Nat Commun. 2019;10(1):1523.
37 Ku A, Lim HC, Evander M, Lilja H, Laurell T, Scheding S, et al. Acoustic enrichment of extracellular vesicles from biological fluids. Anal Chem. 2018;90(13):8011–9.
38 Ambrose AR, Alsahli MA, Kurmani SA, Goodall AH. Comparison of the release of microRNAs and extracellular vesicles from platelets in response to different agonists. Platelets. 2018;29(5):446–54.
39 Ferreira PM, Bozbas E, Tannetta SD, Alroqaiba N, Zhou R, Crawley JTB, et al. Mode of induction of platelet-derived extracellular vesicles is a critical determinant of their phenotype and function. Sci Rep. 2020;10(1):18061.
40 Guo L, Rondina MT. The Era of thromboinflammation: platelets are dynamic sensors and effector cells during infectious diseases. Front Immunol. 2019;10:2204.
41 Tőkés-Füzesi M, Woth G, Ernyey B, Vermes I, Mühl D, Bogár L, et al. Microparticles and acute renal dysfunction in septic patients. J Crit Care. 2013;28(2):141–7.
42 Boscolo A, Campello E, Bertini D, Spiezia L, Lucchetta V, Piasentini E, et al. Levels of circulating microparticles in septic shock and sepsis-related complications: a case-control study. Minerva Anestesiol. 2019;85(6):625–34.
43 Puskarich MA, Cornelius DC, Bandyopadhyay S, McCalmon M, Tramel R, Dale WD, et al. Phosphatidylserine expressing platelet microparticle levels at hospital presentation are decreased in sepsis non-survivors and correlate with thrombocytopenia. Thromb Res. 2018;168:138–44.
44 Mostefai HA, Meziani F, Mastronardi ML, Agouni A, Heymes C, Sargentini C, et al. Circulating microparticles from patients with septic shock exert protective role in

vascular function. Am J Respir Crit Care Med. 2008;178(11):1148–55.
45 Mooberry MJ, Bradford R, Hobl EL, Lin FC, Jilma B, Key NS. Procoagulant microparticles promote coagulation in a factor XI-dependent manner in human endotoxemia. J Thromb Haemost. 2016;14(5):1031–42.
46 Tripisciano C, Weiss R, Karuthedom George S, Fischer MB, Weber V. Extracellular vesicles derived from platelets, red blood cells, and monocyte-like cells differ regarding their ability to induce factor XII-dependent thrombin generation. Front Cell Dev Biol. 2020;8:298.
47 Meziani F, Delabranche X, Asfar P, Toti F. Bench-to-bedside review: circulating microparticles–a new player in sepsis? Crit Care. 2010;14(5):236.
48 Sartori MT, Zurlo C, Bon M, Bertomoro A, Bendo R, Bertozzi I, et al. Platelet-derived microparticles bearing PF4 and anti-GAGS immunoglobulins in patients with sepsis. Diagnostics. 2020;10(9):627.
49 Reid VL, Webster NR. Role of microparticles in sepsis. Br J Anaesth. 2012;109(4):503–13.
50 Fendl B, Eichhorn T, Weiss R, Tripisciano C, Spittler A, Fischer MB, et al. Differential interaction of platelet-derived extracellular vesicles with circulating immune cells: roles of TAM receptors, CD11b, and phosphatidylserine. Front Immunol. 2018;9:2797.
51 Stahl AL, Arvidsson I, Johansson KE, Chromek M, Rebetz J, Loos S, et al. A novel mechanism of bacterial toxin transfer within host blood cell-derived microvesicles. PLoS Pathog. 2015;11(2):e1004619.
52 Brown GT, McIntyre TM. Lipopolysaccharide signaling without a nucleus: kinase cascades stimulate platelet shedding of proinflammatory IL-1β-rich microparticles. J Immunol. 2011;186(9):5489–96.

Supplementary Information

Phenotypic Characterization of Acoustically Enriched Extracellular Vesicles from Pathogen-Activated Platelets

Frida Palm[a*], Axel Broman[b*], Genevieve Marcoux[c], John W. Semple[c,d,e], Thomas L. Laurell[b], Johan Malmström[a], Oonagh Shannon[a,f]

a. Division of Infection Medicine, Department of Clinical Sciences, Lund University, Lund, Sweden
b. Department of Biomedical Engineering, Lund University, Lund, Sweden
c. Division of Hematology and Transfusion Medicine, Department of Laboratory Medicine, Lund University, Lund, Sweden
d. Clinical Immunology and Transfusion Medicine, Office of Medical Services, Region Skåne, Lund, Sweden
e. Department of Pharmacology and Toxicology, University of Toronto, Toronto, ON, Canada
f. Section for Oral Biology and Pathology, Faculty of Odontology, Malmö University, Malmö, Sweden

** These authors contributed equally.*

Supplementary Figures

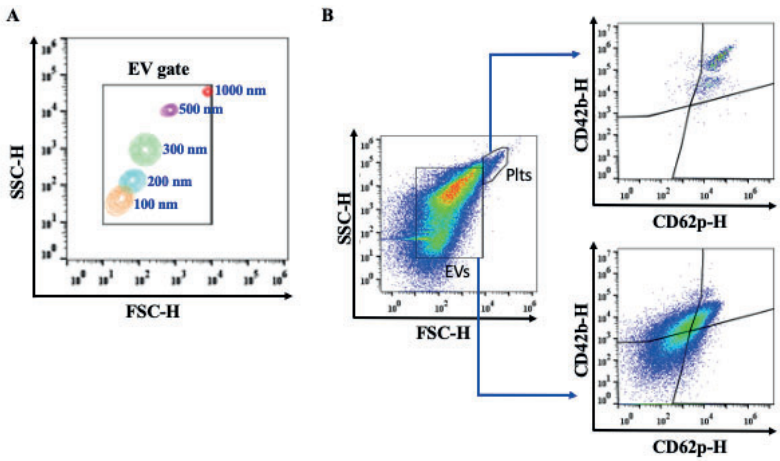

Supplementary figure 1. Assessment of platelet and platelet EV subpopulation by high-sensitivity flow cytometry. (A) Acquisition by flow cytometry (Amnis CellStream, Luminex) of silica beads of various size (100, 200, 300, 500 and 1000 nm) displayed in side scatter (SSC)-H and forward scatter (FSC)-H design the lower (100 nm) and upper (1000 nm) limits of the EV gate. (B) Representative SSC-H and FSC-PMT-H dot plots of platelet (Plts) and platelet EVs (EVs) from a stimulated PRP (left). Platelets detected from this sample in the Plts gate (upper right) and from the EV gate (lower right) are displayed according to their expression of a platelet marker (CD42b-H) and of an activation marker (CD62p-H).

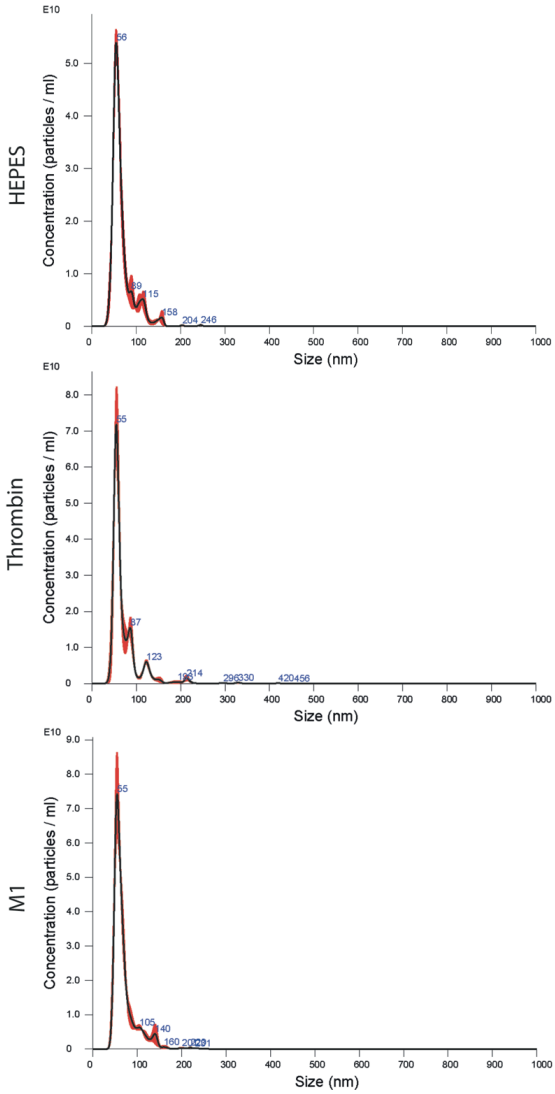

Supplementary figure 2. Nanoparticle tracking analysis of plasma samples containing EVs from platelets stimulated with HEPES-buffer, Thrombin or the M1 protein, performed using Nanosight LM10C. The size distributions are calculated based on all particles found in the plasma samples, not exclusively EVs.

S3A

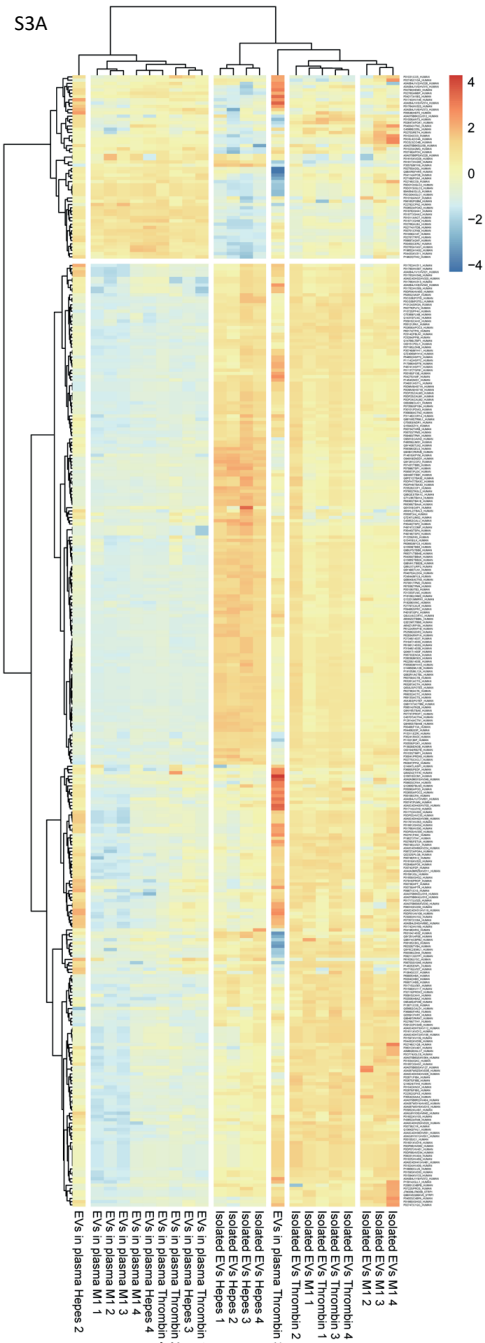
4
2
0
−2
−4
EVs in plasma Hepes 2
EVs in plasma M1 1
EVs in plasma M1 3
EVs in plasma M1 2
EVs in plasma M1 4
EVs in plasma Thrombin 2
EVs in plasma Thrombin 4
EVs in plasma Hepes 4
EVs in plasma Hepes 3
EVs in plasma Thrombin 1
Isolated EVs Hepes 1
Isolated EVs Hepes 2
Isolated EVs Hepes 3
Isolated EVs Hepes 4
EVs in plasma Thrombin 3
Isolated EVs M1 1
Isolated EVs Thrombin 1
Isolated EVs Thrombin 3
Isolated EVs Thrombin 4
Isolated EVs M1 2
Isolated EVs M1 3
Isolated EVs M1 4

S3B

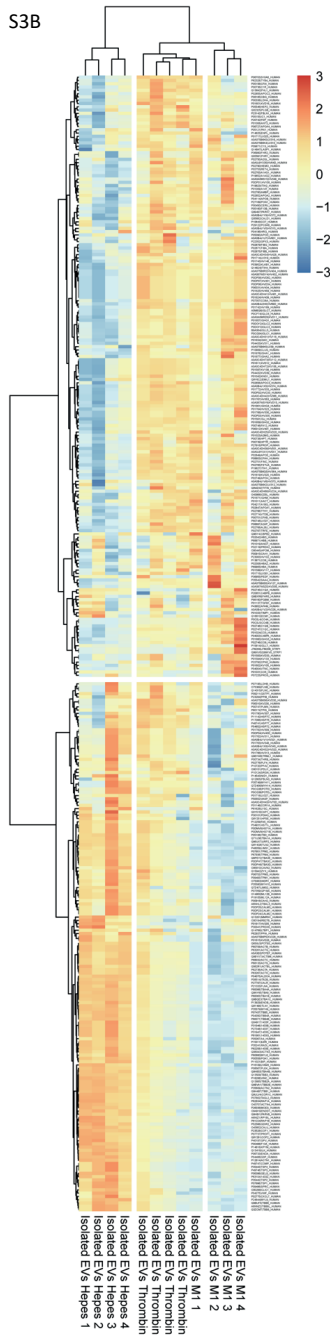
3
2
1
0
−1
−2
−3
Isolated EVs Hepes 1
Isolated EVs Hepes 2
Isolated EVs Hepes 3
Isolated EVs Hepes 4
Isolated EVs Thrombin 2
Isolated EVs Thrombin 3
Isolated EVs Thrombin 1
Isolated EVs Thrombin 4
Isolated EVs M1 1
Isolated EVs M1 2
Isolated EVs M1 3
Isolated EVs M1 4

Supplementary figure 3. Intensities of proteins associated with platelet derived EVs. Heatmaps with intensities for proteins associated with EVs derived from resting platelets (HEPES), and Thrombin- or M1 protein-activated platelets isolated on the acoustic trapping platform and analyzed with quantitative mass spectrometry, in parallel with plasma samples of non-isolated EVs. (A) Heatmap of protein intensities for all samples. (B) Heatmap of protein intensities for isolated EV samples. The intensities shown are the Log 10 of the TIC normalized intensities. The proteins are row normalized and the legend gives the z-score.

Paper III

Paper IV

LUND UNIVERSITY

ISBN: 978-91-8104-272-6 (print)
ISBN: 978-91-8104-273-3 (pdf)
ISRN: LUTEDX/TEEM – 1139– SE
Report-nr: 2/24